Critical Reviews in Solid State and Materials Sciences, 29:1–44, 2004

ISSN: 1040-8436 print
DOI: 10.1080/10408430490442458

Deep Level Transient Spectroscopy of Defects in High-Energy Light-Particle Irradiated Si

F. Danie Auret*
Department of Physics, University of Pretoria, Pretoria 0002, South Africa and
Centre for Electronic Materials, Devices and Nanostructures, UMIST, Manchester, M60 1QD, UK

Prakash N. K. Deenapanray
Department of Electronic Materials Engineering, Research School of Physical Sciences and Engineering, and Centre for Sustainable Energy Systems, Faculty of Engineering and Information Technology, The Australian National University, Canberra ACT 0200, Australia

TABLE OF CONTENTS

*E-mail: fauret@postino.up.ac.za

ABSTRACT: The authors review what has been learned concerning the electrical and annealing properties of point defects in high-energy electron or proton irradiated Si from deep level transient spectroscopy (DLTS). The authors have focused mainly on the properties of electron traps, and to a lesser extent on the properties of hole traps. In addition to an in-depth discussion of hydrogen-related defects in Si, this review article provides a brief tutorial on ion-solid interactions and the theory underlying DLTS. The authors also provide a few examples of the power of high resolution Laplace DLTS in analyzing radiation induced defects. The collection of results gathered in this article may provide the fundamental information for successful defect engineering in light-particle irradiated Si.

KEYWORDS: deep level transient spectroscopy, defects, silicon, irradiation.

1. INTRODUCTION

Radiation of semiconductors has been studied for many years with the aim of establishing firstly, the structure and properties of the defects introduced during irradiation, and secondly, the effects of the radiation-induced defects on semiconductor properties as a function of particle type, energy, dose, and dose rate. The results obtained from these studies served as a basis for several areas in semiconductor materials modification and device fabrication, such as doping, isolation, and carrier lifetime engineering. In many early studies, the focus was on the undesirable effects of radiation-induced defects in electronic devices that have to function in radiation environments, for example, near radiation sources or in outer space where they are exposed to cosmic rays. However, the realization that radiation-induced defects can beneficiate electronic materials and devices by altering their properties, led to new fields of research and novel applications. In the development of new processes for fabrication of Si integrated circuits, the use of ion implantation with energies in the MeV range has steadily increased. This includes, for example, formation of retrograde wells,[1] luminescence centers for optoelectronic devices,[2] conductive silicides and insulating oxides.[3,4] Moreover, irradiation with high-energy electrons, protons, alpha-particles, and heavier ions has received growing interest as a technique to control the carrier lifetime, and thus to improve the switching characteristics, of silicon power devices.[5,6] Compared to gold diffusion, traditionally used for lifetime control, particle irradiation can provide either a uniform lifetime tailoring (when using MeV electrons), or a well defined limited-depth lifetime alteration (when employing keV – MeV ions). Localized layers with a high density of lifetime "killers" can be created at any depth within the device by varying the ion type and energy.[7]

For successfully realizing these and other possible applications, it is imperative to understand the effect of radiation on electronic materials and devices fabricated on them. This is necessary firstly, to avoid the deleterious effects of some defects and, secondly, to utilize the beneficial effects of others, depending on the application. In order to fully understand the role of any defect in a particular electronic device, several properties of the defect need to be known, namely its: energy level(s) in the band gap, concentration, and thermal and optical capture and emission capture cross sections for electrons and holes.[8] This allows a modeling of the effect of a defect on the properties of electronic materials and devices fabricated on them. In addition, the structure, introduction rate, introduction and diffusion mechanisms, and thermal stability of the defect should be determined so that it can be reproducibly introduced, avoided, or eliminated, depending on the application.

Deep level transient spectroscopy (DLTS)[9,10] has been instrumental in determining most of the aforementioned properties of defects introduced in several semiconductors during crystal growth, radiation with different particle types, and by several device fabrication processes. DLTS has also provided important information pertaining to the behavior of defects in electric and magnetic fields and under uniaxial stress. The latter type of study can provide valuable information about the symmetry of defects, which in turn aids in determining their structure. DLTS is particularly attractive because it can be used to characterize defects using various kinds of space-charge–based devices, ranging from simple Schottky barrier diodes (SBDs) and p–n junctions to device structures with higher degrees of complexity.[11] Furthermore, the recent development of high-resolution DLTS, for example by Laplace inversion,[12] has significantly increased its spectroscopic ability, thereby facilitating the separation of closely spaced energy levels that show up as a single broad feature in conventional DLTS. A case in point is the splitting of the DLTS peaks of the divacancy and the E-center in Si, the signals of which are normally observed as a single, sometimes broadened and asymmetric, peak.[13]

In this review the authors shall attempt to provide as much information as possible regarding key results obtained using DLTS in the analysis of radiation- and implantation-induced

defects in Si. The review shall focus mainly on electron-, proton- and alpha-particle irradiation, but it shall also provide some examples of recent results to illustrate the separation of vacancy and interstitial depth profiles in Si implanted with high-energy heavier particles. In order to provide an understanding of the process of particle-induced defect introduction and the extent of this damage in semiconductors, the authors briefly introduce the terminology and key concepts of particle–solid interaction in Section 2. Then, in Section 3, the authors provide the background for applying DLTS, and analyzing and interpreting the data thus obtained regarding the characteristics of deep level defects. In Section 4 the authors treat specialized topics in particle irradiation of Si and the analyses of these by DLTS. In all the examples provided the authors endeavor to place the DLTS results in perspective by comparing them, where possible, with results obtained from other techniques that provide structural information about defects.

2. PARTICLE IRRADIATION OF SEMICONDUCTORS

When energetic particles enter a material, they are decelerated and the energy thus transferred to the material can modify its structure and properties. In the case of crystalline semiconductors, particle-induced materials modification, traditionally known as radiation damage, will occur as long as the projectile particles can transfer energy, E, larger than the displacement energy, E_d, to the lattice atoms. The extent to which a material is modified depends on the energy deposited per unit volume. Two key issues in ion–solid interaction experiments are the depth distributions of (1) the implanted species, and (2) the defects that are created in the lattice. In this section, the authors provide a summary of the theory pertaining to these issues, starting with the main energy-loss mechanisms of energetic ions in a solid.

2.1 Energy-Loss Mechanisms

Energetic particles transfer energy by primarily two mechanisms: (1) screened Coulomb collisions with target atoms (nuclear stopping), and (2) interactions with bound or free electrons in the solid (electronic stopping). The relative effect of the two mechanisms depends on the target species as well as the energy and type (mass and charge) of the incident projectile particle. Figure 1 is a convenient "universal" representation of the velocity (which is proportional to $\varepsilon^{1/2}$) dependence of nuclear stopping $\nu = (d\varepsilon/d\rho)_n$ and electronic stopping $(d\varepsilon/d\rho)_e$, in terms of the reduced energy, ε. Both ε and the reduced path length, ρ,[14] are dimensionless and can be expressed in terms of laboratory units E and x as:

$$\varepsilon = \frac{4\pi\varepsilon_0 a M_2}{Z_1 Z_2 e^2 (M_1 + M_2)} E, \qquad [1]$$

and

$$\rho = N\pi a^2 \frac{4M_1 M_2}{(M_1 + M_2)^2} x, \qquad [2]$$

where M_1 and M_2, and Z_1 and Z_2 are the mass numbers and atomic numbers of the incident particle and target atoms, respectively, e is the electronic charge, N is the number of atoms per unit volume, ε_0 is the permittivity of free space and a is the screening radius. Several expressions exist for the screening

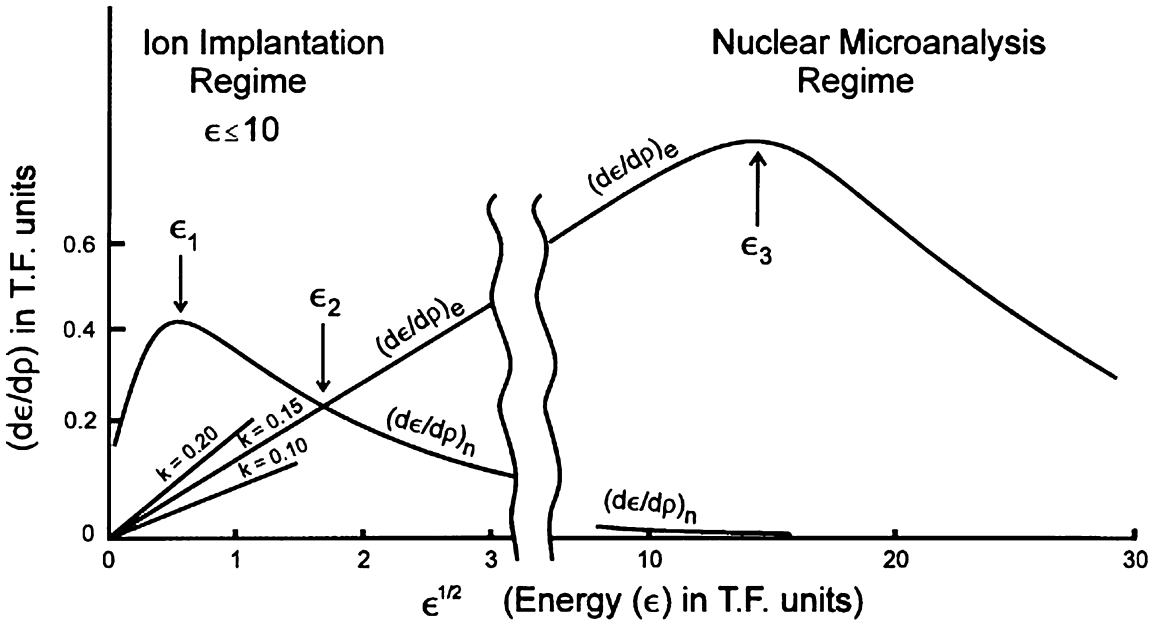

FIG. 1. Nuclear and electronic stopping versus the reduced energy of an implanted ion.[14]

radius,[15,16] with the most frequently used being that given by:[17]

$$a = \frac{0.8853 a_0}{\left(Z_1^{2/3} + Z_2^{2/3}\right)^{1/2}}, \quad [3]$$

where $a_0 = 0.529$ Å is the Bohr radius. In order to facilitate an interpretation of Figure 1 in terms of "real" energies used in experiments, Figure 2 plots the values of ε for protons, He-ions and Si-ions implanted into Si as a function of their energy in keV.

Using the reduced energy has two advantages, namely: (1) nuclear stopping and associated quantities, such as damage production and sputtering, can be approximated by a universal curve for all particle–target combinations (Figure 1), and (2) ion bombardment studies can be separated into two distinct regimes. In the first regime, called the ion implantation regime ($\varepsilon < 10$), both nuclear and electronic stopping contribute significantly to energy loss, and theoretical treatments in this regime are complex. In the second regime, referred to as the nuclear analysis regime ($\varepsilon \gg 10$), where ions are sufficiently fast so that they are virtually stripped of all their electrons, electronic stopping is the dominant energy-loss process. In this regime, the ion trajectory is almost linear, sputtering and collision cascade effects are practically negligible, and the Bethe–Bloch formalism can be used for determining energy loss and penetration.[18]

Figure 1 shows that at low energies (relevant to sputtering and ion beam etching), nuclear stopping is the more important process and that it reaches a maximum value (ε_1) around $\varepsilon^{1/2} = 0.6$, and thereafter decreases. From Figures 1 and 2 it is seen that for protons and He-ions in Si this corresponds to energies of approximately 0.4 keV and 1 keV, respectively. Figure 1 also shows that electronic stopping becomes the dominant energy-loss mechanism for $\varepsilon^{1/2} > 2$ (ε_2) and that it increases linearly with velocity up to about $\varepsilon^{1/2} = 14$ (ε_3). It should be pointed out that whereas $(d\varepsilon/d\rho)_n$ is only a function of ε (*i.e.*, independent of incident particle type and host atoms), the electronic stopping can be written as

$$(d\varepsilon/d\rho)_e = k\varepsilon^{1/2}, \quad [4]$$

where k is a function of Z_1, Z_2, M_1, and M_2. Consequently, electronic stopping does not exhibit true ε-scaling and can consequently not be described by a universal curve.

2.2 Range Distribution of Implanted Ions

The deceleration of a projectile in an amorphous solid is a statistical process. The range, R, of the projectile is related

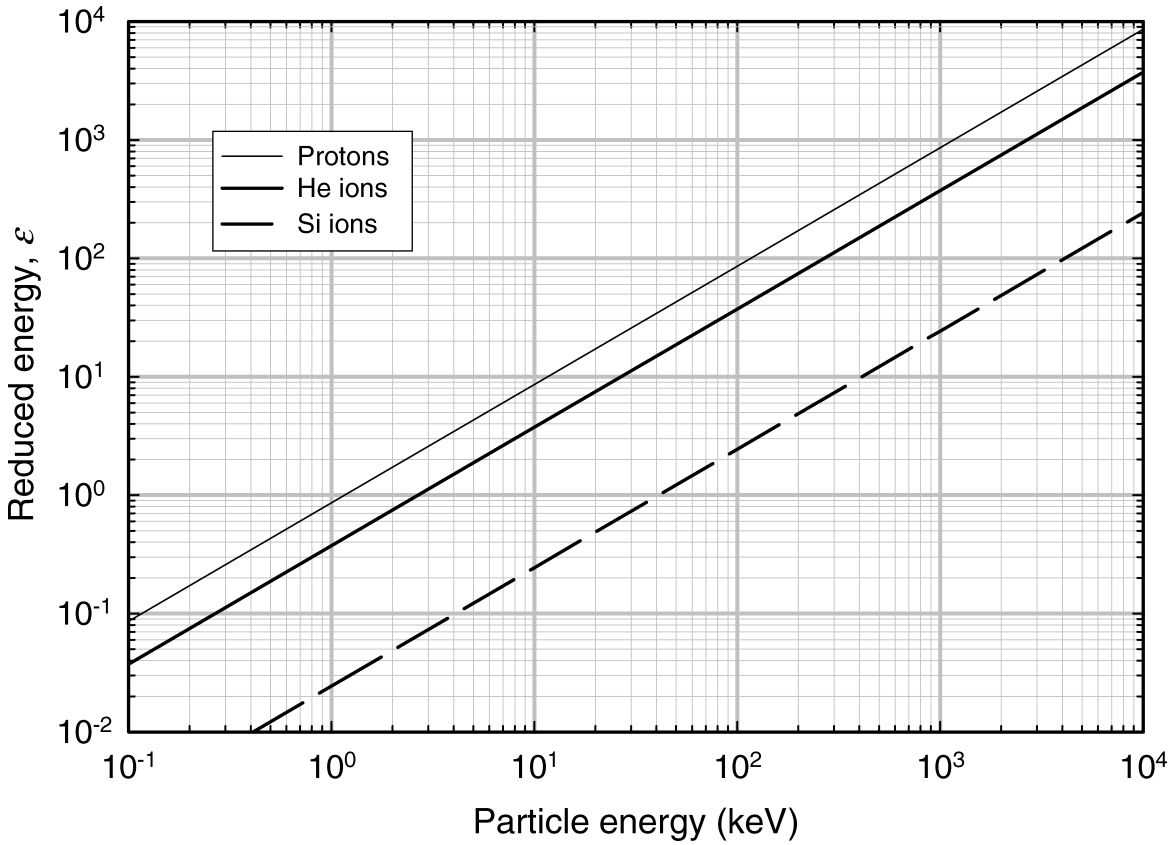

FIG. 2. Reduced energy, ε, as function of energy (in keV) of protons, He-ions and Si-ions implanted into Si.

to its mean track length before coming to rest, whereas the projected range R_p gives the mean penetration depth of the projectile relative to the surface and is the parameter of practical significance. The range, R, of a bombarding ion with initial energy, ε_i, is given by:

$$R = \int_{\varepsilon_i}^{0} \frac{1}{(d\varepsilon/d\rho)_{\text{total}}} d\varepsilon, \qquad [5]$$

where

$$(d\varepsilon/d\rho)_{\text{total}} = (d\varepsilon/d\rho)_n + (d\varepsilon/d\rho)_e. \qquad [6]$$

For $M_1 \geq M_2$, the projected range, R_p, is obtained by multiplying the range, R, with the projection factor, approximately equal to $(1 + M_2/3M_1)^{-1}$.[17] At this point it is important to point out that in the case of a crystalline target, the deviations in predicted and measured projected ranges can be significantly different when channeling effects occur.[19]

A more exact knowledge about the depth distribution calls for an evaluation of the range straggling. If the spatial distribution of implanted ions is approximately gaussian, then the straggle can be described by the standard deviation ΔR. According to the Lindhard–Scharff–Schiott (LSS) theory,[20] the total straggling per ion path length, that is $\Delta R/R$, for $\varepsilon < 3$ approaches a constant value of:

$$\frac{\Delta R}{R} = 0.35 \frac{2(M_1 M_2)^{1/2}}{M_1 + M_2} \qquad [7]$$

As electronic stopping increases at higher energies, the relative straggling becomes smaller. The relative straggling in projected range, $\Delta R_p/R_p$, is almost identical to $\Delta R/R$ because the path length correction terms for the numerator and denominator are virtually identical.

Simulations of implantation profiles and ranges can be computed using Monte Carlo–based techniques, for example, the TRIM (TRansport of Ions in Matter) code of Biersack and Haggmark.[16] For example, Figure 3 depicts the distribution profiles of 1 MeV protons and the vacancies that they create as a function of distance into Si, calculated using TRIM. In order to obtain the number of vacancies or H distribution, the value of the curves at a given depth in Figure 3 should simply be multiplied with the H-dose. Figure 4 depicts the range and straggle of protons in Si as a function of projectile energy as determined from TRIM.

An extensive review of computer simulations of ion–solid interactions can be found in Ref. 21. Although being widely employed, these codes should be used with caution, especially in crystalline substrates, as they generally do not take channeling into account and do not make provisions, for possible

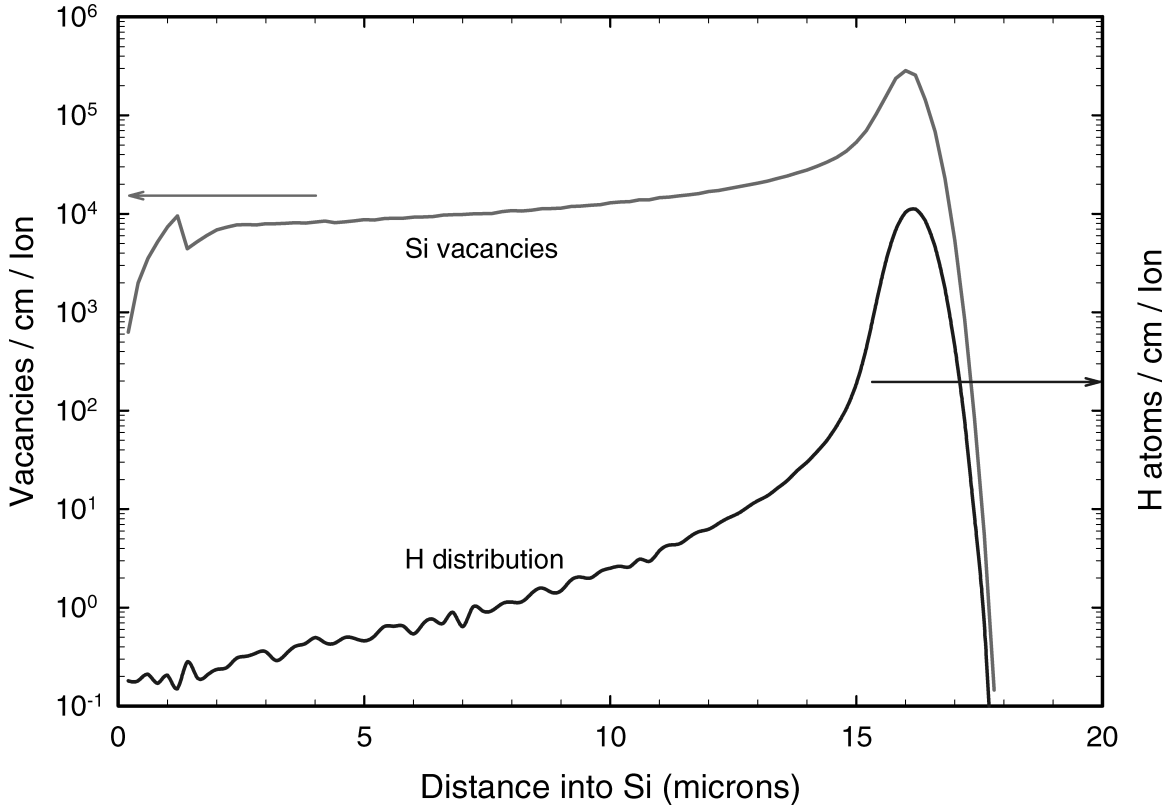

FIG. 3. Distribution of H and Si vacancies for 1 MeV H-implantation into Si, calculated using TRIM.[16]

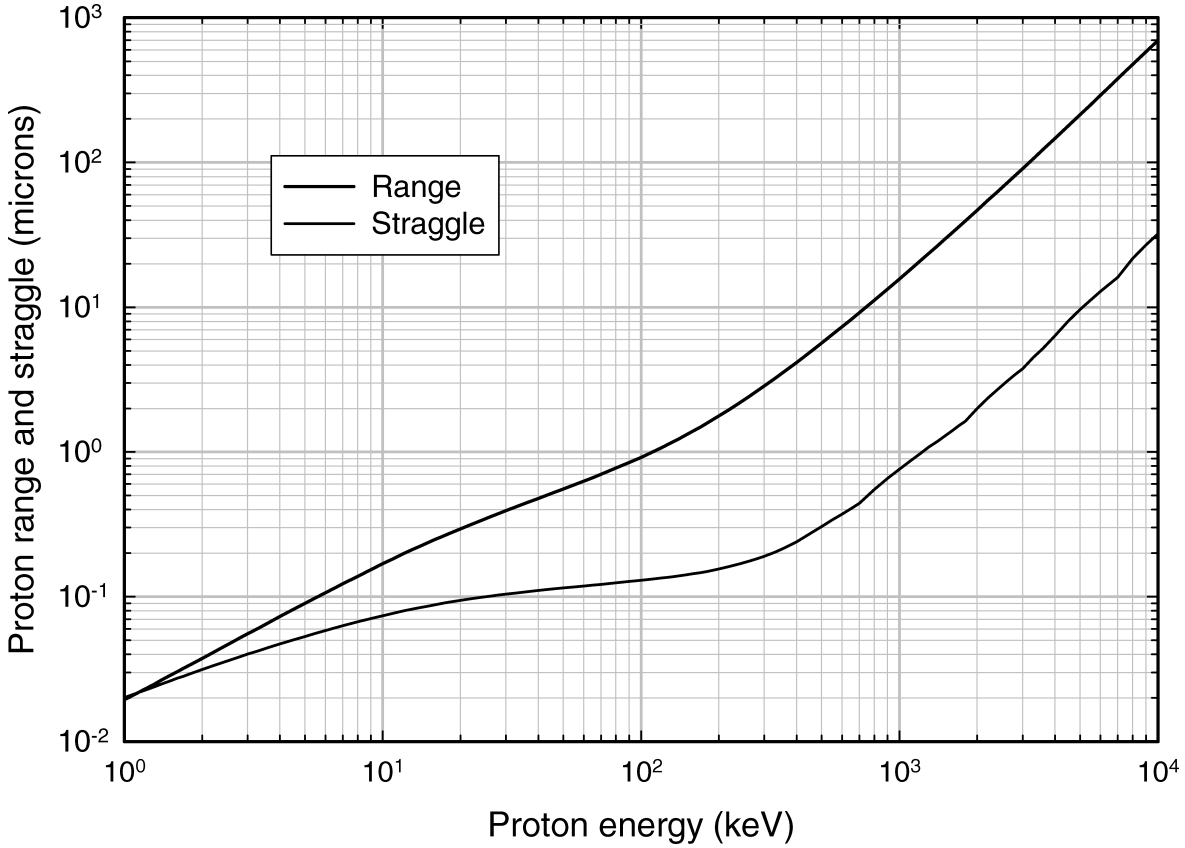

FIG. 4. Range and straggle of protons and He-ions in Si as function of energy, calculated using TRIM.[16]

diffusion effects during and after the implantation. Another important point worth noting is that the generic versions of most computer codes do not account for dynamic annealing of Frenkel pairs (*i.e.*, annihilation of vacancies and interstitials), and, therefore, overestimate the total number of vacancies and interstitials produced by implantation. One of the exceptions to this is the Marlowe code,[22–24] which does take into account the crystallinity of the material, including channeling effects, and offers the possibility to correct for the annihilation of Frenkel pairs.

2.3 Distribution of Radiation Damage

Radiation damage will be created in crystalline materials as long as the energy that the projectile can transfer, E, exceeds the displacement energy, E_d, of the lattice atoms. Atomic replacements and interstitials can occur for $E_d < E < 2E_d$, whereas vacancies and interstitials are formed for $E > 2E_d$. In the case of electron irradiation, only E_d is required to form a vacancy and an interstitial because, after having knocked an atom off its lattice site, the electron is mobile and rapidly diffuses away, leaving behind the Frenkel pair. This is not necessarily the case for protons and heavier atoms.

The energy transferred in an elastic collision depends on the masses of the particles involved and the impact parameter. In the non-relativistic limit the maximum energy, T_{max}, transferred in a head-on collision, is given by:

$$T_{max} = \frac{4M_1M_2}{(M_1+M_2)^2}E, \qquad [8a]$$

where E is the energy of the bombarding particle with mass M_1. In the case of electron irradiation, the relativistic expression:

$$T_{max} = \left(\frac{2M_1}{M_2}\right)\left(\frac{E}{M_1c^2}\right)(E+2M_1c^2) \qquad [8b]$$

must be used, which can be expressed to a convenient approximation as:

$$T_{max} = \frac{2148}{Z}E^2, \qquad [8c]$$

where Z is the atomic number of the target atom, E is in MeV and T_{max} in eV. From Eq. 8c it follows that the minimum electron energy required to displace a silicon ion with a typical displacement energy of 15 eV is about 313 keV.

If the energy of an atom that is knocked out of its lattice site is large enough, this atom may in turn displace other atoms, and if this process continues, a cascade of atomic displacements is

created. This results in a distribution of vacancies, interstitial atoms, and higher order defects in the region surrounding the ion track. The extent of these collision cascades is governed by nuclear and electronic energy-loss processes. However, only the nuclear component, ν, contributes to the production of energetic recoil atoms. For $\varepsilon < 1$ (linear cascade regime for sputtering), a constant fraction of approximately 80% of the total energy ($\nu/\varepsilon \approx 0.8$) is consumed in recoil processes, whereas the ratio ν/ε decreases rapidly when $\varepsilon > 1$.

3. DEFECT CHARACTERIZATION BY DEEP LEVEL TRANSIENT SPECTROSCOPY

Impurities or structural disorder can be intentionally or unintentionally introduced in the crystal lattice, resulting in what is commonly termed "defects." These defects introduce electronic states in the band gap that lie deeper in the band than dopant levels, and these states are commonly referred to as "deep levels." Deep level defects are present in all semiconductors in concentrations that depend on the semiconductor type and the method by which it is grown and processed, and these deep levels affect the electronic properties of semiconductors, among others. Sometimes deep level defects are intentionally introduced in order to modify a specific materials property. For example, radiation-induced defects have been effective in reducing the lifetime of carriers in Si,[5,6,25] thereby enhancing the switching time of high frequency oscillators fabricated on it. The challenge in the area of radiation-induced materials modification lies in innovative defect engineering through which the deleterious effects of defects can be avoided, and their beneficial effects harnessed to tailor the properties of materials and devices for specific applications. Clearly, this requires an intimate knowledge of the properties and behavior of defects.

Deep level transient spectroscopy (DLTS) has become a widely used technique to determine the electronic properties of defects in semiconductors. It yields the position of the energy level of a defect in the band gap, the capture cross section of this level for electrons and holes, as well as the concentration of the defect. Defects in concentrations of as low as 10^{10} cm^{-3} can be detected. When using DLTS in a capacitance mode, it facilitates a distinction between majority and minority carrier defects—a unique feature that distinguishes it from other junction spectroscopic techniques. DLTS has been used to study growth- and process-induced point and extended defects, as well as numerous impurities in a variety of semiconductors. In the next few sections, the most important aspects of deep level defects and DLTS, used for the determination of the electronic properties of these defects, are reviewed.

3.1 Carrier Capture and Emission Characteristics of Deep Level Defects

Defects with deep states in the band gap are often referred to as traps, recombination centers, generation centers, or deep level defects. In a neutral semiconductor an electron trap can be defined as a defect for which the electron capture rate, c_n, is much larger than the hole capture rate, c_p. In contrast, a recombination center is one for which c_n and c_p are about the same. The capture cross section, σ_n, for electron capture is related to the electron capture rate, c_n, by:[9,26]

$$c_n = \sigma_n < v_n > n \qquad [9]$$

where n is the electron concentration and $\langle v_n \rangle$ its average thermal velocity. An analogous expression holds for c_p in terms of σ_p. Traps are further categorized as majority or minority carrier traps. In $n(p)$–type material an electron (hole) trap is a majority carrier trap although it will be a minority carrier trap in $p(n)$–type material.

The thermal emission rate, e_n, of carriers from traps is proportional to a Boltzmann factor, $\exp(-E_T/kT)$, and for traps emitting electrons to the conduction band, e_n can be expressed as:[26]

$$e_n = \frac{\sigma_n \langle v_n \rangle N_C}{g} \exp\left[-\frac{E_T}{kT}\right] \qquad [10]$$

Here E_T is the energy of the defect level below the conduction band minimum, N_C is the effective density of states in the conduction band, g is the degeneracy of the defect level and T is the absolute temperature. An analogous expression holds for hole emission to the valence band. The quantity $\langle v_n \rangle N_C$ varies as T^2, and therefore, if e_n is measured as function of temperature, an Arrhenius plot of e_n/T^2 vs. $1/T$ will yield E_T (slope of Arrhenius plot) and σ_n (intercept at $T^{-1} = 0$). In fact, the capture cross section thus calculated is an *apparent* capture cross section because, in general, the electron and hole capture cross sections are temperature dependent.[26] This may, among other reasons, be the result of carrier capture and multiphonon emission due to lattice relaxation,[27,28] in which case the capture cross section, σ, has the form

$$\sigma = \sigma_\infty \exp\left[-\frac{\Delta E_\sigma}{kT}\right] \qquad [11]$$

where ΔE_σ is the thermal activation energy of the capture cross section, sometimes referred to as the capture barrier. Thus, a more general expression for the thermal emission rate of electrons to the conduction band is:

$$e_n = \frac{\sigma_n \langle v_n \rangle N_C}{g} \exp\left[-\frac{(E_T + \Delta E_\sigma)}{kT}\right] \qquad [12]$$

The thermal activation energy for emission of an electron to the conduction band, $\Delta E_a = E_T + \Delta E_\sigma$, determined from an Arrhenius plot, therefore, has two components: (1) the energy difference between the trap level and the bottom of the conduction band, E_T, and (2) the thermal activation energy of the capture cross section, ΔE_σ, as illustrated in Figure 5 (where ΔE is the same as E_T).

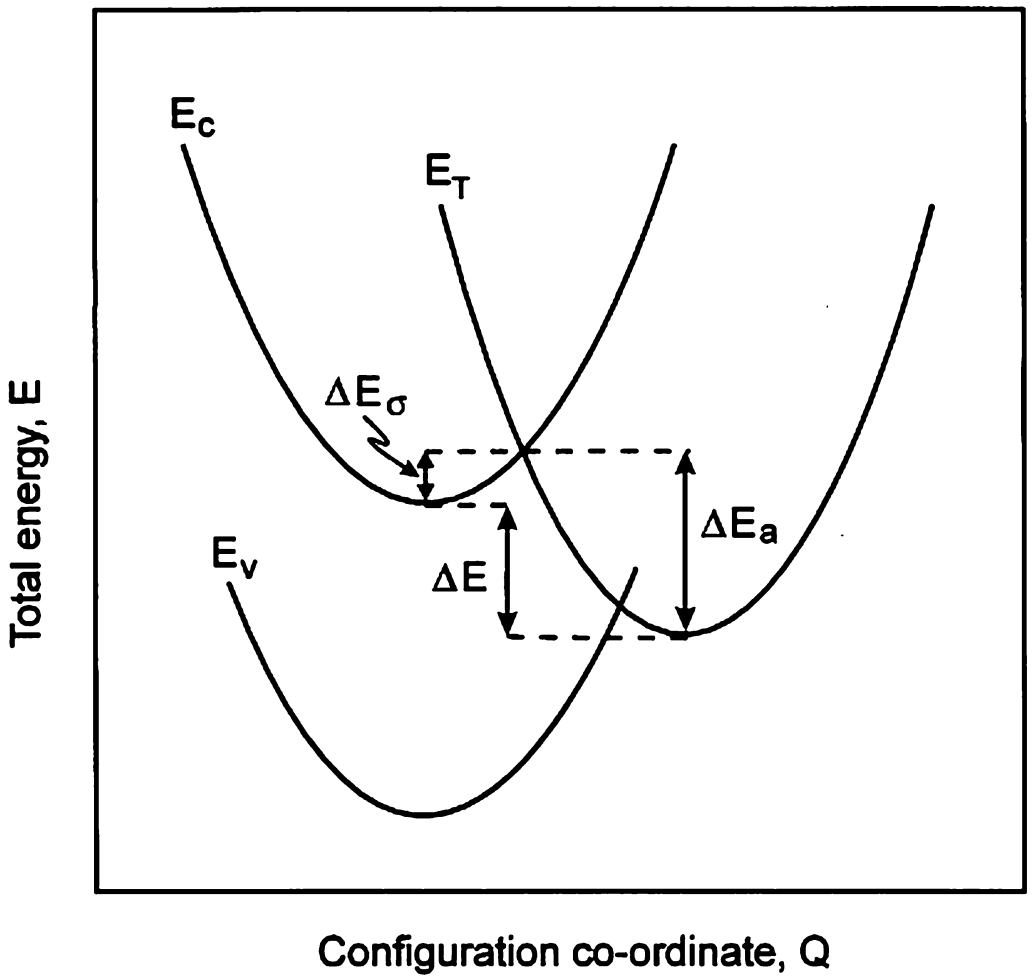

FIG. 5. Configuration co-ordinate (CC) diagram depicting the energy level of the defect below the conduction band, $\Delta E(=E_T)$, the thermal activation energy of the capture cross section, ΔE_σ, and the total energy an electron requires to escape from the trap level to the conduction band, ΔE_a.

The activation energy for thermal emission is the most commonly used parameter to characterize a deep level. However, the physical parameter E_T in Eqs. 10 and 12 is the Gibbs free energy:

$$E_T = \Delta H - T\Delta S \qquad [13]$$

where ΔH and ΔS are the changes in enthalpy and entropy due to the change in charge state of the level. When combining Eqs. 10 and 13, it follows that

$$e_n = \frac{\sigma_n \langle v_n \rangle N_C}{g} \exp\left[\frac{\Delta S}{k}\right] \exp\left[-\frac{\Delta H}{kT}\right] \qquad [14]$$

Therefore, the slope of an Arrhenius plot yields the enthalpy of the deep level, not the free energy, which can only be determined from optical measurements.[26,29,30]

3.2 Deep Level Transient Spectroscopy (DLTS)

In this section the concepts required for DLTS measurements and the interpretation of the results will be briefly reviewed.

With DLTS, defects in semiconductors are analyzed by probing the space-charge layer, also referred to as the depletion region, which exists in a p–n junction, Schottky barrier diode (SBD) or metal-oxide (or insulator)-silicon (MO(I)S) structure.[26,31] The width, w, of the depletion region of a SBD or p^+–n junction varies with the applied voltage according to:

$$w = \sqrt{\frac{2\varepsilon(V_{bi} + V)}{qN}} \qquad [15]$$

Here ε is the dielectric constant of the depleted semiconductor, V_{bi} is the built-in voltage of the junction, V is the externally applied voltage, q is the charge on the electron, and N is the density of the ionized impurities due to dopants and other

defects with levels in the band gap. The junction capacitance due to the depletion layer is:

$$C = \frac{\varepsilon A}{w} = A\sqrt{\frac{q\varepsilon N}{2(V_{bi} + V)}} \quad [16]$$

where A is the area of the junction. It is clear from Eqs. 15 and 16 that if the concentration of electrons or holes trapped at deep levels is changed (*e.g.*, by the thermally or optically stimulated emission of carriers to the conduction or valance bands), this change can be monitored by measuring the variation in the junction capacitance.[32,33] The variation in junction capacitance at constant applied voltage as a result of the temperature dependent variation of N forms the basis of capacitance-based DLTS.

The capture and emission of carriers are shown schematically in Figure 6 for a SBD on a semiconductor containing electron traps. In equilibrium, when the defect level is below the Fermi level, it is usually assumed filled with electrons, while it is likewise assumed to be empty when above the Fermi level. This is, of course, not exact because of the statistical nature of the Fermi distribution function. Under a steady-state reverse bias voltage (Figure 6a), the traps in the depletion region, above the Fermi level, are therefore empty. Reducing the applied voltage to $V - V_p$, (fix Figure 6b), reduces the width of the depletion region and allows electrons to be trapped at the deep levels. Electron capture into an initially empty trap is given by

$$N(t) = N_T[1 - \exp(-c_n t)] \quad [17]$$

where N_T is the trap density and c_n is the capture rate as defined in Eq. 9. When the voltage is restored to its original steady-state value, V, the filled traps lie within the depletion region, as shown in Figure 6c. The thermal emission of trapped electrons to the conduction band, where they are instantaneously swept away by the junction electric field, is observed as a majority carrier capacitance transient.

Experimentally, the electron emission rate can be determined from the time dependence of the capacitance transient. The density of occupied traps at time t after removing the filling pulse is

$$N(t) = N_T \exp(-e_n t) \quad [18]$$

where e_n is the thermal emission rate and N_T is the trap concentration, assuming that all the traps are initially occupied. From Eqs. 10 and 18 it can be shown that the change in trap population gives rise to a corresponding change in diode capacitance, which is time dependent, and if $N_T \ll N_D$, can be expressed as:

$$C(t) = C_o - \Delta C_o \exp(-e_n t) \quad [19]$$

Here C_o is the equilibrium reverse bias (V) capacitance and ΔC_o the change in capacitance directly after removal of the filling pulse.

The procedure for determining the energy level, E_T, and capture cross section, σ_n, of a defect is to extract e_n from the transient, $C(t)$, in Eq. 19 at several temperatures and then use

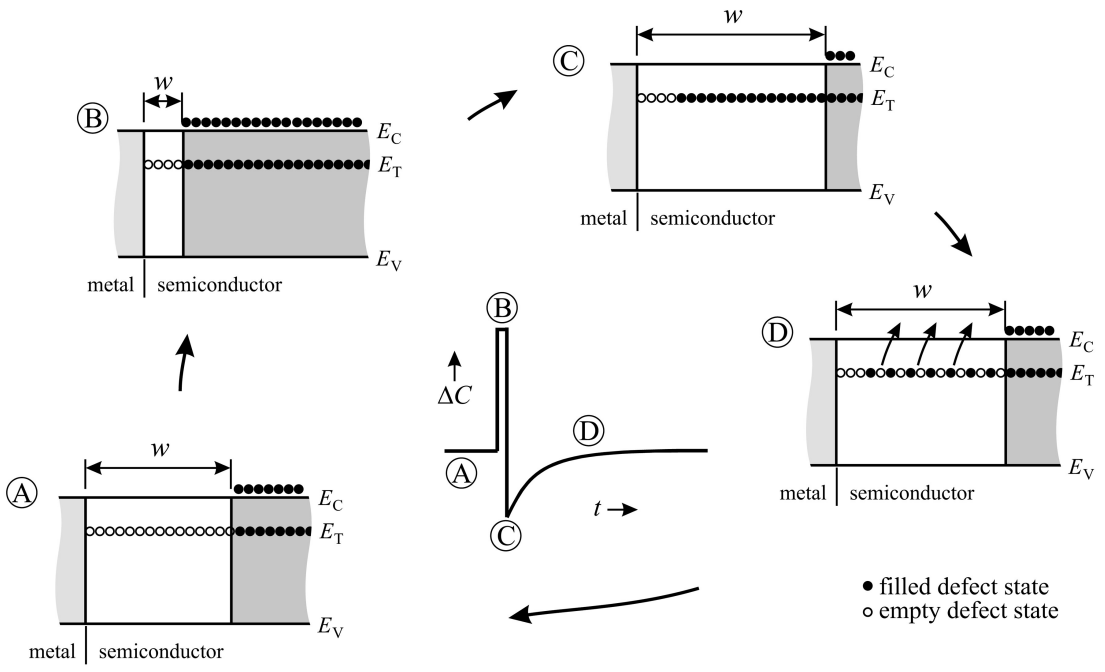

FIG. 6. Variation of depletion region width and trap population of an electron trap in n-type semiconductor for a DLTS bias and filling pulse cycle. (A) and (B) are during reverse bias and the filling pulse, respectively, whereas (C) and (D) are directly, and at a time t, after removing the filling pulse. The resultant capacitance transient is qualitatively shown in the center of the figure.

Eq. 10 to obtain E_T and σ_n, the combination of which is commonly referred to as the defect's "signature." The key step in this process is to obtain e_n from the transient for which several analogue and digital methods exist. Most of the early DLTS experiments were performed using boxcar averagers[9,10] or lock-in amplifiers[26] to analyze the transient resulting from the application of a repetitive bias/pulse sequence. For both these methods, DLTS proceeds by scanning the sample temperature and feeding the repetitive thermal emission transient, which varies with temperature, into the analyzer (boxcar or lock-in amplifier). A DLTS spectrum is obtained by plotting the output signal of the analyzer versus temperature. The resulting signal is a maximum when the thermal emission rate matches the "rate window" of the analyzer. Each peak on the DLTS spectrum is indicative of an energy level with a specific E_T and σ_n. The emission rate of the transient at the peak temperature is a function of the analyzer used. For example, for a lock-in amplifier with a sine wave mixing function, the emission rate is $e_n = f/0.424$ (provided that the filling pulse width is much shorter than the pulsing period), where f is the pulse frequency.[34] By varying the frequency of the lock-in amplifier (or "rate window" in the case of the boxcar analyzer), the peak temperature value shifts, and thus the emission rate can be measured as a function of temperature. From Eq. 10 it follows that an Arrhenius plot of log (e_n/T^2) versus $1/T$ yields E_T and σ_n. Note that the σ_n thus obtained, is an apparent capture cross section as discussed earlier. The real capture cross section may be temperature dependent and has to be determined by measuring the DLTS signal as a function of the filling pulse width at a specific temperature.[9,13]

As opposed to a conventional single phase lock-in amplifier (LIA), a two-phase LIA yields both the first sine and cosine Fourier components of the DLTS transient. If both these components are recorded during a DLTS scan, two peaks at different temperatures are found. For the "in-phase" signal, $e_{nI} = f/0.424$ and for the "quadrature" signal, $e_{nQ} = f/0.157$. From these two emission rates, the defect's signature can be estimated during a single temperature scan.[35] Modern digital LIAs can operate at frequencies as low as 1 mHz (as opposed to the 1–2 Hz of the older analogue LIAs), thereby significantly extending the frequency range and facilitating defect characterization over 5–6 decades of log (e_n/T^2).

An attractive alternative to these traditionally used techniques is to digitize the full transient, which is readily achieved using modern electronics and instrumentation. Digital methods digitize the analogue or digital transient output of the capacitance meter, typically with a sample held at a fixed temperature and average many digitized transients to reduce the noise level. This approach forms the basis of isothermal DLTS measurements.[36,37] All of the accessible decay time constants can then be numerically extracted from the acquired wave-form. The problem of what algorithm to use for this purpose is difficult and several detailed considerations of this problem have been presented. Among others, Ikossi-Anastasiou *et al.*[38] used a "method of moments" approach, whereas Nolte and Haller[39] used an approximation to the inverse Laplace transform. Nolte and Haller also discussed the theoretical limit of time constant separation in the presence of noise. Eiche *et al.*[40] used the "Tikhonov regularization" method to separate the constituent exponentials in a photo-induced current transient spectroscopy (PICTS) signal. Thereafter, a simple scheme using a binomial expansion of the boxcar weighting function was reported by Thurzo *et al.*[41] During this scheme a temperature scanning measurement was combined with a simple digital signal processing method to obtain sharper peaks, however, at the expense of considerably more noise.

A common approach to the description of non-exponentiality observed in DLTS transients is to assume that they are the superposition of exponential emission rates:

$$f(t) = \int_0^x F(s)\, e^{-st} ds \qquad [20]$$

where $f(t)$ is the recorded transient and $F(s)$ is the spectral density function. A mathematical representation of the transients given by Eq. 20 is the Laplace transform of the true spectral function $F(s)$. In this case, to find the real spectrum of the emission rates present in the transient, it is necessary to perform an inverse Laplace transform for $f(t)$ using some mathematical method. In the case of multi- or mono-exponential transients the result of such a procedure is a spectrum of delta-like peaks. Despite the fact that the problem as defined here is very general, it should be remembered that Eq. 20 does not have a general solution for any given function $f(t)$. For an analytical multi-exponential function such a solution exists and, according to Lerch's theorem,[42] it is unique. However, if noise is superimposed on this function, the number of possible solutions can be infinite. Consequently, the problem is to find the best estimate for $F(s)$ and, according to the prior knowledge about the system being investigated and its boundary conditions, to exclude unphysical solutions and to choose only the simplest one, that is, the one that reveals the least amount of detail or information that was not already known or expected.[12]

Laplace-DLTS–based methods, applied to simple point defects as well as complex problems, have led to an extensive quantitative improvement in the DLTS measurement resolution. In Figure 7 a comparison between a conventional DLTS (inset) and Laplace DLTS (full figure) of the G4 center in Si is depicted. The most important observation from this and other similar studies is that whereas the standard DLTS (Figure 7, inset) gave featureless peaks, the Laplace DLTS spectra revealed a fine structure in the thermal emission process.[43]

The evolution of the Laplace DLTS technique over the last few years has facilitated achieving the theoretical limit of the resolution of DLTS. For relatively shallow states that emit at low temperatures, the reduction in line-width is remarkable and can result in more than two orders of magnitude increase in resolution over the original DLTS technique of Lang.[43]

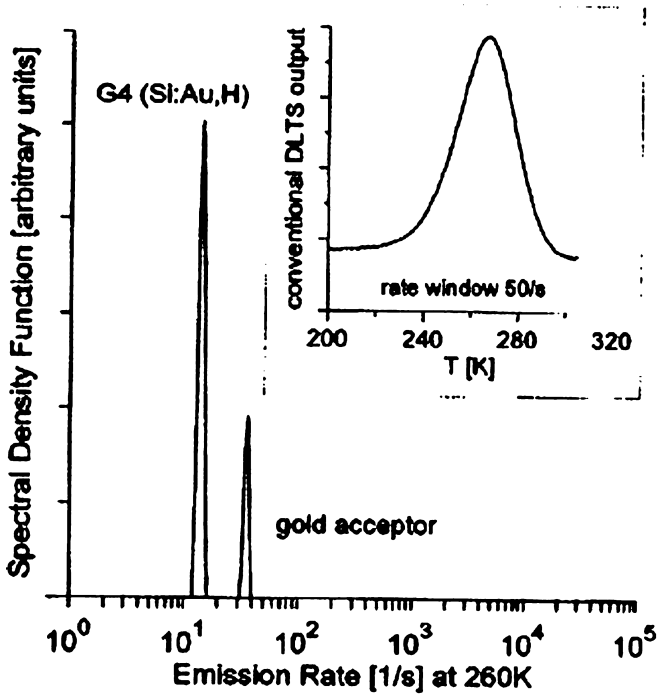

FIG. 7. DLTS and LDLTS spectra of hydrogenated silicon containing gold. The conventional DLTS spectrum is shown as an inset at the top right of the figure. The broad peak centered at 260 K is attributed to electron emission from the gold acceptor $G4$. The main spectrum was obtained by the Laplace technique and clearly separates the gold-acceptor level and the gold-hydrogen level $G4$ (redrawn from Ref. 43).

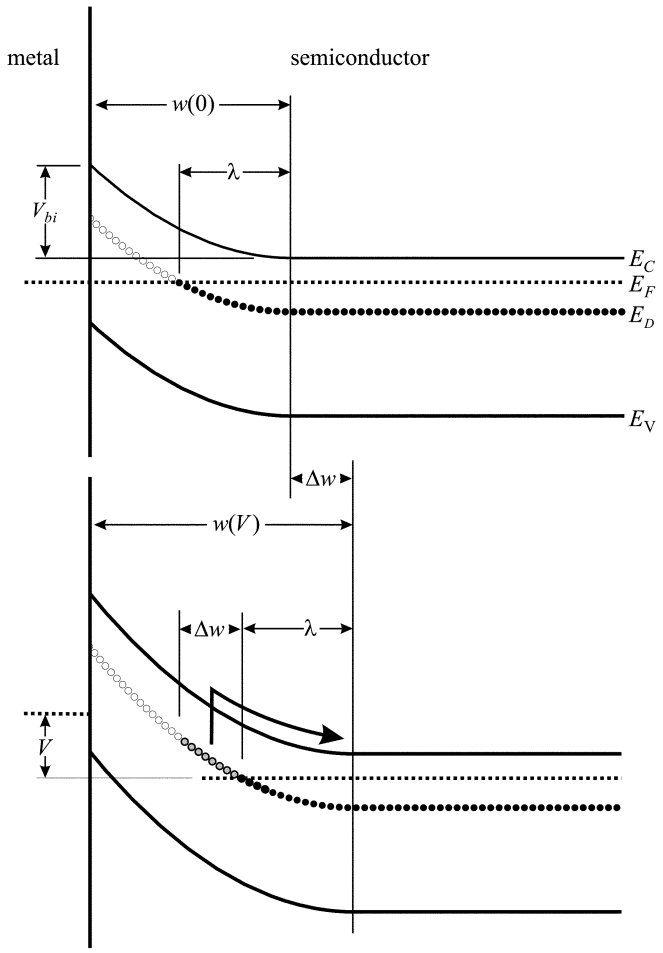

FIG. 8. Depletion region of a Schottky barrier diode with built-in voltage V_{bi}, on n-GaAs under zero bias and reverse bias, V. The widths of the depletion layer (w) and transition region (λ) are defined in Eqs. 17 and 23, respectively.

In order to obtain the defect concentration, N_T, the total signal due to a majority carrier pulse of amplitude V_p, superimposed onto the reverse bias, V, and duration long enough to fill all traps below the Fermi level, has to be determined by double integration of the Poisson equation.[44] The limits of this integration are determined by the location in the space-charge layer where emission takes place, that is from $w(V)-\lambda$ to $w(0)$ $-\lambda$ (Figure 8, for pulsing to 0 Volt), where λ is the width of the transition region:

$$\lambda = \sqrt{\frac{2\varepsilon(E_F - E_T)}{q^2 N}} \qquad [21]$$

For a constant free carrier density, N_T can be related to the magnitude of the total signal, $\Delta C/C$, thus found by:[44]

$$N_T(x_m - \lambda) = 2N(x)\left(\frac{\Delta C}{C}\right)_{t=0} \times \left[\left(\frac{x-\lambda}{x}\right)^2 - \left(\frac{x_p-\lambda}{x}\right)^2\right]^{-1} \qquad [22]$$

where x and x_p are the depletion widths during application of the reverse and filling pulses, respectively, and $x_m - \lambda$ is the mean distance from the interface to the region from which traps emit carriers. In a noise-free environment, $\Delta C/C$ values of 10^{-5}–10^{-6} can readily be achieved, implying that defect concentrations of as low as 10^{10} cm^{-3} can be detected. Using Eq. 22, the deep level concentration profile can be measured through the variation of the depletion width with applied bias, if the shallow level concentration profile is known. Trap concentration profiles can be measured either by filling defects to a constant filling voltage level and varying the reverse bias voltage, or by using a constant reverse bias and varying the filling pulse amplitude.[31]

Finally, an important issue is the influence of an electric field on the emission of carriers from traps in the depletion region. The average electric field of typically 10^5 V m^{-1}–10^7 V m^{-1}

in the depletion layer (depending on the doping level and applied bias) can influence the shape of defect potentials and may, therefore, enhance charge emission from potential wells, by for example the Poole–Frenkel effect[45] or phonon-assisted tunneling.[46,47] Detecting the Poole–Frenkel effect establishes an important characteristic of a defect. It evidences the presence of donor-like electron traps in an *n*-type semiconductor or acceptor-like hole traps in a *p*-type semiconductor, that is, states that are neutral when occupied and charged when empty. It has, for example, been shown that oxygen-related thermal donors in Si exhibit Poole–Frenkel enhanced emission.[11] On the other hand, ignoring the effect of the electric field can lead to erroneous defect level energies and capture cross sections, and consequently incorrect defect identification. Ideally, any comparison of defect properties should be done under equal electric field conditions in a narrow spatial region to limit the electric field variation. This is the essence of the double DLTS (DDLTS) measurement technique.[48]

For a complete electrical characterization of a defect, its majority as well as minority carrier capture cross sections must be determined. Minority carrier capture in SBDs is usually achieved either optically, by illuminating semi-transparent Schottky contacts with above band gap light, or electrically, by applying a large forward bias to the SBD. For *p–n* diodes, minority carrier injection occurs when the filling voltage pulse causes the diode to be forward biased. After minority carrier injection, the occupation of the traps in the depletion region is the net result of the capture of both types of carriers. Note that the sign of the resulting capacitance transient is negative for the emission of majority carriers (Figure 6), and positive for minority carriers because their charge has the opposite sign,[26] making it easy to distinguish between the type of carriers being emitted.

From the knowledge of energy level, E_T, concentration, N_T, and capture cross section, σ_n and σ_p, of a defect for minority and majority carriers, it is possible to establish whether the defect will act as a trap (and thus cause carrier reduction according to Eqs. 12 and 20), or whether it will act as a recombination center. Markvart *et al.*[49] have demonstrated that a modified version of DLTS, referred to as recombination DLTS, can be used to identify defects that act as recombination centers. These centers act as "stepping stones" for carriers and contribute to the current-voltage characteristics of rectifying junctions at a recombination rate, U:[50,51]

$$U = \frac{\sigma_p \sigma_n \upsilon_{th}\left(pn - n_i^2\right) N_T}{\sigma_n[n - n_i \exp\{(E_T - E_i)/kT\}] + \sigma_p[n + n_i \exp\{-(E_T - E_i)/kT\}]} \quad [23]$$

where E_i and n_i are the intrinsic Fermi level and intrinsic carrier density, respectively, and the other symbols have previously been defined. Clearly, the most efficient recombination centers are those with levels close to the middle of the band gap, and with approximately equal capture cross section for electrons and holes.

3.3 Summary

The recent introduction of Laplace DLTS has rendered DLTS a true spectroscopic technique facilitating a distinction between discrete traps with energy separations of as little as a few meV. The spectroscopic nature of DLTS allows independent studies of different defect species in the same semiconductor. Furthermore, because DLTS is a space-charge–related technique, it facilitates control of the charge state of defects in the space-charge region that enables charge state dependent processes to be studied and metastable defect configurations to be revealed. DLTS is further attractive because it can be used to characterize defects using various kinds of space-charge–based devices. This includes simple Schottky barrier diodes (SBDs), as well as device structures with higher degrees of complexity. Finally, the sensitivity of DLTS for detecting defects in concentrations of as low as 10^{10} cm^{-3} is superior to any other electrical characterization technique.

4. RADIATION-INDUCED DEFECTS IN SI

Point defects created in crystalline Si by high-energy electrons and protons have been studied extensively by various experimental techniques, including DLTS, over the past four decades. Despite the relatively vast knowledge that exists on the electronic and annealing properties, and the physical structure of these defects, they have attracted renewed interest during the past few years due to their key role in, among others, promoting transient enhanced diffusion (TED) of dopant atoms during post-implantation annealing. TED currently stands as one of the major stumbling blocks preventing the realization of the sub-100 nm node in the Si microelectronics devices technology.[52] Furthermore, the following points are worth noting concerning recent interests for increased investigations of defect properties in Si. First, the increased availability of MeV ion implanters has allowed defects created by ions heavier than alpha-particles to be be studied. Unlike MeV electrons, which create uniform distributions of isolated point defects in the regions of interest, the heavier ions produce non-uniform defect distributions along their paths and with localized regions of high defect concentrations around their projected ranges. The types of defects created by light and heavy ions may, therefore, be quite different. Second, during various device processing steps, such as exposure to a plasma for anisotropic etching and metallization using either an electron beam or sputter deposition, the semiconductor surface is subject to low-energy (less than a few keV) particles. These defects, created in the near-surface region ($\lesssim 0.1\ \mu$m)

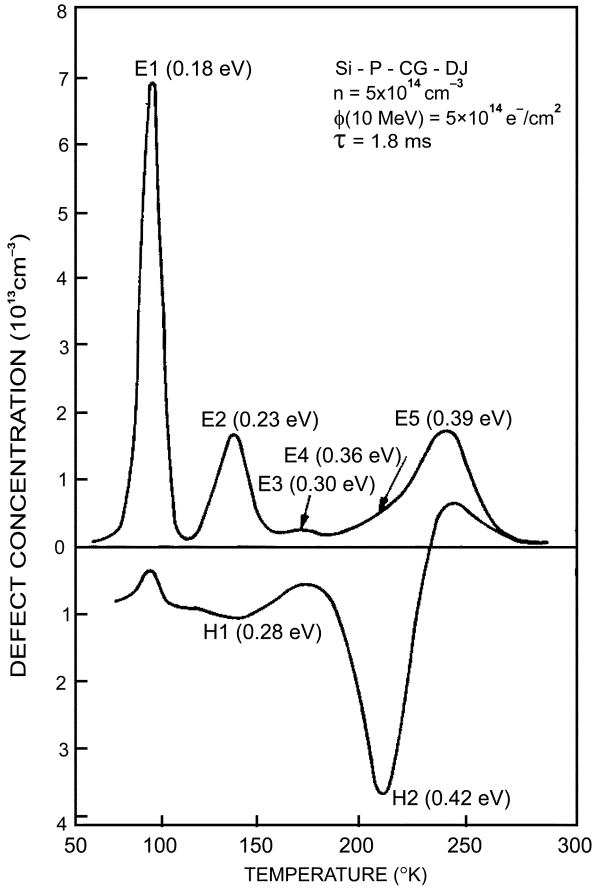

FIG. 9. Typical DLTS spectra observed following electron irradiation of silicon at 300 K. (a) Phosphorus-doped crucible grown Si; (b) boron-doped, crucible grown Si; (c) aluminum-doped float zoned Si [26].

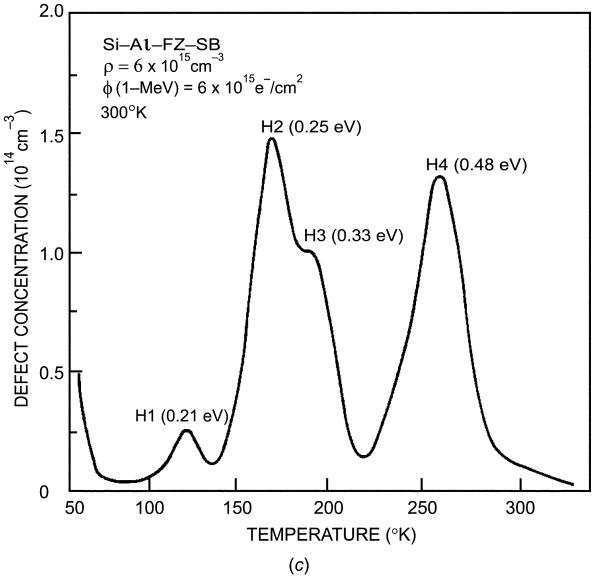

FIG. 9. Continued.

of the semiconductor material and which diffuse into the bulk, may also have different properties than the point defects generated by MeV electron irradiation. In addition, hydrogen-related defects can be formed intentionally during proton irradiation of Si for minority carrier lifetime control or unintentionally in pre-irradiated Si during chemical cleaning with solutions containing HF. Thus, the study of defects is of both technological and scientific interests.

4.1 High-Energy Electron Irradiation

As an introduction, the authors note that the first DLTS results regarding the electronic properties of radiation-induced defects in a semiconductor were reported by Kimerling *et al.* after irradiating *n*- and *p*-type Si with 1–10 MeV electrons (Figures 9a–c).[26,53–57] It was demonstrated that the presence of electrically inactive impurities, such as C and O in Si, can be detected by DLTS through their interaction with radiation-induced vacancies and interstitials. For some of these defects detailed annealing studies were performed. Tentative assignments of defect structures were made based on a comparison of defect state introduction, thermal stability, and impurity dependence with earlier EPR and IR absorption identifications. The main background-impurity–related defects were found to be the V-O center (A-center), the carbon interstitial (C_i) and the C_i-C_s pair. In *n*-type Si, a dopant dependent defect, the V-P center (E-center) was detected, whereas in *p*-type Si the dopant dependent defects were found to be the V-Al, Al_i and Al_i-Al_s pair. Although the assignments of some of these levels have subsequently been shown to be incorrect, these pioneering studies proved that DLTS is a remarkably sensitive technique for defect detection.

Previous studies employing Hall-effect and minority carrier lifetime techniques were less specific and did not allow

convenient correlation between material background effects and defect electronic properties. It was pointed out, however, that a direct comparison can be made between the majority carrier compensation observed by Hall-effect and capacitance transient measurements on the same material.[58] In the following sections, the authors present a more detailed discussion regarding the identification of a number of radiation-induced defects by DLTS combined with other techniques, such as EPR.

4.1.1 Primary Radiation-Induced Defects

4.1.1.1 Silicon vacancies and interstitials. The conventional method of quenching in vacancies for analytical purposes by rapid cooling from high temperatures, successful for many materials, does not work for Si. The lattice vacancy is too mobile and consequently the material simply cannot be quenched rapidly enough to freeze in measurable concentrations of vacancies. The only successful method so far for isolated vacancy production has been radiation damage at cryogenic temperatures. Provided the energy of the incoming particle is sufficiently high, it displaces the Si atom from its regular lattice site by transferring recoil energy to it.

The primary defect creation process is the formation of a Frenkel pair (vacancy-interstitial). One of the surprising findings in the case of Si irradiated with 1–3 MeV electrons, is that the silicon interstitial (Si_i) is mobile even at 4.2 K.[59] As a result, the Frenkel pair either annihilates itself, or the Si_i escapes and is subsequently trapped by some impurity, leaving behind an isolated vacancy. In *p*-type Si, isolated vacancy (V) production was found to be a relatively efficient process, perhaps reflecting the long-range Coulomb attraction of the interstitial to dominant interstitial traps, which have been shown by EPR studies to be the group III doping atoms. In *n*-type Si the formation of isolated vacancies was shown to be very inefficient (a factor of ≈100 lower than in *p*-type Si), with Frenkel pair annihilation apparently dominating.[59] Consistent also with this simple model for defect formation is the observation in *n*-type Si that low temperature vacancy production efficiencies, comparable to that found in *p*-type material, can be achieved at higher electron bombardment energies (5, 50 MeV).[60–62] Here, the recoiling interstitial is displaced farther from the vacancy, reducing correlated vacancy-interstitial annihilation. Consistent is also the observation that low-temperature vacancy production efficiencies in *n*-type Si can be increased by counterdoping with group III atoms, thereby providing efficient traps for Si_i.

4.1.1.2 The isolated vacancy. The structure of the silicon vacancy has been well established and reviewed. A simple one-electron orbital model can account for the electronic properties observed for the isolated vacancy. The dangling bonds on the four nearest neighbours to the vacancy form a single symmetric (a_1) and triply degenerate (t_2) set of orbitals.[59,63,64] The states in the gap to which this model apply are V^{++}, V^{+}, V^{0} and V^{-}. In addition, $V^{=}$ is also believed to exist as a stable state in the gap, but being non-paramagnetic, no direct evidence of its structure has been obtained. Jahn-Teller distortions occur for V^{+}, V^{0}, and V^{-} and significantly influence their properties, as has been discussed in detail.[59] In general, the effect of increasing Jahn-Teller distortions is to lower the defect's energy level.

The energy levels of the Si vacancy are diagramatically shown in Figure 10.[63] The levels in panel (a) represent the consensus of recent theoretical estimates for the location of the neutral vacancy t_2 and a_1 orbitals with respect to the Si band edges. In panel (b) the corresponding level positions are indicated assuming a Hubbard correlation energy of $U \approx 0.3$ eV, a typical value found experimentally for deep levels in Si. In panel (c) the levels are shown after the effect of the Jahn-Teller distortions. Each level drops in the gap because with each added electron, the Jahn-Teller distortions increase. In the case of the two donor states, the effect is strong enough to produce negative-U ordering, the indicated level positions having been measured directly by EPR and correlated DLTS studies.[63] This effect was first predicted theoretically, and later experimentally confirmed. This remarkable prediction served as a noteworthy early indication of the power of the emerging theoretical techniques.

The experimental evidence in support of negative-U ordering was presented by Watkins and Troxell.[65] The kinetics for the loss of the EPR signal in the dark after photoionization in indium-doped *p*-type Si (Figure 11) has been interpreted as hole-release to the valence band

$$V^{+} \rightarrow V^{0} + h^{+}. \qquad [24]$$

This lead to an estimate for the single donor state (0/+) location as $E_V + 0.05$ eV, as indicated in Figure 10. A different hole-release process is monitored in DLTS studies,[56,66–68] as shown in Figure 11. There, a single dominant hole emission peak at $E_V + 0.13$ eV is observed in *p*-type Si irradiated by electrons at 4.2 K which, in its production and annealing kinetics, can be correlated directly with the vacancy. Emission rate kinetics, however, clearly showed (Figure 11) that the process observed by DLTS was not the same as that studied by EPR, that is, for which Eq. 24 applies. It was therefore tentatively postulated that the process observed by DLTS corresponds to emission from a second donor state, as indicated in Figure 10.[65,69–71]

A critical argument in this identification was the recognition that for negative-U ordering, hole emission from V^{++} is a two-hole emission process:[65]

$$V^{++} \rightarrow V^{+} + h^{+} \rightarrow V^{0} + 2h^{+}. \qquad [25]$$

The limiting process is the first one. At temperatures where this is being observed as thermally activated emission, the second hole-release will follow immediately because it has the shallower energy level. Therefore a single DLTS peak will be observed associated with the first hole level position, but its amplitude will be twice its normal size. The evidence for this was provided by Watkins *et al.* who studied floating zone Si doped to 10^{18} cm^{-3} with Sn and irradiated with 1.5 MeV electrons

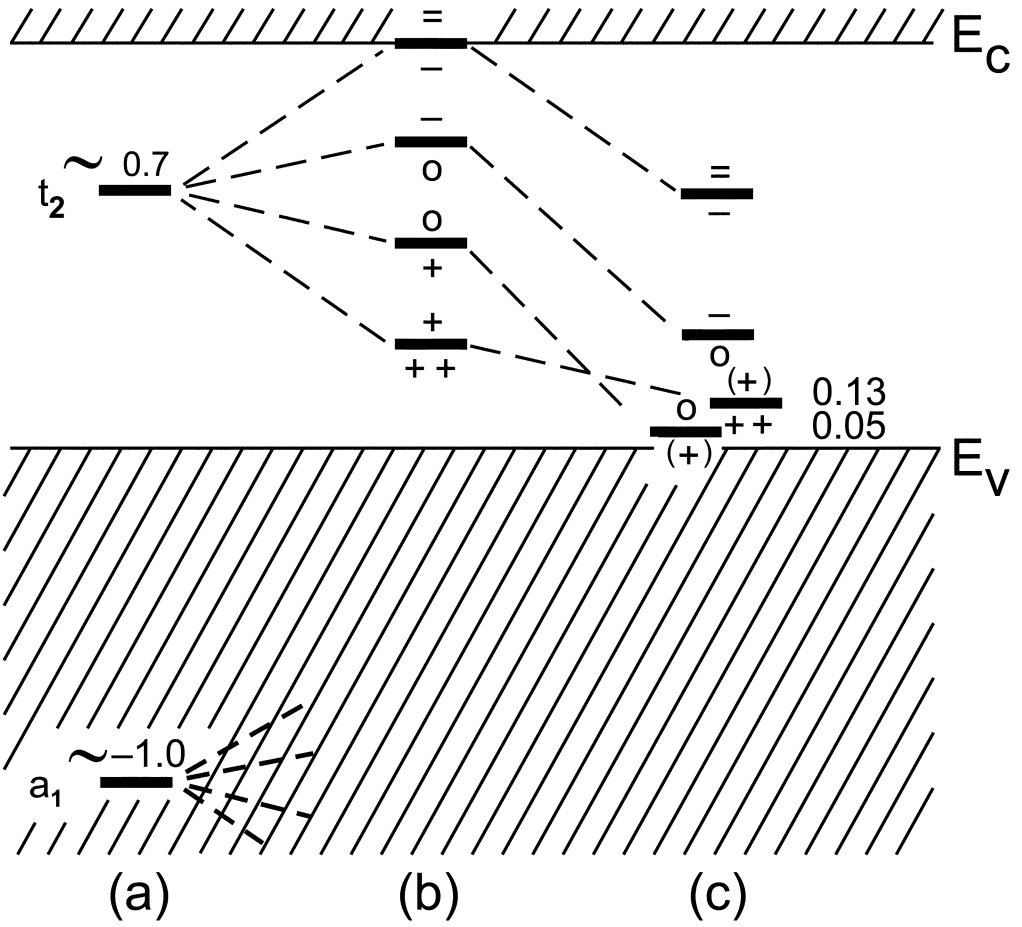

FIG. 10. Electrical level positions for the Si vacancy: (a) calculated single particle energies for relaxed V^0; (b) Corresponding estimates for the level positions; (c) Experimental results after Jahn-Teller relaxations (level positions in eV from the valence band (redrawn from Ref. 66, with permission).

at 4.2 K.[70] From previous EPR studies[72] it was known that for this specific system, almost 100% conversion of vacancies to vacancy-tin pairs occurs upon annealing as the vacancies become mobile and diffuse through the crystal. The key observation here was that the DLTS peak of the $E_V + 0.13$ eV vacancy level was twice that of the V-Sn signal (Figure 12). Because EPR studies have confirmed that the V-Sn is a "normal" defect with a one-hole emission, this was taken as evidence that the vacancy emits two holes (Eq. 25) for negative-U ordering, as predicted.

The removal kinetics of the single vacancy upon annealing has been studied using both EPR and DLTS. The results are summarized in Figure 13.[59] An activation energy of 0.18 ± 0.02 eV was measured by EPR for the migration and trapping of the $V^=$ by oxygen in low resistivity *n*-type Si. DLTS studies in the low resistivity *p*-type Si showed that the activation energy for annealing of V^{++} (zero bias annealing) was 0.32 ± 0.02 eV, which agreed remarkably well with the value (0.33 ± 0.03) eV obtained from EPR measurements. The annealing process of the vacancy in high resistivity *p*-type Si under reverse bias is also characterized by a third activation energy of (0.45 ± 0.04) eV. Correlative EPR measurements provided the evidence for the higher thermal stability of V^0, to which this higher activation energy has been assigned.

Finally, it should be noted that no acceptor-like levels, $(= /-)$ and $(-/0)$, of the vacancy could be observed by DLTS in *n*-type Si. This was interpreted as indicating that these levels must be deeper than ≈0.17 eV below the conduction band.[59,73]

For the vacancy, once mobile above 150–200 K, the dominant trapping centers are oxygen, leading to the formation of the A-center (V-O),[74] substitutional dopants such as P, Sb, and As, resulting in vacancy-dopant pairs, and other vacancies, leading to divacancy formation.[75–77] Also note that because the isolated vacancy is mobile below room temperature and migrates until trapped by impurities, DLTS studies of room temperature irradiated Si (such as in Figures 9a–c), will therefore not show any peaks of single vacancies.

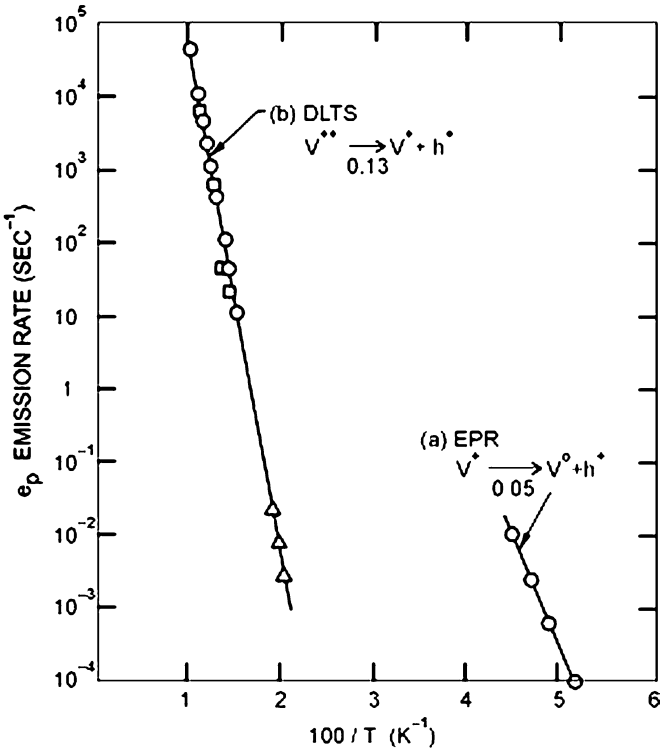

FIG. 11. Kinetics for the EPR V^+ spectrum decay after photo-generation,[74] and hole emission rate observed by DLTS[56,66–68] for the $E_V + 0.13$ eV level identified with the vacancy (redrawn from Ref. 63, with permission).

4.1.1.3 The silicon interstitial. No direct experimental information exists concerning the structure or electronic properties of the isolated silicon interstitial, Si_i. As mentioned earlier, in *p*-type Si its high mobility (even at 4.2 K) assures that all of the interstitials produced are present only as trapped by impurities. No DLTS signals can therefore be expected for the isolated Si_i in *p*-type Si. In *n*-type Si there is some indirect evidence that Si_i may be less mobile (≈150 K), with some still present, therefore, after a 4.2 K irradiation. However, no EPR spectrum has been detected that can be identified with it.[64] The only way to learn something about the interstitial is to study its interaction with impurities. From such studies, complimented by theoretical calculations, it turned out that a simple model analogous to the molecular orbital model that successfully describes the silicon lattice vacancy can be used to describe the properties of interstitial Si.[64] As will be discussed in more detail later, interstitial Si is trapped primarily by substitutional carbon (C_s), thereby forming "interstitial" carbon, C_i.[64]

4.1.2 Secondary Radiation-Induced Defects

4.1.2.1 Defects due to migration of Si vacancies. As the temperature of irradiated Si is raised to 150–200 K, the vacancies become mobile and migrate through the crystal. Here, they

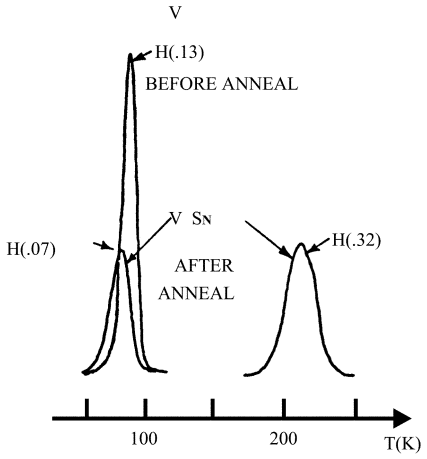

FIG. 12. Conversion of vacancies to tin-vacancy pairs as monitored by DLTS in electron irradiated *p*-type Si containing 10^{18} Sn/cm^3.[70]

recombine either with each other to form divacancies (V-V or V_2), or with other impurities in the crystal to form vacancy-impurity pairs. In what follows, the authors briefly describe the formation and properties of the divacancy and of some well-studied vacancy-donor pairs.

4.1.2.2 The divacancy. From early EPR studies it was deduced that the divacancy introduces three energy levels in the band gap, namely $E_C - 0.40$ eV,[78,79] $E_C - 0.54$ eV[78] and $E_V + 0.25$ eV.[79] However, DLTS measurements[26,56,57,80] (Figure 9) revealed that two electron traps at $E_C - 0.23$ eV (V-$V^{=/-}$) and $E_C - 0.41$ eV (V-$V^{-/0}$), and one hole trap at $E_V + 0.21$ eV (V-$V^{0/+}$) can be associated with the divacancy. This identification was based on a comparison of the annealing kinetics observed by DLTS and EPR. In lightly doped *n*-type Si, it was found that the V-V anneals at between 270°C and 340°C in a first order process for which $\nu = 1.08 \times 10^9$ s^{-1} and $E_a = 1.47$ eV.[80] From the value of ν it would appear that the diacancy anneals by diffusing through the crystal until trapped by a sink where its structure changes. It was established by EPR measurements that the divacancy anneals faster in Cz than in FZ Si, a clear indication that oxygen acts as a trap for the diffusing divacancy. It was subsequently shown that the divacancy anneals in two stages with quite different annealing parameters.[81]

It is worth pointing out that there is some controversy regarding the relationship between the concentrations and nature of the two charge states in ion-implanted and electron-irradiated material.[82,83] However, the evidence from Laplace DLTS measurements suggests that in ion-implanted Si there are other states with similar emission and capture properties to V-$V^{-/0}$, thus the confusion over the apparent concentrations. In electron-irradiated Si the divacancy in the diamagnetic doubly negative charge state has a static trigonal symmetry with inward breathing mode lattice relaxation. However, it exhibits

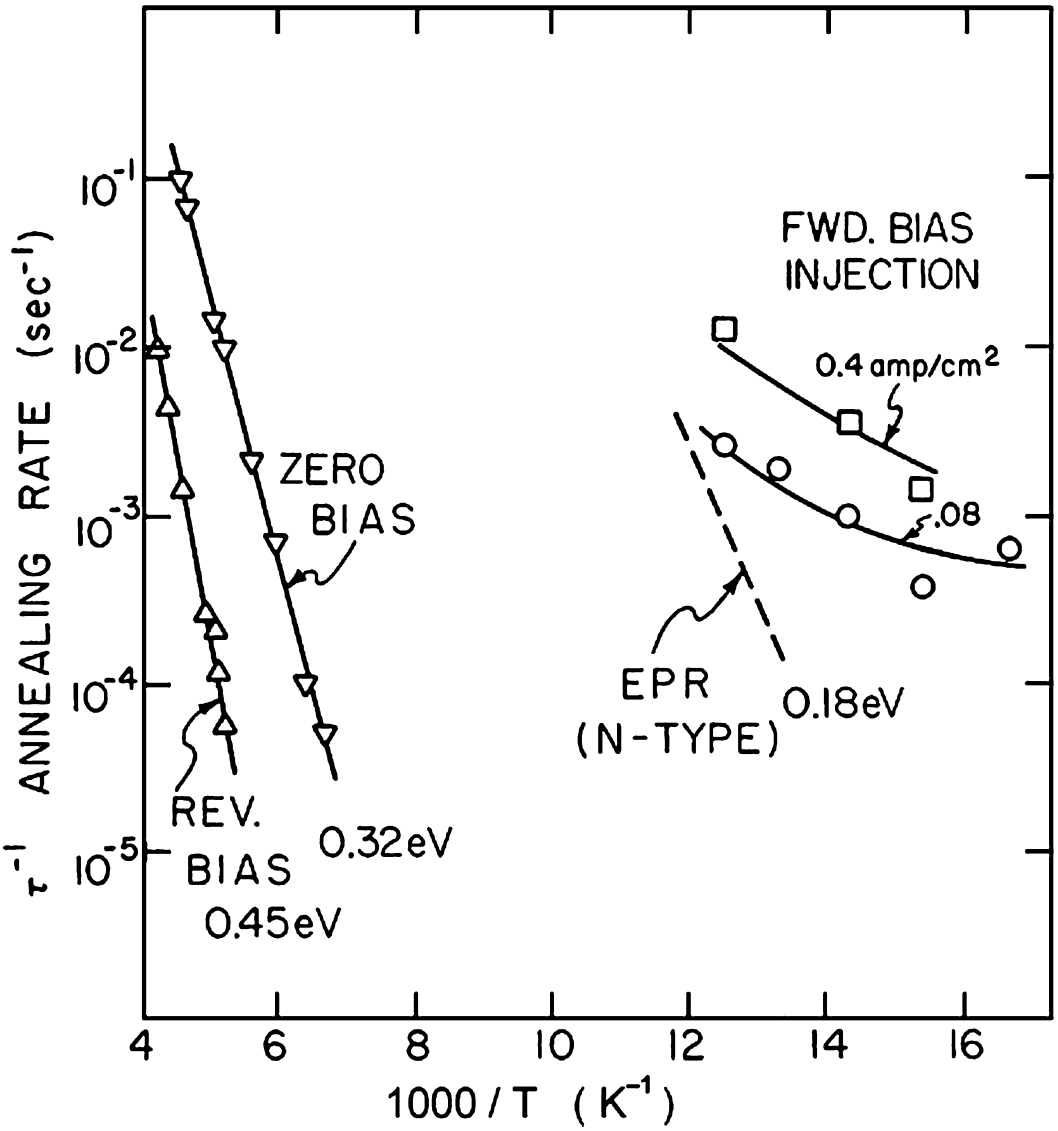

FIG. 13. Annealing kinetics for the vacancy determined by DLTS studies of the $E_V + 0.13$ eV level in p-type Si. Shown also are the kinetics for vacancy annealing in low resistivity n-type silicon from EPR studies (from Ref. 59, with permission).

no measurable Jahn-Teller effect, unlike other charge states of the defect.[84]

4.1.2.3 Vacancy-oxygen pairs (V-O). The vacancy-oxygen (V-O) pair results from the trapping of mono-vacancies by interstitial oxygen (O_i), a common impurity in Si. In samples containing O_i as the main impurity with $[O_i] \gg$ [V-O] (where square brackets denote concentration]), the production of V-O reflects the concentration of vacancies escaping annihilation. Correlation between annealing behavior as monitored by EPR and DLTS measurements, as well as a comparison of material properties, showed that the electron trap at $E_C - 0.18$ eV is the $V\text{-}O^{-/0}$ transition of the V-O pair. It anneals at 360°C with annealing parameters of $E_a = 1.3$ eV and $\nu = 108\ s^{-1}$.[81] The low value of ν implies that V-O annealing occurs via long-range migration and subsequent trapping by sinks to change its properties. The stable microscopic structure of the V-O pair was first established by magnetic resonance techniques to have the orthorhombic C_{2v} symmetry.[85] The recent results obtained through a combination of Laplace DLTS and uniaxial stress measurements (Figure 14) are in agreement with this structure[86]. For the ⟨100⟩ stress direction the peak of the V-O pair splits into two peaks with the amplitude ratio 2:4, whereas it splits into two equally intense peaks with amplitude ratio 3:3 when the stress is applied along the ⟨111⟩ direction. An orthorhombic defect is expected to split into three distinct peaks with amplitudes in the ratio 1:4:1. Only two peaks with

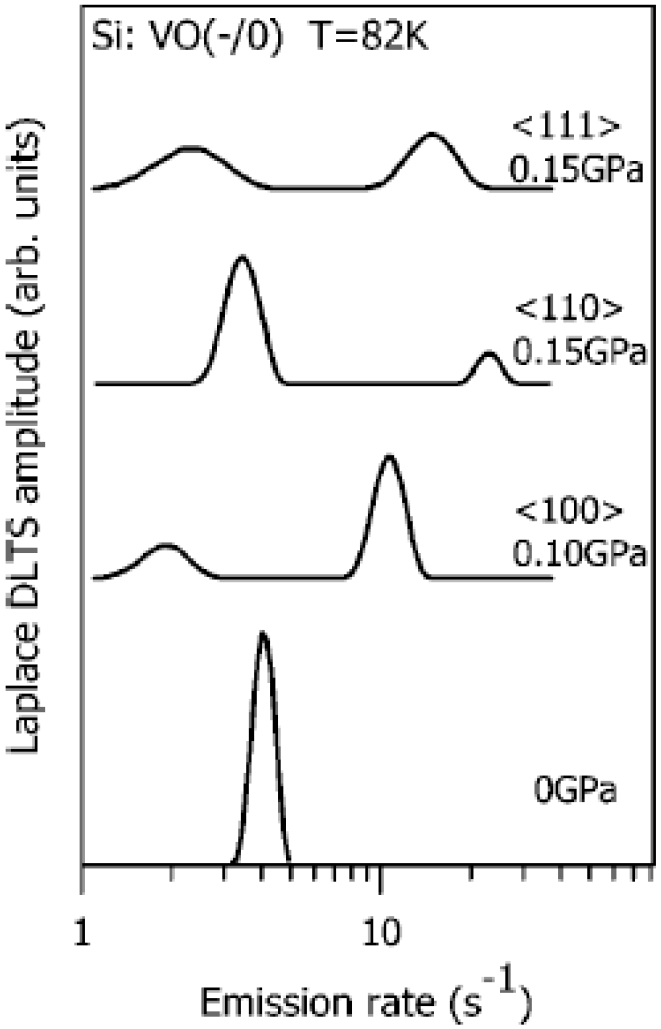

FIG. 14. Laplace DLTS spectra for the V-O complex taken without stress and with stress applied along three major crystallographic directions. The amplitudes of the stress-split peaks sum up to the value observed without stress. Note the small stress values needed to observe the Laplace DLTS peak splitting (from Ref. 86, with permission).

an amplitude ratio 5:1 are, however, observed because the first two lines at low stress cannot be resolved.

4.1.2.4 Vacancy-donor pairs (V-D_s). A well known group of defects that form as the vacancy moves through Si is the combination of vacancies with substitutional donor (D_s) dopant atoms, such as P, As and Sb, to form V-P_s, V-As_s and V-Sb_s pairs.[87] The energy levels of these defects are all close to $E_C - 0.4$ eV, that is, very close to that of the divacancy. It is not possible to distinguish between the **V-D_s** and V_2 signals if conventional DLTS is used without first removing the **V-D_s** by annealing (as described in more detail later). However, when employing Laplace DLTS, Evans-Freeman *et al.*[13] reported a clear separation between the V_2 and V-P signals because of the much higher resolution of this Laplace DLTS.

Annealing of the V-As complex has been shown to occur primarily via two mechanisms.[88] Isochronal annealing at 180°C clearly indicated a fast and a slow process. The slow process could be analyzed in detail and in diffused junctions it is a first order process with $\nu = 7\times10^{13}\ s^{-1}$ and $E_a = 1.40$ eV during reverse bias and $\nu = 1.4\times10^{12}\ s^{-1}$ and $E_a = 1.38$ eV during zero bias. For implanted junctions annealed simultaneously with the diffused junctions, the parameters were $\nu = 7.7\times10^{14}\ s^{-1}$ and $E_a = 1.53$ eV for reverse bias annealing and $\nu = 7.2\times10^{14}\ s^{-1}$ and $E_a = 1.71$ eV for zero bias annealing. At a given temperature (162°C in Ref. 88), it was found that the annealing rate was higher when the E-center is in its neutral charge state (zero bias) than when it is in the negative charge state. This can be explained by assuming that E-center anneals by dissociation. Then the Coulomb binding energy between V^- and As^+ for the dissociation of $(V\text{-}As)^0$ is smaller than the binding energy between $V^=$ and As^+ for the dissociation of $(V\text{-}As)^-$.

These results show several further interesting aspects. First, from the magnitude of the pre-factors it is clear that the defect annealed out by dissociation. This contrasts the original thought that annealing occurs by diffusion and subsequent trapping by defect/impurity sinks. However, it should be kept in mind that the data given earlier only reflect what is happening during the slow process. Annealing by dissociation and migration could be taking place in parallel, but with dissociation being the dominant process. Second, when the V-As center is in its neutral charge state, its annealing rate is about 30 times faster than when in its negative charge state. Finally, from a detailed set of reaction equations in devices with the lower oxygen content (implanted junctions), it followed that the rate of vacancy removal during dissociation is slower than in devices with higher oxygen concentrations (where vacancies are captured by the oxygen), and thus the dissociation process is slowed down.

Recently, it was demonstrated that there is also an alternative path for the removal of the E-center.[89] In the 125–175°C annealing range of electron irradiated FZ-Si it was found that the disappearance of the E-center is accompanied by a significant increase in the concentration of the C_i-C_s complexes and by the formation of a defect with an acceptor level at $E_C - 0.21$ eV. It was suggested that this level is related to a pair of substitutional carbon atoms, C_s-C_s, which is formed when a free vacancy that is released upon E-center annealing is captured by the C_i-C_s complex.

4.1.2.5 Defects due to motion of interstitial Si: Carbon-related defects. Carbon is a common impurity in crystalline silicon. Substitutional carbon (C_s) may exceed a concentration of $10^{17}\ cm^{-3}$ in as-grown Czochralski (Cz) and floating-zone (FZ) silicon and gives rise to an infrared localized vibrational mode at 607 cm^{-1}.[90] When such samples are irradiated with electrons below 300 K, mobile silicon interstitials (Si_i) and vacancies (V) are produced, and reactions between Si_i and C_s take

place to produce isolated interstitial carbon (C_i).[62,91] The first detection of C_i was made using infrared absorption via localized vibrational modes at 930 and 921 cm^{-1}.[91] The C_i defect was subsequently identified in *p*-type Si (the Si-G12 center) through EPR,[62] and more recently an electronic absorption band at 856 meV has also been identified as arising from the C_i defect.[92,93]

4.1.2.5.1 Interstitial carbon. In DLTS studies it was found that a peak at $E_V + 0.28$ eV[55,57,94] in room temperature irradiated *p*-Si had a very similar formation and annealing behavior as the Si-G12 center in EPR[62] and the 930 and 921 cm^{-1} vibrational modes in IR studies.[91] The introduction rates of the defects were found to be independent of the acceptor doping impurity or growth technique. The defect was therefore assigned to the single donor level (0/+) of the isolated carbon interstitial, known to exist from the EPR observation of C_i^+.[62] In *n*-type Si, on the other hand, a similarly behaved DLTS peak at $E_C - 0.10$ eV was also observed.[57] By injecting minority carriers in the *n*-type Si diodes, the $E_V + 0.28$ eV peak could be monitored in the same diodes as the $E_C - 0.10$ eV peak. It was found that the two peaks were introduced and annealed out together.[57] Based on these observations, the $E_C - 0.10$ eV peak was assigned as arising from a single-acceptor level (−/0) of C_i.[57,95] Somewhat later, the first evidence followed from EPR studies that the ionised C_i^- acceptor is the same as the $E_C - 0.10$ eV DLTS center.[96]

4.1.2.5.2 Interstitial-carbon − substitutional carbon. At $T > 300$ K, C_i atoms become mobile[55] and have a tendency to complex with other impurities.[97] In *p*-type Si it has been established that one of the complexes formed due to the mobile C_i is the C_i-C_s pair. From EPR spectra (Si-G11 line) it was proposed that the two carbon atoms in the donor $(C_i\text{-}C_s)^+$ pair share a single lattice site.[98] On the other hand, optically detected magnetic resonance (OMDR) showed a luminescence band with a zero phonon line at 0.97 eV and it was proposed that this arises from exciton recombination at a neutral complex also involving two carbon atoms. The model deduced for this OMDR center consisted of two adjacent and equivalent substitutional carbon atoms with an interstitial Si atom that has distorted out from a bond-centered position between them. The formation and annealing characteristics suggested that the 0.97 eV luminescence and the Si-G11 EPR center arise from the same C_i-C_s pair, but the different proposed structural models argued against it. In a more recent, detailed investigation, using several spectroscopic techniques, it was shown that C_i-C_s is bistable.[97] In the positive and negative charge states, the stable configuration of the defect involves a carbon-silicon "molecule" that occupies a single lattice site (each atom being three-fold coordinated) next to a substitutional carbon atom (four-fold coordinated). In the neutral charge state, the defect rearranges its bonds so that both carbon atoms become substitutional (four-fold coordinated) with a two-fold coordinated Si atom nestled between them.

The C_i-C_s pair has also been extensively studied by DLTS. In *p*-type Si a level at $E_V + 0.33$ eV was initially assigned to it based on the fact that the DLTS peak corresponding to this level grew in with a 1:1 correspondence when C_i^+ ($E_V + 0.28$ eV) annealed around 300–350 K.[56] It was noted in a subsequent study that the $E_V + 0.33$ eV level annealed around 400°C, much higher than the C_i-C_s^+.[94] In a more recent DLTS study of irradiated *p*-type Si, where oxygen contamination was minimized, the radiation induced hole traps were monitored before and after annealing in the 300–350 K range.[97] It was observed that as the $E_V + 0.28$ eV level (C_i) disappeared, a new level at $E_V + 0.09$ eV was detected. No level at $E_V + 0.33$ eV was observed. About 70% of the $E_V + 0.28$ eV level was converted to the $E_V + 0.09$ eV in this sample. The remainder could be accounted for by assuming that the reduction in the divacancy signal observed during annealing is due to the trapping of C_i at divacancy centers, thereby annihilating them or changing their character. This defect was shown to exhibit bistability: cooldown under reverse bias or with minority carrier injection at $T < 50$ K, independent of cooling bias condition, almost eliminates the $E_V + 0.09$ eV level, without the detection of any new DLTS peaks. This behavior of $E_V + 0.09$ eV is very similar to that of the EPR Si-G11 spectrum under photo-injection. The annealing behavior of $E_V + 0.09$ eV is also similar to that of the EPR Si-G11 center. It was therefore concluded that the $E_V + 0.09$ eV level is directly associated with the Si-G11 center $(C_i\text{-}C_s)^+$. This implies that the donor state of the C_i-C_s pair has a level at $E_V + 0.09$ eV, and not at $E_V + 0.33$ eV as suggested before.[56] It is believed that this misinterpretation was due to oxygen introduction into the junction during the junction diffusion process. The origin of the level at $E_V + 0.33$ eV is not clear, but it may be related to the C_i-O_i pair, which has a level in the same energy region.

Using the bistability of the $E_V + 0.09$ eV level, the interconversion between the two configurations of the $(C_i\text{-}C_s)^+$ defect could be determined. The $B^+ \rightarrow A^+$ conversion was measured under reverse bias cooling followed by isothermal annealing at 60–70 K under zero bias, and has a time constant that can be written as:[97]

$$\tau(T) = 4x10^{-13} \exp[0.21\,\text{eV}/kT], \qquad [26]$$

which is in good agreement with the recovery kinetics measured by EPR. This confirmed that the same process was monitored by DLTS and EPR, and that the $E_V + 0.09$ eV level results from hole emission from $(C_i\text{-}C_s)^+$. The reverse bias conversion $A^0 \rightarrow B^0$ was also measured and can be described by

$$\tau(T) = 9x10^{-12} \exp[0.16\,\text{eV}/kT] \qquad [27]$$

The bistability of the C_i-C_s pair has also been studied by capacitance spectroscopy in *n*-type Si, although it was initially not realized that the levels involved were those of the C_i-C_s pair. Isothermal capacitance transient measurements revealed that part of a DLTS peak at $E_C - 0.17$ eV could be converted to a level at $E_C - 0.11$ eV under special pulsing conditions.[100]

Subsequently, it has been shown that there are several ways to generate the bistable $E_C - 0.11$ eV level. In addition to cooling down under reverse bias,[101–103] it can also be generated by minority carrier injection at $T < 50$ K, regardless of the cooling conditions. Either forward bias injection or photo-excitation with 1.16 eV light is effective. DLTS studies further showed that the bistable $E_C - 0.17$ eV peak is a direct product when the $E_C - 0.10$ eV level of C_i^- anneals at 300–350 K.[103] This is consistent with DLTS and EPR findings that the intensity of the bistable $E_C - 0.17$ eV defect is proportional to [C], but not to [O].[96,103]

The annealing behavior of the $E_C - 0.17$ eV DLTS level clearly indicated that it consists of two components: the V-O center detected by EPR and the bistable center.[97] The bistable component anneals out first at about 280°C, closely matching the annealing behavior reported for the $(C_i\text{-}C_s)^+$ pairs in EPR Si-G11 studies. The V-O pairs provide the stable component of $E_C - 0.17$ eV, which anneals out at about 360°C.[74,104] These observations, plus the dependence of the $E_C - 0.17$ eV level on carbon concentration, supports the original conclusion that the bistable defect responsible for the $E_C - 0.17$ eV $\rightarrow E_C -$ 0.11 eV intraconversion is a carbon-carbon pair, arising from a single acceptor level $(-/0)$ of the defect.[103]

It is worth mentioning here that the bistable C_i-C_s defect and the V-O center can also be distinguished following the significant difference between their capture cross sections. Pellegrino *et al.*[105] have recently shown that the concentration versus depth-profiles of V-O center and C_i-C_s pair could be separated by varying the filling pulse width during DLTS depth profiling measurements. The C_i-C_s pair is predominantly observed in oxygen-lean samples, wherein the competing O_i trap for migrating C_i is suppressed. They used P-doped (100) oriented FZ Si having a resistivity of 65 Ωcm ($\sim 8 \times 10^{13}$ P/cm^{-3}), and containing O_i and C_s with a concentration $\sim 5 \times 10^{15}$ cm^{-3} each. The sample was implanted with 6 MeV ^{11}B ions to a dose of 1×10^8 cm^{-2} at room temperature. The V-O center has a relatively large capture cross section ($\sim 9 \times 10^{-15}$ cm^{-2}), whereas that of the C_i-C_s pair is $\sim 8 \times 10^{-18}$ cm^{-2}.[97] Hence, a 10 μs filling pulse width was sufficient to obtain the depth profile of the V-O center, whereas the cumulative depth distribution of both the V-O center and the C_i-C_s pair was obtained with a 50 ms pulse width. The depth profile of the bistable C_i-C_s defect was determined by subtracting [V-O] from the cumulative defects profile. A shift of ~ 0.5 μm was observed between the depth profiles of the V-O center and the C_i-C_s pair and it was attributed to the preferential forward momentum of recoiling Si atoms.

4.1.2.5.3 Carbon-oxygen pairs. In high oxygen content material (Cz), the C_i atom can be trapped by oxygen, leading to the formation of the C_i-O_i pair. The resulting defect can be detected by a DLTS peak corresponding to a level at $E_V + 0.38$ eV,[94] local mode absorption (C(3) center),[106] and IR electronic absorption or luminescence at 0.79 eV (C-line).[107] In p-type material, an EPR spectrum (Si-G15) has been shown to arise from the ionized donor state of the same complex as gives rise to the DLTS peak at $E_V + 0.38$ eV, allowing a microscopic identification of the $E_V + 0.38$ eV defect as a simple C_i-O_i pair.[108]

4.1.2.5.4 Interstitial-carbon – donor-atom pairs: C_iD_s. DLTS provided evidence regarding another interesting group of defects that form above room temperature as C_i migrates and pairs up with substitutional dopant atoms, such as P_s, Sb_s, and As_s, to form more stable defects such as C_i-P_s,[109,110] C_i-Sb_s[111] and C_i-As_s.[109]

An example is the complex behavior of C_i-Sb_s that was carefully monitored by DLTS.[111] The DLTS peaks observed immediately after room temperature irradiation (Figure 15, curve a) are due to C_i at $E_C - 0.10$ eV and V-Sb_s at $E_C -$ 0.4 eV. A weak signal due to the divacancy is also observed at $E_C - 0.23$ eV. After a 350 K anneal, the C_i signal disappears and new DLTS peaks appear from C_i-C_s pairs at $E_C - 0.17$ eV and from C_i-Sb_s pairs at $E_C - 0.39$ eV on the shoulder of the V-Sb_s peak (Figure 15, curve b). An interesting observation was made after hole injection at 300 K followed by cooldown under zero or reverse bias:[111] The $E_C - 0.39$ eV peak disappeared and three new peaks emerge at $E_C - 0.13$ eV, $E_C - 0.27$ eV and $E_C - 0.46$ eV (Figure 15, curve c), with the relative intensity of the $E_C - 0.13$ eV peak depending strongly on the cooldown bias condition. Subsequent injection at 140 K replaced the $E_C - 0.13$ eV and $E_C - 0.27$ eV peaks by a new one at $E_C - 0.16$ eV (Figure 15, curve e). This process was found to be completely reversible, thermal annealing at discrete temperature stages reversing the process sequentially through each of the peaks, finally back to the original peak at $E_C - 0.39$ eV after annealing at 350 K. This whole process is also completely reproducible. These findings indicate that the C_i-Sb_s pair must have several possible configurations, each with distinctly different electrical properties, and that it converts from one to another as a result of electron and hole capture during electrical injection. Similar behavior has been reported for the C_i-P_s pairs[109,110] and C_i-As_s pairs,[109] with five configurations having actually been detected in the case of phosphorus.[109]

An explanation for this behavior, presented later, has been proposed by Watkins.[112] Substitutional group V atoms are single donors and therefore have a positive $^+$e core. Isolated interstitial carbon has an acceptor level $(-/0)$ at $E_C - 0.10$ eV and a simple molecular orbital model for it predicts a second acceptor level $(= /-) \approx 0.3$ eV higher, resonant in the conduction band. Three charge states for the pair can therefore be expected: $(C_i^{=}\text{-}Sb_s^+)^-$, $(C_i^-\text{-}Sb_s^+)^0$, and $(C_i^0\text{-}Sb_s^+)^+$ with Coulomb binding energies of approximately $2e^2/\varepsilon r$, $e^2/\varepsilon r$, and 0, respectively, where r is the pair separation. In removing an electron from the pair, the difference in Coulomb energy must also be supplied, the net result being that the level positions of the defect are simply lowered by $e^2/\varepsilon r$ from those for isolated interstitial carbon

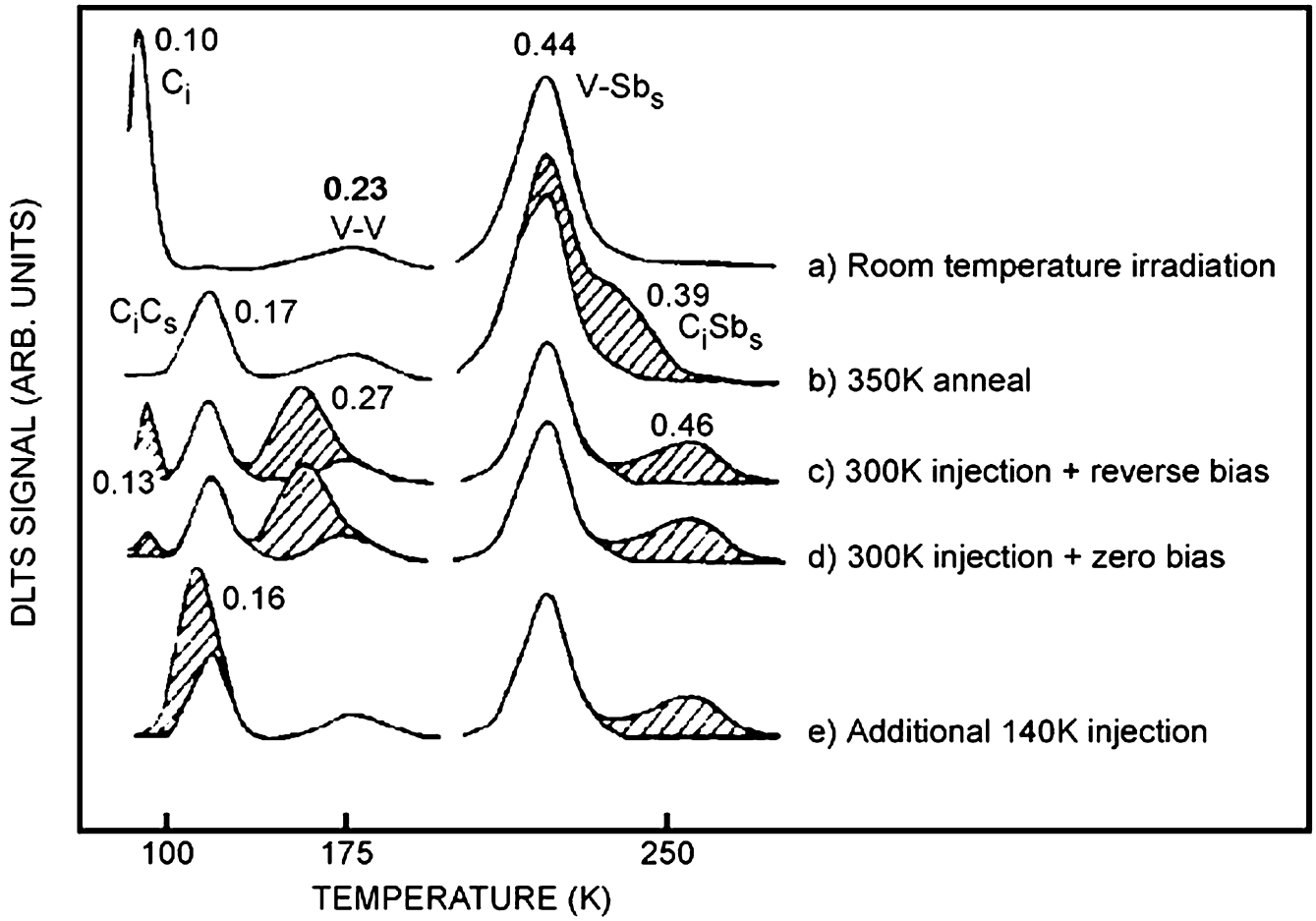

FIG. 15. DLTS spectra of electron irradiated Si(Sb,C) revealing levels (shaded) of four distinct configurations of the $C_i - Sb_s$ pairs produced by the indicated injection and bias conditions. Level positions are indicated in eV from the conduction band edge (from Ref. 112, with permission).

(from which the electron is being removed). This is illustrated in Figure 16, where the different configurations are identified as the donor-acceptor pairs formed when the interstitial carbon acceptor takes on the different lattice positions available near the substitutional Sb donor. In the model, the ground stable configuration (I) corresponds to the closest pair separation, the $e^2/\varepsilon r$. Coulomb lowering of the levels indicating $r \approx 2$ Å, a value typical of a nearest neighbor carbon-antimony molecular bond length. Electronic excitation provided by electron-hole recombination during minority carrier injection serves to partially separate the pair and, in subsequent thermal annealing, the interstitial carbon works its way back in several discrete annealing stages to the ground close-pair configuration. The Coulomb energy lowering for the most distant separation (III) indicates $r \approx 3.4$ Å, again a reasonable value. In Figure 16, the levels monitored by DLTS are indicated in solid lines. The two configurations labeled IIA and IIB are interesting in that they form a bistable set, the A configuration being the stable one for the negative charge state, and B the stable one for the neutral state. This is evident in Figures 15c and d where the presence or absence of the 0.13 eV DLTS peak depends on whether the diode is cooled under reverse bias (defect neutral) or zero bias (negatively charged). By studying the kinetics of the conversion and emission processes, the CC diagram for the two configurations has been deduced[111] and is shown in the inset of Figure 16. The barrier for intraconversion between IIA and IIB (0.25 eV) is significantly smaller than that determined[109] for III $\rightarrow$ II (0.62 eV) or II $\rightarrow$ I (1.2 eV). The latter is comparable to the diffusion activation barrier determined for isolated C_i (0.73 eV[96,97], 0.87 eV),[113] suggesting that conversion between the sets I, II, and III involves the normal diffusional motion of C_i. The results suggest, however, that for the IIA $\rightarrow$ IIB conversion, a different type of rearrangement may be occurring. A clue of what this might be is found by noting that the CC diagrams of the acceptor state of the C_i-C_s and that for the IIA $\rightarrow$ IIB configurations of the C_i-Sb_s

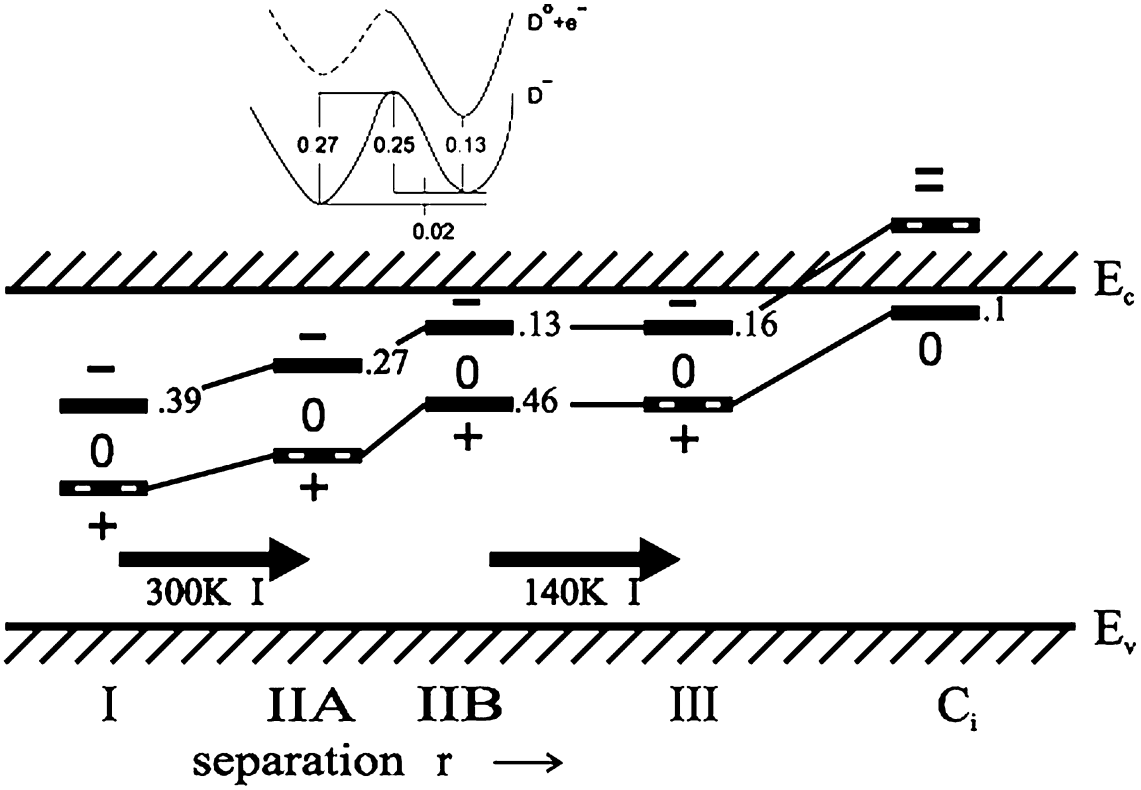

FIG. 16. Electrical levels (in eV, from the conduction band edge) for the four configurations of the $C_i - Sb_s$ pair interpreted as those of C_i lowered by the Coulomb interaction with Sb^+ vs. separation, r. CC diagram determined for the IIA–IIB pair shown in the inset (from Ref. 112, with permission).

pair is strikingly similar. This suggests that for the IIA → IIB conversion of the C_i-Sb_s pair, a similar bond switching to that of the acceptor state of the C_i-C_s may be involved. Such easy motion could serve to change the C_i-Sb_s, but only between two configurations. Further separation would require C_i-Si interchange as in long-range diffusion.

Detailed DLTS studies have also been undertaken for the C_i-P_s pair.[109,110,114] Curves a–e in Figure 17 shows the DLTS spectra related to the C_i-P_s pair for different bias and annealing conditions. Conversion kinetics studies suggested that C_i moves in the lattice during the conversions among four configurations of C_i-P_s pairs, whereas a fifth configuration is more likely to be a result of a bond rearrangement.[109] Experimentally determined energy level diagrams and CC energy surfaces are consistent with the simple ionic model, which takes into account Coulomb interactions between C_i and P_s atoms at different lattice separations in a uniform dielectric medium (silicon). The energy level diagram proposed by Gürer *et al.*[109] for the four configurations of C_i-P_s originally detected is shown in Figure 18. It consists of a pair of an acceptor $(-/0)$ and a donor $(0/+)$ that are separated by $U \approx 0.3$ eV for each configuration. These authors were the first to observe the donor $(0/+)$ levels of IA and IIA. According to Figure 18, the energy levels get shallower as the conversions IA → IIA → IIB → III are induced. Figure 18b shows the charge state assignment for the two energy levels of the fifth configuration. It consists of a single acceptor $(-/0)$ level at $E_C - 0.07$ eV and a single donor level $(0/+)$ at $E_C - 0.39$ eV. It was also observed that after 140 K injection, the junction capacitance increases, consistent with the introduction with a donor at $E_C - 0.39$ eV in the upper half of the Si band gap. This assignment is also consistent with the observed hole emission $(C_i\text{-}P_s)^+ \rightarrow (C_i\text{-}P_s)^0 + h^+$ during the conversion back to the stable configuration.

Based on arguments similar to those made earlier for the C_i-Sb_s pair, a structural model has been proposed for the stable (close pair) configuration of C_i-P_s pairs (Figure 19). The pair separation for the stable configuration was estimated as 1.9 A, which is very close to a typical C-P bond length. It is a ⟨100⟩ oriented C-P molecule (each atom is three fold coordinated) that occupies a single lattice site. This structure is very similar to that of C_i^+ and C_i^- and has a C_{2v} symmetry as determined by EPR.[115]

4.1.3 Annealing of Radiation-Induced Defects

In Figure 20 the stability of the vacancy and several first generation vacancy-defect pairs is schematically summarized.

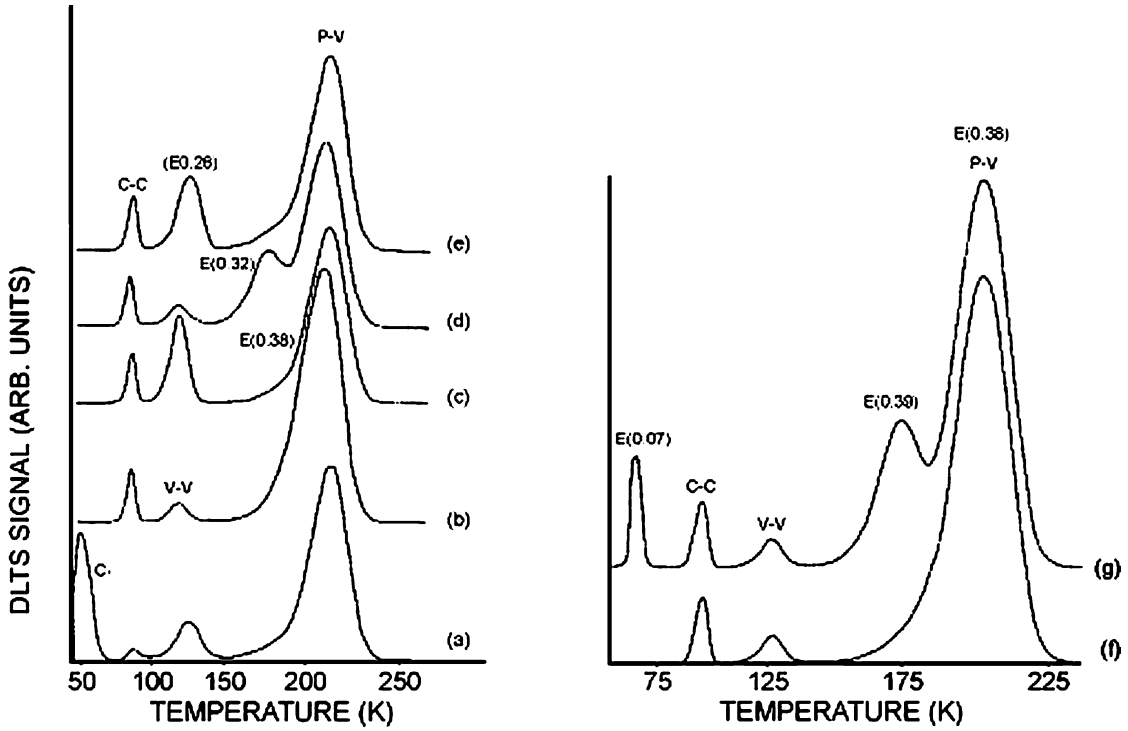

FIG. 17. DLTS spectra showing the five configurations of C_iP_s pairs: (a) After e^--irradiation at 295 K; (b) After 350 K, 1800 s zero bias (ZB) annealing of C_i; (c) After injection at 240 K, 300 s (0.38 → 0.23 eV); (d) After ZB annealing at 260 K, 300 s (0.23 → 0.32 eV); (e) After ZB annealing at 290 K, 300 s (0.32 → 0.26 eV); (f) Same as (b); (g) After injection of holes at 140 K, 300 s (0.38 → 0.07/0.39 eV) (redrawn from Ref. 109, with permission).

This data was obtained after isochronal annealing cycles of typically 15 min duration.[59] The stability of each defect pair reflects a binding energy between the vacancy and its partner. Some of these defects were discussed in the preceding sections.

4.2 High-Energy Proton Irradiation

The first DLTS of proton bombarded Si was reported by Kimerling *et al.* after irradiating Si with 400 keV protons at room temperature.[54] They reported that the proton damage is very similar to 1 MeV electron damage. In a

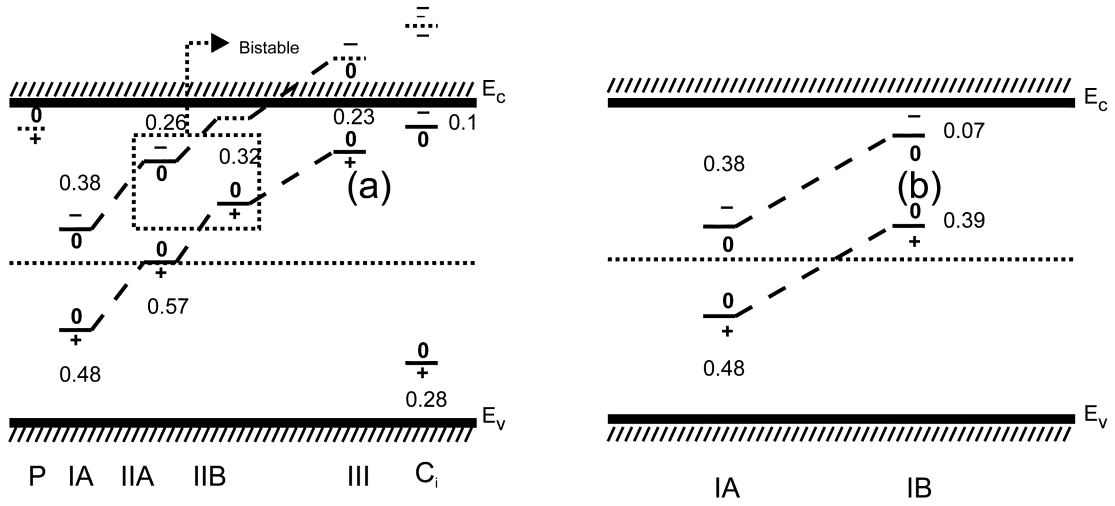

FIG. 18. Charge state assignment for the (a) four original configurations; (b) fifth configuration of the $C_i - P_s$ pair (redrawn from Ref. 103, with permission).

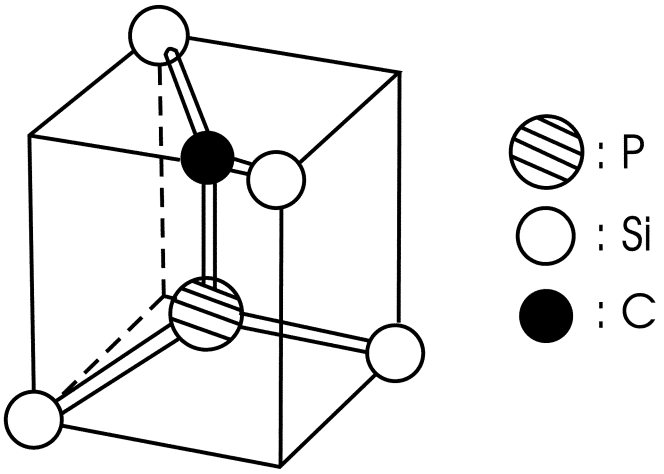

FIG. 19. Proposed structure for the stable configuration of the $C_i - P_s$ defect pair (redrawn from Ref. 109, with permission).

follow-up investigation, FZ and Cz Si was bombarded with (100–300) keV protons at temperatures of between 10 and 300 K.[57] The most important data of that report was the assignments of defect states to the single Si vacancy and the carbon interstitial. The $V^{=/-}$ was found to have an energy of 0.09 eV below the conduction band. This identification was based on its annealing behavior (90 K) and the charge state dependence.[72] The data for the $V^{0/+}$ transition was found to be consistent of two signals being from the same state (negative U). The $C_i^{-/0}$ at $E_C - 0.12$ eV and $C_i^{0/+}$ at $E_V + 0.28$ eV had the same stability and concentrations. The positive charge state was observed in *n*-type Si at $E_V + 0.28$ eV after injection and in *p*-type Si at $E_V + 0.27$ eV by using Schottky contacts. No defects related to the presence of hydrogen in Si were observed in this experiment. Such defects will be discussed in more detail later as observed in more recent experiments.

4.3 Hydrogen and Its Interaction with Other Defects

The role of hydrogen in semiconductor materials is of interest to both the scientific community and the electronics devices manufacturing industry. Hydrogen can be introduced into the semiconductor material both intentionally and unintentionally through a host of ways, including the growth stage, ion implantation, chemical cleaning of the surface, or exposure to a plasma containing hydrogen.[117] It is very mobile and exhibits a wide range of interactions with impurities and defects in crystalline semiconductors, especially by passivating dangling bonds and impurities, and decorating irradiation-induced defects.[118,119] Benton *et al.*[120] have used atomic hydrogen to neutralize electrically active point defects in Si. Similarly, the deep levels introduced by metals, such as Au, Ni, Fe, and Cu, can also be passivated by reaction with atomic hydrogen.[119] Atomic hydrogen also passivates the shallow acceptors in Si. One of the first-neighbor Si atoms around the trivalent acceptor atom has

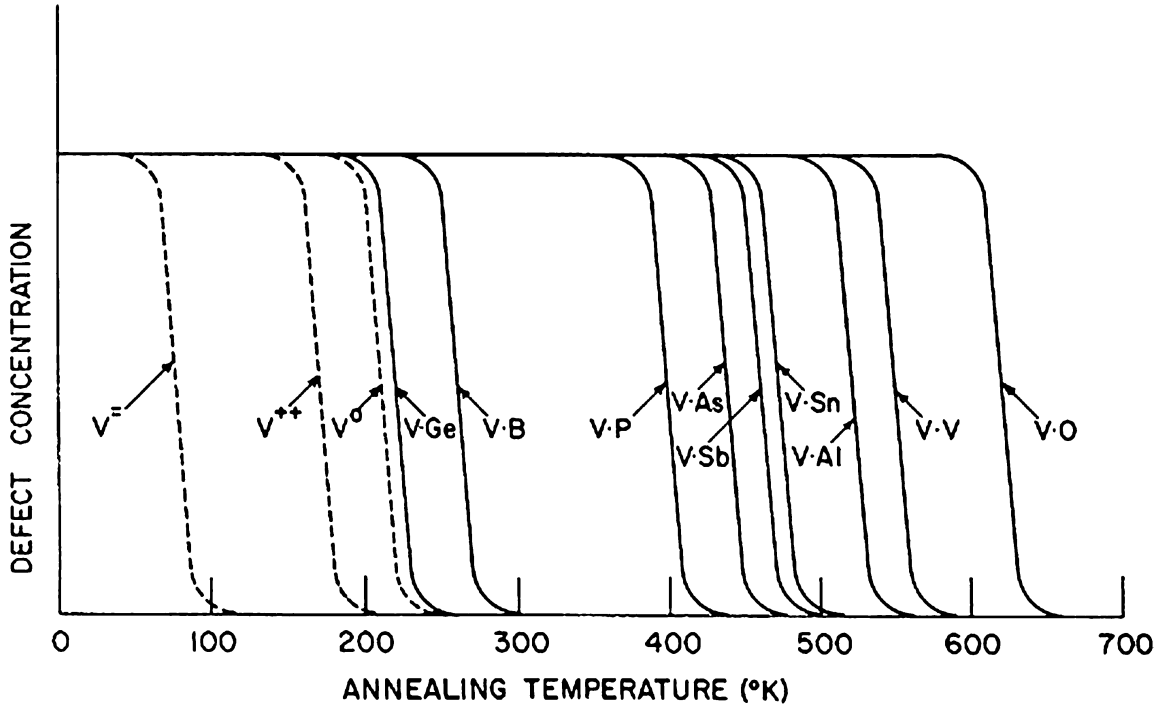

FIG. 20. Schematic of vacancy and vacancy-defect pair annealing stages (15 min isochronal annealing); (from Ref. 59, with permission).

a hydrogen atom attached to its dangling bond to form Si-H and a neutralized 3-fold coordinated acceptor.[121–123] Pankove *et al.*[122] have proposed a structural model in which the H is in the interstitial configuration along the ⟨111⟩ axis between the B acceptor and one of its Si neighbors with the H bonded primarily to Si. This model was later confirmed by theoretical cluster calculations,[124,125] localized vibrational mode spectroscopy,[126] and channeling experiments.[127,128]

The properties of hydrogen in elemental and compound semiconductors have previously been reviewed by Pearton *et al.*[129] and Haller.[130] In this section the authors concentrate on the properties of hydrogen-related defects studied in irradiated crystalline Si by DLTS. Being the lightest element, ion implantation of hydrogen can be conveniently done in many types of implanters or accelerators with fluences that do not result in a carrier reduction of more than 10%, as is required for quantitative DLTS analysis. The same does not apply for the heavier ions. For example, Irmscher *et al.*[131] have found that for 0.3 MeV proton implantation two defects observable by DLTS were produced per incident proton at room temperature, whereas defect production per helium ion was ten times higher, and therefore also the effect on the free carrier density. The relatively higher fluences of hydrogen that can be achieved without causing too much carrier compensation, therefore, allow for interactions between hydrogen and impurities and defects in the Si crystal to be studied.

4.3.1 The Isolated Hydrogen Atom

Irmscher *et al.*[131] have shown that implantation of protons into both n- and p-type Si at 80 K produced only one H-related level, E3′ at approximately $E_C - 0.18$ eV, which dominated over all other levels. This defect could not be observed after bombardment at room temperature. Their results indicated that E3′ was an electron trap with a donor nature, but mentioned that an ultimate charge state assignment would necessitate more detailed measurements. The defect was tentatively identified as a V-H complex or a hydrogen atom in a well-defined interstitial site. The E3′ defect anneals out at about 100 K in n-type and 250 K in p-type Si. Holm *et al.*[132] have observed a bistable center with a level at $E_C - 0.16$ eV in proton irradiated n-type Si at 45 K, which they associated with E3′. This center annealed out at ∼100 K under zero bias at a rate of $\nu = (3.0 \times 10^{12}\ \mathrm{s}^{-1})\exp[(-0.29\ \mathrm{eV})/kT]$ and at ∼200 K under reverse bias at a rate of $\nu = (1.3 \times 10^{8}\ \mathrm{s}^{-1})\exp[(-0.44\ \mathrm{eV})/kT]$. The two defect states could be recovered by forward bias injection at low temperatures. The decay without (with) reverse bias reflected capture of one (two) electron(s), and the metastability was ascribed to hydrogen jumps between bond-center (BC) and tetrahedral sites due to changes in charge states. Theoretical predictions demonstrate that the isolated neutral and positively charged hydrogen atoms occupy the BC site, whereas negatively charged hydrogen enters the interstitial tetrahedral site (T site).[133,134] The fact that the annealing properties of E3′ and the level at $E_C - 0.16$ eV were similar to the AA9 center [135] and the 1990 cm^{-1} Si-H mode originating from hydrogen at bond-center sites, prompted them to identify E3′ as the isolated neutral hydrogen atom (H^0) occupying the BC site.

Endrös[136] has reported the electronic properties of hydrogen in carbon-doped n-type Si. It was shown that hydrogen in the presence of carbon formed a charge-state-dependent center located ∼0.16 eV below the conduction band edge. This H-C complex was found to be only stable in the more positively charged state and annealed after capture of electrons above 300 K. In his work, Endrös studied the level at $E_C - 0.16$ eV in both hydrogen plasma exposed p^+n junction diodes and hydrogenated Schottky barrier samples by wet chemical etching in a mixture consisting of HNO_3:HF = 5:1. A model was proposed whereby reverse bias annealing led to the dissociation of hydrogen-passivated phosphorous donors according to the reaction $(\mathrm{P\text{-}H})^0 \rightarrow \mathrm{P}^+ + \mathrm{H}^0 + \mathrm{e}^-$. The Fermi level position would determine the charge state of hydrogen ($\mathrm{H}^0 \rightarrow \mathrm{H}^+ + \mathrm{e}^-$) in the depletion region. The deep donor level (H-C complex) is then formed through the drift of H^+ in the electric field of the space-charge region and its trapping at substitutional carbon impurities. The formation of molecular hydrogen ($\mathrm{H}^0 + \mathrm{H}^0 \rightarrow \mathrm{H}_2$) is the probable reason for loss of the deep level for $T \geq 300$ K. In a later study, Endrös *et al.*[137] determined an activation energy of 0.73 eV for the dissociation kinetics of the H-C complex. Because of the isoelectronic behavior of substitutional carbon in crystalline Si, the deep level at $E_C - 0.16$ eV reflected mainly the electronic properties of hydrogen. In fact, pseudopotential density functional calculations showed that the H-C pair has an energy level that is virtually identical to that of an H atom at the same atomic site but without the impurity.[138] Both the E3′ center and the H-C complex, therefore, seem to reflect similar basic properties of the isolated H in Si.

Further investigations of the electronic properties of the H-C complex by double-correlation DLTS[139] revealed an anomalously strong dependence of its activation energy on the electric field to the extent of ∼31 meV/10^4 Vcm^{-1}. The zero-field activation energy for electron emission from the H-C complex was found to be 185 meV, which is close to the T^2 corrected estimate of Irmscher *et al.*[131] It was argued that such a strong field dependence could not be explained satisfactorily in terms of the Poole–Frenkel effect or in terms of the quantum-mechanical tunneling model. Csaszar and Endrös[139] proposed a model that takes into account the electronic properties of H on its lattice site as predicted by theory. In the presence of an electric field in the space-charge region the H^+ is altered from its BC interstitial site (zero field condition) in line with the field strength. This results in a change in the energetic position of the H^+/H^0 defect level in the Si band gap.[138] Consequently, the field dependence of the H-C activation energy is the sum of two effects: (1) a contribution of ∼6 meV/10^4 Vcm^{-1} attributed to the Poole–Frenkel field-assisted electron emission from a Coulombic potential well associated with the ionized proton, and (2) a structural term to the extent of ∼25 meV/10^4 Vcm^{-1}

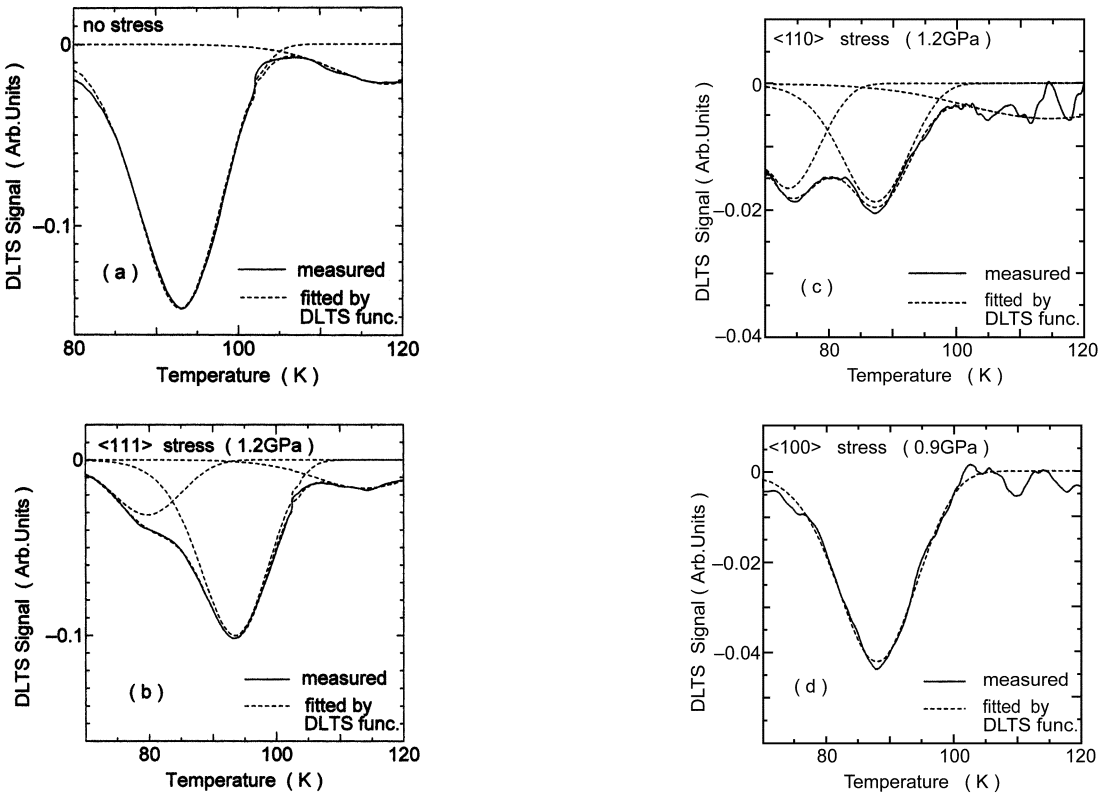

FIG. 21. DLTS spectra of the H-C complex in Si under no stress (a) and under compressive stresses along the ⟨111⟩ (b), ⟨110⟩ (c), or ⟨100⟩ (d) directions. Solid curves are measured spectra, and broken lines are the fitting using usual DLTS function considering the presence of the maximum three peaks: the split peaks of the E3 trap at 75–95 K and the unidentified peak around 115 K. The application of the ⟨111⟩ and ⟨110⟩ stresses splits the E3 trap peak into two as intensity ratios of 1:3 and 2:2, respectively, which are the ratios of the low-energy peak to the high-temperature peak. There is no splitting under the ⟨100⟩ stress. These results clearly indicate the trigonal symmetry of the H-C complex.[140].

that results from the position-dependent electronic properties of hydrogen.

DLTS has been applied to study the structure and bonding nature of the H-C complex in Si under uniaxial stress.[140] As shown in Figure 21 the application of ⟨111⟩ and ⟨110⟩ compressive stresses split the DLTS peak of the H-C complex into the ratios of 1:3 and 2:2, respectively. The ratios are of the low-temperature peak to the high-temperature peak. No splitting of the defect peak was observed under the ⟨100⟩ stress. Kamiura *et al.*[140] deduced a trigonal symmetry $C3_V$ for the H-C complex, and proposed a structural model for the complex consistent with theoretical predictions,[139,140] where a hydrogen atom occupied a BC site between carbon and silicon atoms. The peak splitting under the ⟨111⟩ stress meant that the configuration of the complex whose ⟨111⟩ symmetry axis along the C-H-Si bond was parallel to the ⟨111⟩ axial stress was favored, suggesting the anti-bonding nature of the H-C complex. Stress-induced preferential alignment of the H-C complex was also observed at 250 K (Figure 22). The observed growth of the high-temperature peak together with the decay of the low-temperature peak under 1 GPa stress along the ⟨110⟩ axis was explained by the increase in the bonding energy under a compressive stress parallel to the bonding direction. In a subsequent study, the same group[141] demonstrated that the alignment was suppressed under reverse bias annealing (RBA), indicating that stress-induced alignment occurred preferentially in the neutral charge state. This result meant that hydrogen moved more easily in the neutral charge state under compressive stress. Relaxation of this preferential alignment could be achieved by zero bias annealing (ZRB) above 260 K following removal of the stress. ZBA at 280 K for 15 min resulted in complete recovery of the low-temperature peak and an original 1:1 ratio of the split peaks. Because four BC sites around carbon are equivalent during ZBA under no stress, this result was explained as the loss of stress-induced alignment due to random jumps of hydrogen from bond to bond to recover the initial random orientations of the H-C complex. It was again found that relaxation (*i.e.*, random jumps of hydrogen) was suppressed under RBA, indicating that hydrogen moved more easily in the neutral charge state also under no stress.

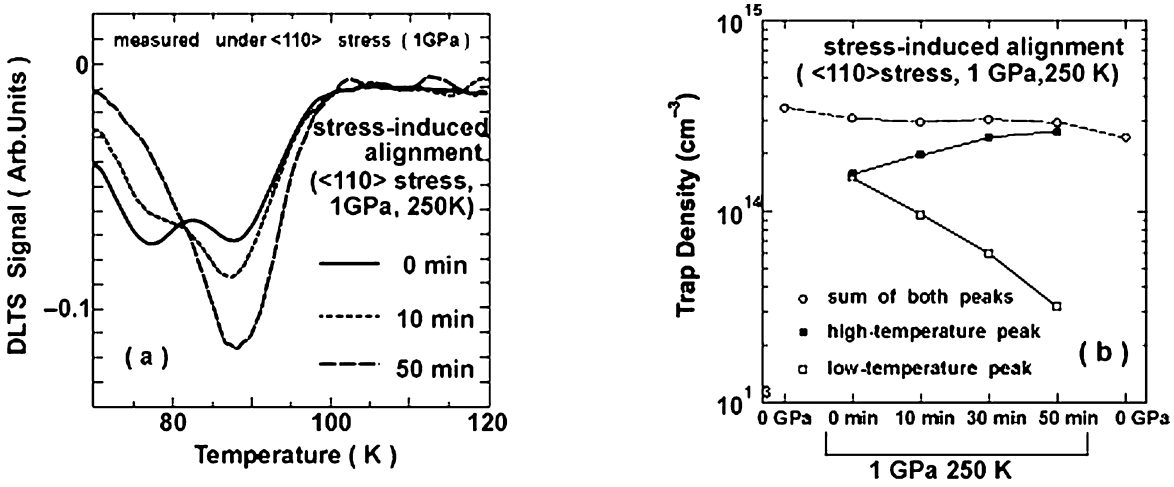

FIG. 22. Stress-induced preferential alignment of the H-C complex at 250 K: (a) changes in DLTS spectrum due to stress annealing, and (b) the densities of split peaks and their total density as a function of annealing time and the densities of the unsplit peak measured under no stress before and after stress annealing. The observed growth of the high-temperature peak together with the decay of the low-temperature peak can be reasonably explained by an increase in the bonding energy under a compressive stress parallel to the bonding direction.[140]

Kamiura and coworkers[142,143] have performed a detailed study of the thermal stability of the H-C complex under various conditions, such as in the dark, under light illumination, and with or without the application of a reverse bias, and proposed a model for its dissociation mechanism. One key observation was that annihilation of the H-C complex was enhanced under light illumination, but was suppressed during the application of reverse bias. Annihilation of the complex occurred only outside the depletion region of the Schottky diode. A deviation from first order annealing kinetics was observed and attributed to the reverse reaction to reform the H-C complex after its dissociation. Their results further clearly showed that below-gap excitation is essential for the photoinduced dissociation of the H-C complex. Using the theory of Lucovsky[144] on the photon-energy dependence of photoionization cross section for deep centers in semiconductor materials, Kamiura *et al.*[142] extracted a threshold energy of 0.98 eV for the photoionization of the H-C complex. This allowed them to conclude that the photoexcitation of an electron from the valence band to the E3 defect induced the H-C complex to become unstable.

From the Arrhenius-like temperature dependence of the dissociation rate, $1/\tau$, of the H-C complex that the authors observed, they proposed two possible mechanisms (illustrated in Figure 23) for the zero bias photoinduced dissociation of the H-C complex. The first mechanism—charge-state-enhanced dissociation—may proceed via two pathways. Being of donor character, the charge state of E3 is positive at annealing temperatures (trap level located above the Fermi level). In mechanism A1 (see Figure 23), below-gap excitation of an electron from the valence band to the trap level changes its charge state to neutral. Alternatively, the trap level can also be neutralized when the defect traps an electron from the conduction band following above-gap excitation. The authors assumed that neutralization of the H-C complex reduced its activation energy for dissociation. The second mechanism, recombination-enhanced dissociation, can also proceed via two different routes (B1 and B2 in Figure 23). In B1 and B2, neutralization of the trap results from capture of a hole from the valence band, that is, by electron-hole pair recombination at the defect level. If the energy released by the recombination is converted into vibrational energy of hydrogen through the electron-lattice interaction, the dissociation of the defect complex may be enhanced by the emitted phonons. However, the authors pointed out that

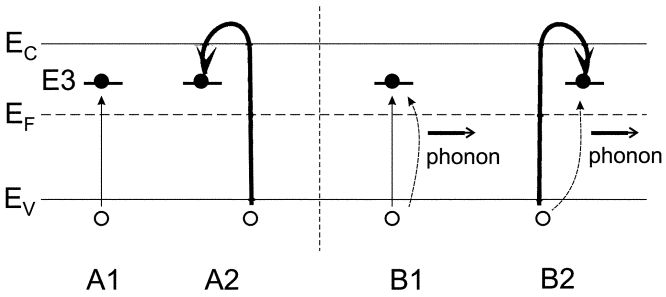

FIG. 23. Two possible mechanisms of the photoinduced dissociation of the H-C complex in zero-bias annealing experiments: charge-state-enhanced dissociation (A1, A2) and recombination-enhanced dissociation (B1 and B2) (redrawn from Ref. 142, with permission).

their experimental data could not be used to identify whether charge-state-enhanced dissociation or recombination-enhanced dissociation was the actual mechanism responsible for the dissociation of the H-C complex.

The results obtained by these authors were explained in relation to the atomic and electronic model of the H-C complex. Following the theoretical predictions of the atomic configurations of the isolated hydrogen,[133,134] Kamiura *et al.*[143] proposed a defect model of the H-C complex (see Figure 24), whereby the hydrogen atom resides inside a silicon-carbon bond because of the small size of a carbon atom. The carbon atom being negatively charged (stronger electronegativity than silicon) attracts a proton and repels the donor electron bound to the proton, thus delocalizing its wavefunction. Consequently, the hydrogen donor level, which is located near the midgap in its isolated state, is raised to $E_C - 0.15$ eV for the H-C complex. Theoretical modeling of the H-C complex has presented different results concerning the stability of its three configurations (one BC site and two anti-bonding sites).[145,146] Unlike the results of Maric *et al.*,[145] Kaneta and Katayama-Yoshida[146] have reported that the BC site was more stable than the two anti-bonding sites by 0.6 eV, and that the BC configuration yielded a donor state near the conduction band. Kamiura and coworkers[142] assumed that donor level to correspond to defect E3 in their experiements, and proposed that the BC configuration of the H-C complex in its neutral state was unstable with no binding among hydrogen, carbon, and silicon (*i.e.*, upon electron capture). No binding between these three atoms meant that the activation energy of hydrogen motion should be comparable to that of isolated hydrogen, which had previously been measured to be 0.5 eV by Van Wieringen and Warmoltz.[147] This value is similar to the activation energy for the dissociation of the H-C complex under zero bias light illumination.[142] The authors, therefore, assumed that the complex captured an excess electron, created in the conduction band by above-gap excitation, or accepted an electron from the valence band by below-gap excitation, and lost the binding to become dissociated at a activation energy of 0.5 eV. The activation energy for the dissociation of the H-C complex in the dark is 0.2 eV higher than under light illumination. In the dark, an electron needs to be excited from the Fermi level to produce the neutral H-C complex, which then dissociates with an activation energy of 0.5 eV. Indeed, Kamiura *et al.*[142] estimated the difference between the Fermi level and the H-C complex level in their samples to be 0.2 eV. The configurational coordinate diagram shown in Figure 25a illustrates the total energy of the complex in the positive and neutral states. When the defect charge state is positive (under reverse bias) it is dissociated by atomic jump of hydrogen with a activation energy of 1.3 eV. When the defect becomes electrically neutral by electron capture the activation energy for its dissociation is lowered to 0.5 eV (Figure 25b).

Very recently, it was reported that the H-C center has cross section values that are acceptor-like and no Poole–Frenkel effect could be observed in the expected electric field range.[148] Laplace measurements and *ab initio* calculations lead these authors to believe that the hydrogen can sit in the bond center between C and Si, or on an antibonding site with C, with similar energies of formation. The structure can therefore be expected to be a mix of these two configurations.

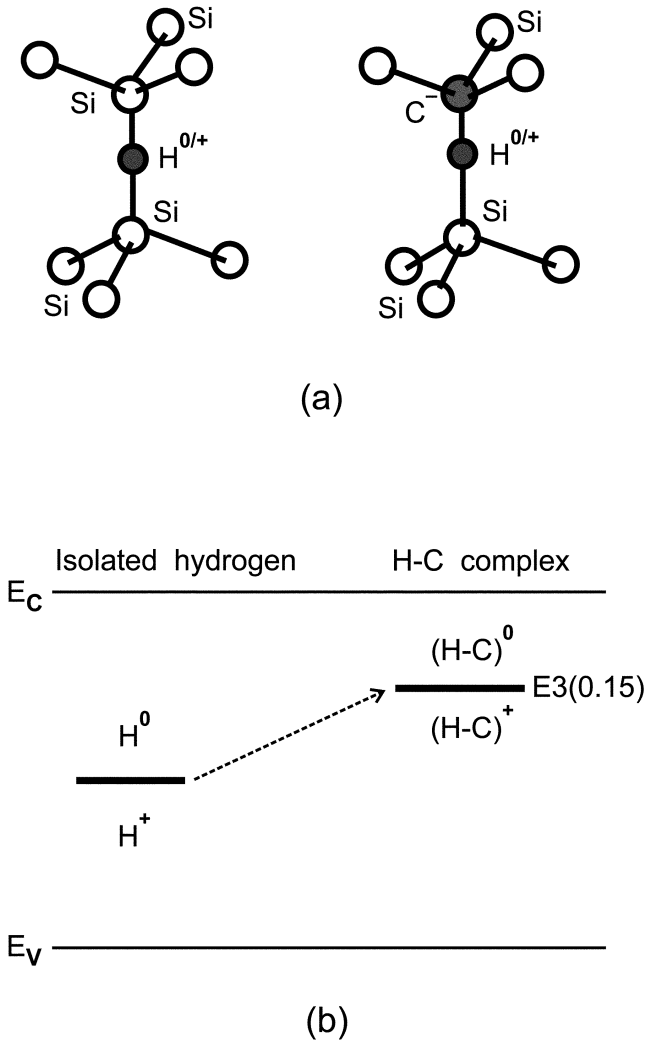

FIG. 24. Defect model of the H-C complex in comparison with that of isolated hydrogen, which tends to reside inside a silicon-silicon bond in the positive and neutral charge states (a), while hydrogen resides inside a silicon-carbon in the H-C complex (b). Because carbon has a stronger electronegativity than silicon, it attracts bonding electrons and subsequently has an effectively negative charge state. Such a carbon atom, in turn, attracts a proton and conversely repulses the donor electron bound to the proton thus delocalizing its wavefunction. This raises the hydrogen donor level, which is originally located near the midgap in the isolated state, to $E_C - 0.15$ eV of the H-C complex (redrawn from Ref. 142, with permission).

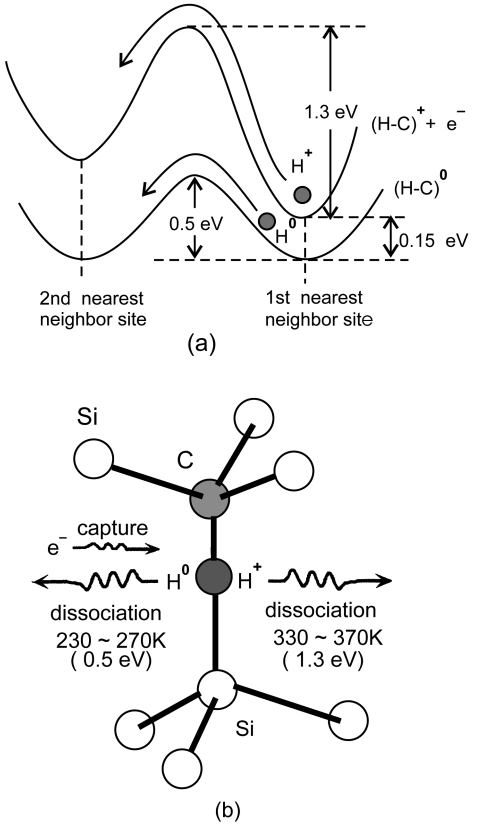

FIG. 25. Configurational coordinate diagram illustrating the total energy of the H-C complex in the positive and neutral charge states (a), and the illustration of the dissociation of the complex using an atomic model (b). In (a), the upper curve represents the potential for hydrogen in the positive charge state around carbon. Hydrogen must break its bond with carbon and silicon when it moves away from them. The lower curve shows that hydrogen moves freely in the neutral state without any attractive force exerted by carbon and silicon. In (b), when its charge state remains positive by reverse-bias annealing, the complex is dissociated by atomic jump of hydrogen with an activation energy of 1.3 eV. If the charge state of the complex is changed to neutral, due to capture of an electron, the barrier height is lowered to 0.5 eV to enhance the dissociation of the complex (redrawn from Ref. 142, with permission).

4.3.2 Hydrogen-Related Defect Complexes

The interaction of hydrogen with defects has been investigated in proton implanted Si,[131,149–155] and in electron irradiated Si samples hydrogenated in either a mixture containing HF[156–159] or in boiling water.[160] Most of these studies have focused on the electron traps related to hydrogen-defect complexes and much has been learned about the vacancy-oxygen-hydrogen (V-O-H) complex ($E_C - 0.32$ eV). However, as will shortly become obvious, there is still controversy concerning the structure of the hydrogen-related hole trap at $E_V + 0.28$ eV. More research work is yet to be carried out in order to confirm the tentative structural assignment of other hydrogen-defect complexes. It is pointed out here that the lowest energy state for hydrogen is bonding to the dangling bond of a vacancy type defect, and irradiation-induced defects, such as V—V (or V_2) and V—O center, involving broken bonds.[161] Using *ab initio* molecular dynamic simulations Hastings *et al.*[162] have found that hydrogen is trapped at vacancy aggregates V_n ($n =$ number of vacancies) by forming a strong Si-H bond around which the rest of the defect reconstructs. They found no correlation between the stability of V_n and the binding energy of H to it. Furthermore, none of the small V_n aggregates ($n \leq 5$) could be passivated by trapping a single H. In the case of V_2, a fully saturated complex contains eights hydrogen atoms assuming a chemically driven partial dissociation of the original V_2 configuration.[167]

Irmscher *et al.*[131] have compared the DLTS spectra for H- and He-ion irradiation of *n*- and *p*-type Cz grown Si. They found that whereas He-ion irradiation introduced the same set of defects as electron irradiation, room temperature H-irradiation introduced five electron traps and one hole trap in addition to the previously observed defects. These levels were named E2 ($E_C - 0.10$ eV), E3 ($E_C - 0.13$eV), E7 ($E_C - 0.32$ eV), E10 ($E_C - 0.41$ eV), E11 ($E_C - 0.45$ eV), and H2 ($E_V + 0.28$ eV). The properties of E3 have been discussed in detail in the previous section. DLTS depth profiling indicated that the distribution of these H-related defects followed the expected ion distribution profile (calculated from TRIM) for 300 keV protons, whereas the profiles of the "pure" radiation induced defects resembled distributions of energy deposited into atomic processes. Isochronal annealing showed that the concentrations of most of the defects could be drastically reduced by annealing in the 400–600 K temperature range. Moreover, it was found that both H-related levels E7 and H2 were always present in the same concentrations in unannealed samples, regardless of the doping level, and change their (equal) concentrations simultaneously during annealing. Therefore Irmscher and co-workers concluded that the E7 and H2 levels represent two charge states of one and the same H-related defect complex. These two levels were somewhat later speculated to be the single acceptor and donor states of an interstitial proton-related carbon defect complex, C_i-H.[164] They further remarked that the production of H-related levels at room temperature depended in a complex manner on charge state and recombination influences, and these levels were dominant in samples implanted before Schottky barrier fabrication.

Hüppi[149] also observed hydrogen-related defects in Si. The samples were p^+-n-n^+ diodes fabricated on ⟨111⟩ oriented, dislocation free, neutron transmutation doped FZ Si with a resistivity of 60 Ωcm. The diodes were implanted with 1.5 MeV protons at an angle of 7° off normal incidence to a dose of 5×10^{10} cm^{-2}. The proton energy and diode thickness were chosen to locate the protons in the low-doped *n*-base. The two most prominent H-related defects that they observed, E(175 K) and H(148K) were located at $E_C - 0.31$ eV and $E_V + 0.26$ eV,

respectively. Following Irmscher,[164] Hüppi assumed that the two defects were the single acceptor and donor states of C_i-H, respectively. Hüppi also used the Schockley-Read-Hall recombination statistics in order to determine the efficiency of the proton-implantation induced defect levels as minority carrier recombination centers. An eight hour anneal at 300°C revealed an increase in the concentration of E(175 K), making it by far the most dominant electron trap. Following the complete annealing of divacancies (V_2), the dominant recombination centers in proton implanted *n*-type Si were the two H-related defects, E(175 K) and H(148 K), as well as the (C_i-O_i) complex H(205K).

In another comparative study of proton, deuterium, and helium ion implanted Cz ($\sim 1 \times 10^{18}$ cm^{-3} oxygen) and Fz ($\leq 3 \times 10^{15}$ cm^{-3} oxygen) *n*-type Si wafers with free carrier concentration in the range from 1×10^{14} to 2.5×10^{15} P cm^{-3}, Palmetshofer and Reisinger[151] detected two hydrogen-related electron traps E(0.30) and E(0.39) with levels at $E_C - 0.30$ eV and $E_C - 0.39$ eV, respectively. E(0.39) was observed as a shoulder on the high-temperature side of the defect peak E(0.41) due to the superposition of the V–P and $V_2^{0/-}$ peaks. Based on its electronic signature, E(0.30) is the same defect as E7[131] and E(175 K).[149] The introduction of E(0.30) during proton implantation exhibited several features, including: (a) a nonlinear production behavior, with its concentration increasing nearly quadratically with fluence below 5×10^{10} cm^{-2}. The investigation of the defect concentration in various samples bombarded with different doses of H^+ ions revealed a universal dependence of the defect concentration on ion dose and phosphorous level. A deviation of the quadratic production behavior was observed at the higher proton fluences; a peak defect profile at a higher depth compared to vacancy-related defects, but coinciding with the peak hydrogen ion distribution; negatively charged vacancies that diffuse via the electric-field-enhanced diffusion mechanism are responsible for its formation. Based on these observations, Palmetshofer and Reisinger[151] concluded that the defect E(0.30) was a H-V complex that is formed along the reaction:

$$\text{(P-V)} + \text{H} \rightarrow \text{(H-V)} + \text{P} \qquad [28]$$

Palmetshofer and Reisinger also found that the production of the defect E(0.30) was drastically reduced to below 10% for bombardment with a negative bias applied to the Schottky contact. They therefore argued that the reaction (Eq. 28), was only efficient when the (V-P) pair was negatively charged.

Two hydrogen-related electron traps E3 and E5 at approximately $E_C - 0.32$ eV and $E_C - 0.45$ eV, respectively, have also been observed by Svensson *et al.*[150] in 1.3 MeV proton implanted high purity *n*-type FZ silicon. Similar to depth distribution of E(0.30) observed by Palmetshofer and Reisinger,[151] the depth distributions of E3 and E5 revealed that the generation process was not only linked to the elastic deposition but also hinged strongly on the hydrogen implantation profile. The broader experimental depth profiles of E3 and E5 compared to the theoretical distribution of the hydrogen was attributed to the relatively mobile hydrogen at room temperature. The dose dependence study of Svensson *et al.*[150] showed that E3 and E5 were caused by low order complexes that could be destroyed during interaction with radiation-induced defects or impurities mobile at room temperature. Because the proportionality constant between the two levels decreased with dose, and σ (E3) $\gg \sigma$ (E5), the two levels could not be due to the same defect. This conclusion is consistent with the results of Hüppi[149] that only E3 was present after annealing for 8 h at 300°C. Svensson *et al.*[150] speculated that E3 and E5 could be complexes involving partly hydrogen-saturated A-center (V-O) and V_2 configurations that could be slightly distorted. Their isothermal annealing experiments of 5.4 MeV self-ion implanted Cz *n*-type Si later showed that the concentration of E3 increased slightly as the concentration of V_2 decreased.[165] This result was interpreted as a limited supply of hydrogen giving rise to an increase of the $\sim E_C - 0.32$ eV trap, a partly saturated divacancy, and a corresponding decrease of V_2.

There is at present ample experimental evidence to show that the hydrogen-related electron trap at $\sim E_C - 0.32$ eV, that is, E7,[131] E3,[150] E(175K),[149] and E(0.30),[151] is a complex involving the V-O center and a single hydrogen, that is, the V-O-H complex. Before turning to the identification of the V-O-H complex, the authors first review the recent results of Lévêque *et al.*,[155] who have investigated the properties of defects E3 and E5 (following nomenclature used in Refs. 150 and 165) in 1.3 MeV proton implanted *n*-type Fz Si and oxygen-lean epitaxial Si layers grown by molecular beam epitaxy. In light of the identification of the E3 defect as the V-O-H complex, Lévêque *et al.* [155] have provided an alternative interpretation of the results obtained previously by Lalita *et al.*[165] During annealing in the temperature range 200°C to 300°C dissociation of V_2 increases the concentration of free vacancies that may become trapped by interstitial oxygen atoms (*i.e.*, enhanced formation of V-O centers), and subsequently, V-O-H complexes are formed in the case of a sufficient supply of migrating hydrogen atoms. They also performed a systematic study of the isochronal annealing behavior of both E3 and E5 in the temperature range 100°C to 300°C. No correlation was observed between the loss of V-P centers and the formation of E3, and they ruled out the reaction described by Eq. 28. Based on the similar annealing behavior of V_2 and E5, they suggested that E5 was most probably a complex involving hydrogen and V_2 with a break-up mechanism similar to that proposed for V-O-H^0 by Johannesen *et al.*[166] Lévêque *et al.*,[155] also observed that the concentration of E5 was two times larger in Epi-Si as compared to Fz-Si, whereas the concentration of V-O centers was four times larger in the Fz-Si. Because of the competition between V-O and V_2 to trap hydrogen, the concentration of E5 is expected to be larger in oxygen-lean Si (*i.e.*, epitaxial Si) if it were indeed a complex involving V_2 and H.

The authors now turn to the identification of the $\sim E_C - 0.32$ eV level as the V-O-H complex. Gutsev *et al.*[167] have used Modified Neglect of Diatomic Overlap (MNDO) calculations to determine the configurations containing one or two hydrogen atoms in the A-center. It was found that the electrical activity of the A-center was decreased by hydrogen passivation of the two silicon dangling bonds, but the resulting defect states were not removed from the band gap. In fact, their MNDO simulations suggested that the V-O-H and V-O-H_2 complexes should have lower energy level positions in the band gap than the V-O-center. Feklisova and Yarykin[156] studied the transformation of deep level spectra of high-energy electron irradiated *n*- and *p*-type Cz Si due to hydrogenation under wet chemical etching. They observed the hydrogen-related electron traps E4 ($E_C - 0.32$ eV) and E5 ($E_C - 0.36$ eV) in the *n*-type Si, and hole traps H3 ($E_V + 0.16$ eV) and H4 ($E_V + 0.27$ eV) in the *p*-type Si. Because the concentration of E4 and E5 close to the surface could exceed the concentration of V_2 deep in the crystal volume, Feklisova and Yarykin inferred that the two traps could originate only from the A- and K-centers. Based on the evolution of the concentration profiles of A-centers and E4 in annealed samples, it became clear that E4 was a complex involving the A-center. Furthermore, the authors developed a model to determine the number of H atoms in the defects from their DLTS profiles and arrived at the conclusion that E4 was a complex involving the V—O center and two hydrogen atoms (*i.e.*, V-O-H_2 complex). However, Peaker *et al.*,[158] have recently expressed the view that the V-O-H_2 complex should be inert and introduce no level in the band gap. Moreover, Bonde Nielsen *et al.*[152] have provided the evidence that the hydrogen-defect with a level at $E_C - 0.31$ eV (*i.e.*, corresponding to defect E4 in Ref. 156 displayed orthorhombic-I symmetry and ruled out that it contained two hydrogen atoms.

More recently, Johannesen *et al.*[166] have characterized proton or deuteron implanted FZ and Cz silicon at ~50 K using EPR measurements. They observed a novel signal in the oxygen-rich Cz Si, which displayed a transition from monoclinic-I to orthorhombic-I symmetry in the temperature ranges 180–240 K and 230–290 K in the proton and deuteron-implanted samples, respectively. The vacancy-type nature of a defect with an unpaired electron confined to a dangling-bond orbital was deduced from the *g* tensor observed at low-temperature as well as the large ^{29}Si hyperfine splitting. Proton hyperfine splitting further showed that a single hydrogen atom was incorporated in the defect. Their observations allowed an unequivocal assignment of the signal to the neutral charge state of the V-O center containing only one hydrogen atom, that is, the V-O-H^0 complex. They also found that the hydrogen atom could jump rather easily between two equivalent sites lying in the ⟨110⟩ mirror plane of the defect.

Tokuda and Seki[159] have also investigated the interaction of hydrogen with the V-O pair produced in *n*-type Cz Si by 10 MeV electron irradiation. They observed a defect labelled NH1 ($E_C - 0.31$ eV) resulting from reaction of the V-O center with hydrogen. Figure 26 illustrates the depth profiles of the A-center and the NH1 defect for the electron-irradiated sample after chemical etching for 10 h and subsequent illumination for 100 h. It can be seen that the concentration of both the A-center and the NH1 defect decrease close to the surface where the concentration of hydrogen is expected to be maximum. They found that the decreased A-center concentration was larger than the NH1 defect concentration over the measured depth. The difference between the decreased A-center concentration and the NH1 defect concentration was considered to be the concentration of passivated A-centers, which lose their electrical activity. Their results supported the idea that the NH1 defect resulted from a partly saturated A-center, and proposed the following reactions between the A-center and hydrogen:

$$\text{A-center (vacancy-oxygen pair)} + x\text{H} \rightarrow \text{NH1} \quad [29]$$

$$\text{NH1} + y\text{H} \rightarrow \text{passivation of the A-center} \quad [30]$$

Although x and y represented undetermined numbers of hydrogen atoms in Ref. 159, values of $x = 1$ and $y = 2$ can be expected following the experimental results of Bonde Nielsen *et al.*,[152] Peaker *et al.*,[158] and Johannesen *et al.*[166] Further, note that the loss of V-O is not equal to the gain in V-O-H on hydrogenation because some V-O-H_2, which is inert, is also formed. The branching ratio was found to depend on the hydrogen concentration [168]. The V-O-H complex was also detected by Ohmura *et al.*[159] in hydrogenated electron beam irradiated *n*-type ⟨111⟩ Si epitaxial layers. Hydrogenation was performed by boiling irradiated samples in H_2O or D_2O at 120°C in a medical autoclave. Reappearance of the V-O center on isochronal annealing in the temperature range 175°C to 250°C after hydrogenation (and the simultaneous disappearance of the V-O-H complex) suggested that the disappearance of the V-O center by hydrogenation was not due to the destruction of the latter, but a mere vanishing of its electronic level due to the formation of the partly saturated V-O-H complex.

It is pointed out here that the comparison between the depth profiles of the A-center and NH1 defect are qualitatively similar to that between the concentration profiles of the A-center and defect E4 from Feklisova *et al.*[156] Peaker *et al.*[158] have also observed that only the V-O-H center could be observed between 0.9 to 1.6 μm in their chemically etched electron irradiated samples. They could, however, detect the V-O-H complex as well as the V-O center when profiling between 0.9 to 2 μm below the surface of the samples. Peaker *et al.*[158] pointed out that the concentration of the V-O-H center could not fully account for the decrease in the number of A-center, modified or otherwise. However, the results obtained by Laplace DLTS were in qualitative agreement with the defect reactions described by Eqs. 29 and 30.

Tokuda *et al.*[153] have also investigated the effect of light illumination on the hydrogen-related electron traps E(0.32) ($E_C - 0.32$ eV) and E(0.49) ($E_C - 0.49$ eV). The defects were

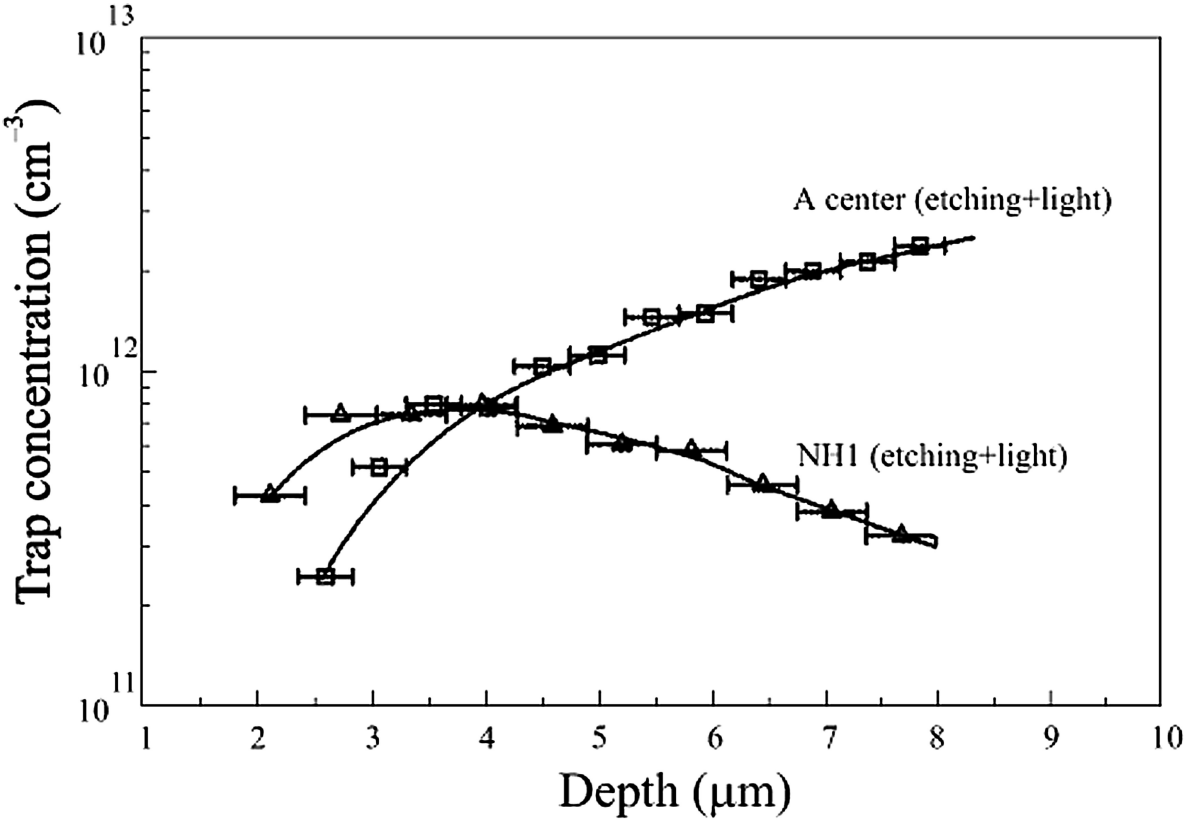

FIG. 26. Depth profiles of the A center and the NH1 defect for the electron-irradiated sample after etching for 10 h and subsequent light illumination for 100 h.[159]

introduced in *n*-type Cz Si by 170 keV hydrogen implantation to a fluence of 2×10^{10} cm^{-2} with a fluence rate of 1×10^{10} cm^{-2} s^{-1} at room temperature. Phosphorous implantation was also performed at an energy of 300 keV (fluence $= 1 \times 10^{9}$ cm^{-2}; fluence rate $= 1 \times 10^{9}$ cm^{-2} s^{-1}) for comparative purposes. Figure 27 shows the DLTS spectra for the sample illuminated by a GaAs LED (peak emission at $\lambda = 940$ nm) for (a) 0, (b) 30, or (c) 300 min under zero bias. The peak heights of the vacancy-related traps: E(0.15), E(0.21) and E(0.39) (V-O, $V_2^{=/-}$, and $V_2^{-/0}$+ V-P, respectively) decrease by light illumination, whereas the peak heights of the hydrogen-related traps: E(0.32) and E(0.49), increase. The changes in peak heights of the defects, $\Delta C/C_\infty$, are illustrated in Figure 28 as a function of illumination time. The solid lines through the data points in Figure 28 were calculated based on a first order reaction with time constant of 36 min. Hydrogen was identified to play an important role in the light-illumination effects because no such effects were observed in phosphorous-implanted samples. Furthermore, the decrement of $\Delta C/C_\infty$ for the E(0.15) trap corresponded to the increment of $\Delta C/C_\infty$ for the E(0.32) trap, which was direct confirmation that the V-O center was transformed by hydrogen into the E(0.32) defect. These results are consistent with the identification of the E(0.32) trap as the V-O-H complex. Based on the results in Figure 28, and those of Svensson *et al.*,[150] the authors proposed that the trap E(0.49) was a complex involving the divacancy and hydrogen, which is consistent with the recent suggestions of Lévêque *et al.*[155]

Tokuda and coworkers[153] also found that the light illumination-induced defect transformations did not take place when the Schottky diode was placed under reverse bias, indicating that the transformations occurred only when the defects were outside the depletion region. They concluded that excess electrons were involved in those defect transformations. In addition, forward current injection without light illumination also transformed the defects, albeit with a reaction time constant of 100 min, which was further support for the idea that excess electrons caused the defect transformations. The difference of the time constants was ascribed to different amounts of excess electrons available between the two methods. They proposed that, similar to the dissociation of the H-C complex under light illumination[142,144] (discussed in section 4.3.1), there exist hydrogen-containing defects that are unstable due to the change of their charge state by capturing electron under light

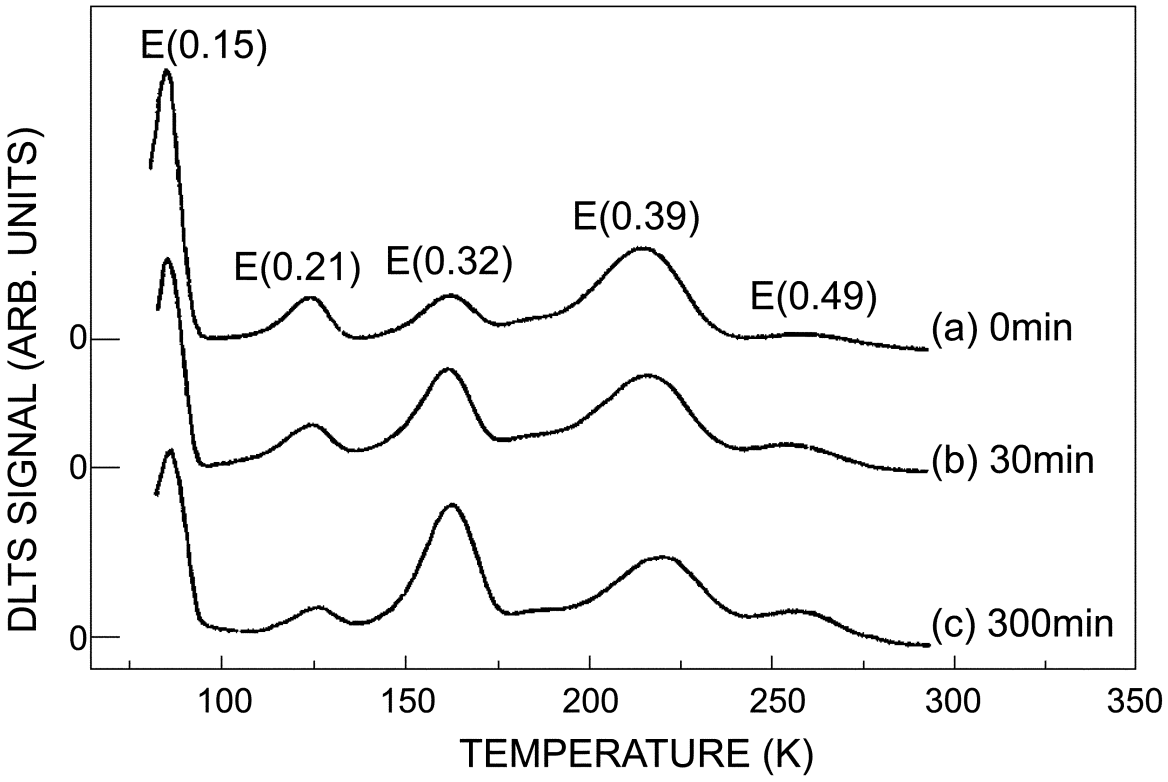

FIG. 27. DLTS spectra for the hydrogen-implanted sample, which is illuminated by light using a GaAs LED for (a) 0, (b) 30, and (c) 300 min with the application of zero bias to a Schottky diode.[153]

illumination and forward current injection. The free hydrogen atoms then complex with the available V-O centers and V_2 to form E(0.32) and E(0.49), respectively. They speculated that the undetected hydrogen-containing defects could have energy levels in the upper half of the band gap (too shallow to be detected by DLTS measurements above 85 K) because defects with energy levels in the lower half of the band gap are less stable due to electron occupation. The limited source of these hydrogen-containing levels results in the saturation effect observed for prolonged light illumination.

The acceptor levels (−/0) of the V-H and V_2-H defects in silicon have been identified by Bonde Nielsen *et al.*[152] from comparison of Laplace DLTS and EPR annealing data. Bech Nielsen *et al.*[169] have identified the EPR signal related to the neutral charge state of the vacancy containing a single hydrogen atom, that is, V-H^0, in proton implanted FZ silicon. The signal displayed monoclinic-I symmetry below 65 K and trigonal symmetry above 100 K. The properties of the V-H^0 complex are determined almost completely by the silicon dangling bonds. They also reported on the striking similarity between the properties of the V-H^0 and the E-center (V-P pair), which indicated that the Si-H fragment could be regarded as a "pseudo-group-V-impurity." Furthermore, as explained by Bonde Nielsen *et al.*,[152] a vacancy-hydrogen defect (V_n-H) should typically contain a dangling bond with an unpaired electron or a lone pair in addition to the bond that has been saturated by hydrogen and may also contain elongated bonds forming bridges between Si-Si neighbors. Then it is the wave function of the dangling bond electrons that predominantly determines the electronic properties of the vacancy-hydrogen complexes. V_n-H defects would, therefore, be expected to give rise to families of very similar deep levels in silicon.

Figure 29 illustrates the Laplace DLTS spectra from He and H implanted p^+n-diodes made on FZ Si. The contribution of V-P-centers to the DLTS spectra was eliminated by annealing samples at 400 K under reverse bias. Only the acceptor level of the divacancy, $V_2^{-/0}$, is common to both spectra. Although the origin of the second main peak in the helium-implanted sample remains unknown, it could be due to a more complex vacancy cluster formed as a result of the denser collision cascades of the He implantation. After 400 K annealing two hydrogen-related defects could be observed, which have been assigned to the V-H and V_2-H complexes. These positive identifications follow from the correlation between the Laplace DLTS and EPR isochronal annealing data shown in Figure 30. Bonde Nielsen *et al.*[152] extracted activation enthalpies of 0.443 eV and ∼0.43 eV for the V-H(0/–) and V_2-H(0/–) complexes, respectively.

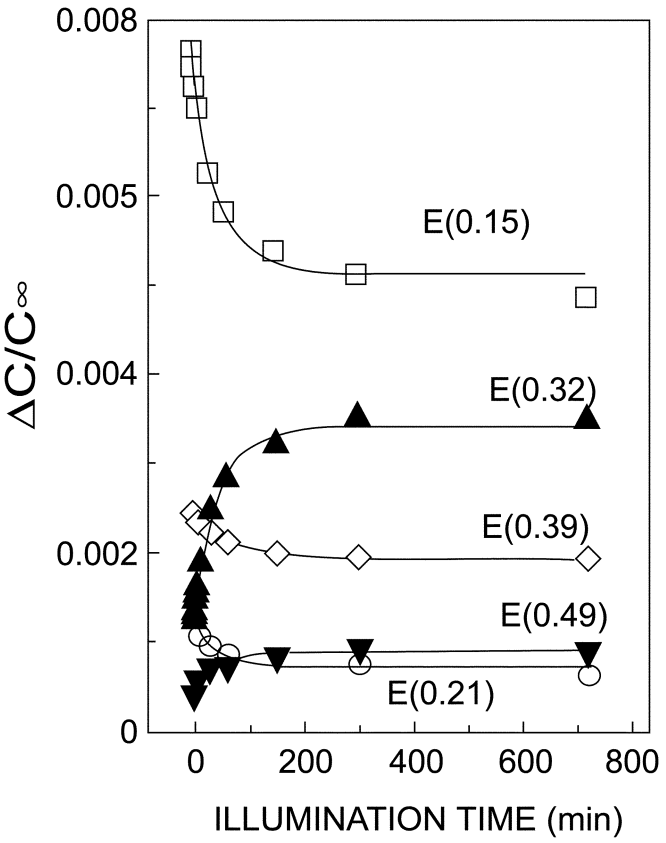

FIG. 28. $\Delta C/C_\infty$ for traps as a function of light illumination time with the application of zero bias to the Schottky diode.[153]

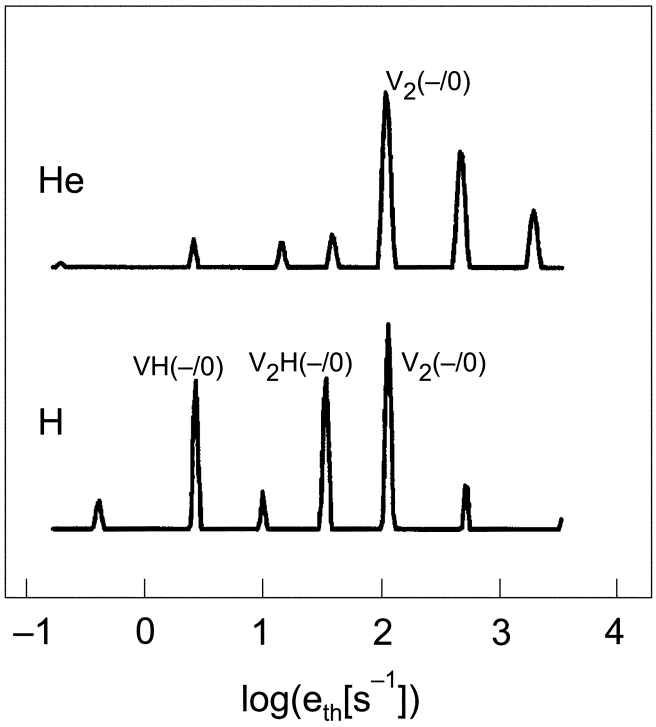

FIG. 29. Comparison of Laplace DLTS spectra measured at 225 K and displayed as function of emission rate (e_{th}).[152] Lower plot: hydrogen-implanted sample ($\sim 10^{10}$ cm^{-2}), upper plot: Helium-implanted sample ($\sim 10^{9}$ cm^{-2}). The samples (FZ silicon) have been implanted at 60 K and reverse bias annealed at 400 K. See Figure 31 for the assignment of the emission-rate peaks to VH and V_2H (redrawn from Ref. 152, with permission).

Only few studies have recently investigated the hydrogen-related hole trap at $\sim E_V + 0.28$ eV (H2 in Ref. 131 and H(148 K) in Ref. 149) in the *p*-type Si.[154,157] Feklisova *et al.*[157] have observed the hole trap H4 ($E_V + 0.28$ eV) in chemically etched high-energy electron irradiated *p*-type Cz Si after RBA at 380 K. Only the defect peaks associated with $V_2(0/+)$ and K-center (C_i-O_i) were detected in the irradiated and hydrogenated samples (*i.e.*, no RBA). The appearance of H4 was accompanied by the partial disappearance of both the divacancy and the K-center. Feklisova *et al.* used the depth profiles of activated boron and those of the H4- and K-centers illustrated in Figure 31 to infer that the H4 center was a product of the K-center hydrogenation. The boron passivation observed around 2 μm was taken as evidence that the defect reactions occurring at that depth were due to hydrogen. For 1 h annealing, the sum of the K- and H4-center concentrations were constant. This constancy remained valid for a wide set of samples (both Cz and FZ) and irradiation doses, which indicated that the H4-centers were formed at the expense of the K-centers. Further annealing, however, broke that constancy and the H4-center depth profile exhibited a local minimum in the region with the highest hydrogen concentration (see Figure 31c). The authors mentioned that this phenomenon was consistent with the model that another hydrogen atom was added to the H4-complex, but did not detect any defect with concentration comparable to those of the K- and H4-centers, and with energy level located between ~0.1 eV above the valence band and the midgap.

In another study, Fatima *et al.*[154] have studied the interaction of hydrogen with implantation-induced point defects in *p*-type epitaxial, Cz and FZ Si (6–8 Ωcm). Defects were created by 0.30 or 0.20 MeV H, 2 MeV B or 2.8 MeV C ion implantation through predeposited Ti Schottky barrier diodes on the *p*-type samples at room temperature and at various ion fluences (10^9–10^{10} cm^{-2}). Prior to implantations the diodes were annealed at 200°C in order to recover the electrical activity of boron that was passivated during the chemical cleaning preceding metallization. No deep levels in the lower half of the band gap were detected in the unimplanted samples. Figure 32 illustrates the DLTS spectra of *p*-type Cz Si implanted with 0.30 MeV H at RT to a dose of 3.5×10^{10} cm^{-2}

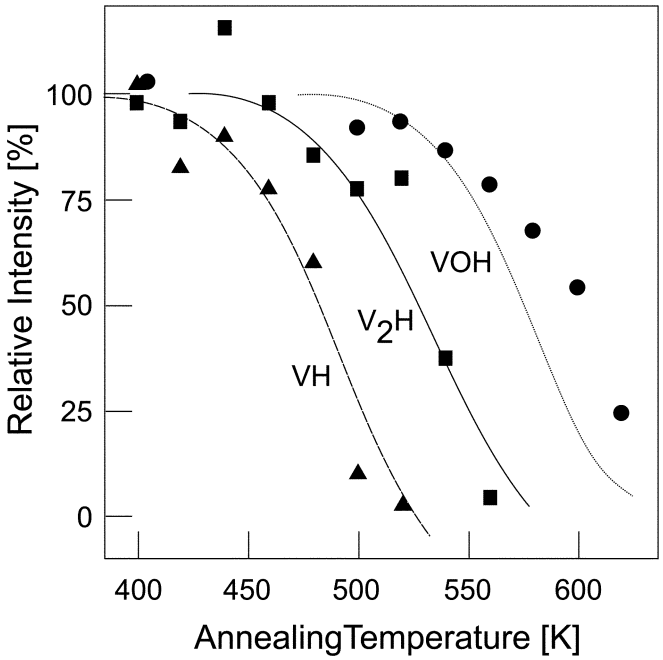

FIG. 30. Correlation of Laplace DLTS and EPR isochronal annealing data. The data points refer to emission peaks and the smoothed curves to EPR data (redrawn from Ref. 152, with permission).

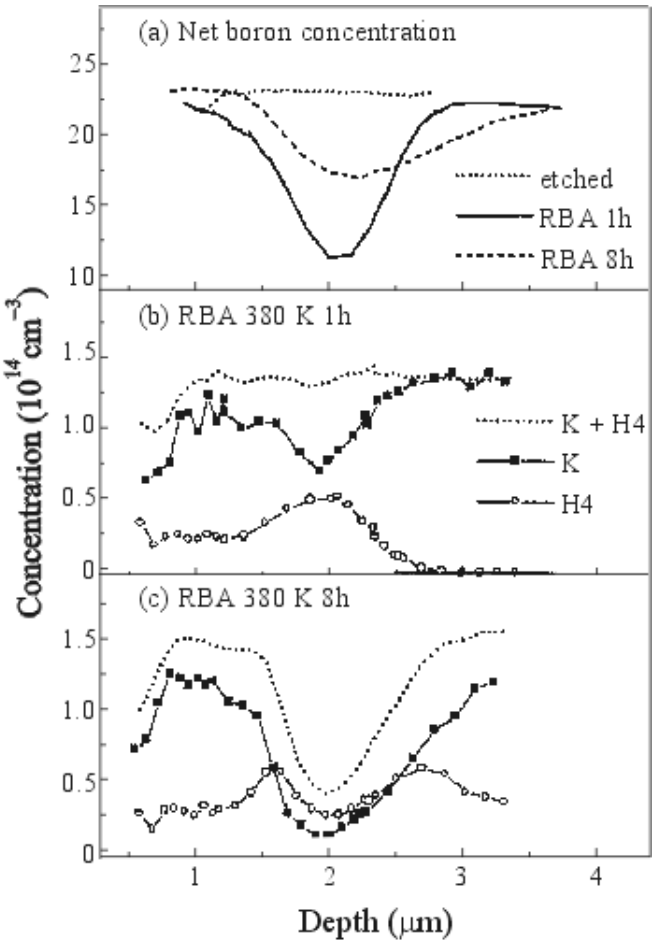

FIG. 31. Depth profiles (a) of the net acceptor concentration at different annealing stages and (b, c) deep-level centers in *p*-type Cz-Si taken after reverse-bias annealing at 380 K during (b) 1 h and (c) 8 h (redrawn from Ref. 157, with permission).

and annealed at 150°C for 30 min. Similar to what has been observed by Feklisova *et al.*,[157] the intensity of the level at $E_V + 0.28$ eV increased upon annealing whereas those of V_2 and K-centers decreased. In order to investigate the role of hydrogen in the annealing of V_2 and C_i-O_i, Si implanted samples were also annealed at 150°C. Fatima *et al.*[154] found that the reduction in the C_i-O_i peak was similar in both hydrogen and silicon implanted samples and, contrary to the results of Feklisova *et al.*,[157] concluded that annihilation of the K-center was not influenced by hydrogen. In other words, the level at $E_V + 0.28$ eV was not a product of hydrogen interaction with the K-center. In addition, the authors did not observe any saturation of the K-center peak intensity with the increasing fluence of hydrogen.

The ion implantation experiments of Fatima *et al.*[154] were also aimed at identifying the origin of the scarcely studied hydrogen-related hole trap at $\sim E_V + 0.51$ eV. Figure 33 shows the DLTS spectra from (a) H and He implanted Fz Si, and (b) B and C implanted Cz Si. It was clearly shown in this study that the level at $E_V + 0.51$ eV was a defect involving hydrogen. In the C implanted samples, no level related $E_V + 0.51$ eV was observed. On the other hand, that peak was quite prominent in the B implanted samples. Another remark made was that the level at $E_V + 0.28$ eV was not introduced in C and B implanted samples. The authors observed a linear dose dependence for the introduction of V_2 in Si implanted samples (doses normalized to yield equivalent number of vacancies/ion as hydrogen). The linear dose dependence revealed a dilute concentration regime, where the concentration of V_2 was not large enough to effect trapping of migrating defects for the formation of larger complexes. The saturation in the concentration of V_2 for the higher fluences was, therefore, attributed to the passivation of V_2 by hydrogen. Based on the results shown in Figure 33, Fatima *et al.*[154,170] have proposed that the level at $E_V + 0.51$ eV was the hydrogen-boron interstitial complex. In *p*-type Si, a competition takes place between acceptors and C_s atoms for capturing migrating Si interstitials, Si_i.[116] Preferential formation of B_i atoms takes place because the capture cross section of Si_i at B_s (substitutional B) is about seven times larger than for Si_i at C_s.[114] These mobile B_i atoms then pair with hydrogen to form the B_i-H complex. At the higher fluences hydrogen partially or fully passivates the V_2 and less are available for complexing with B_i.

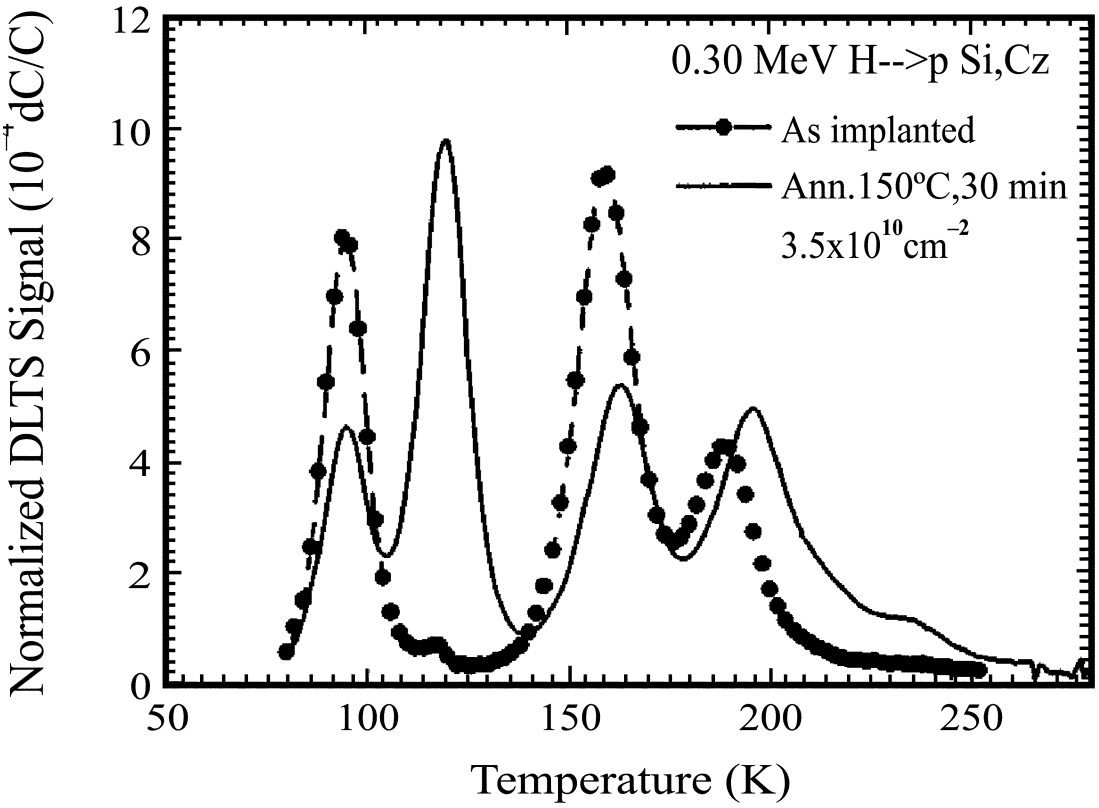

FIG. 32. DLTS spectra of *p*-type Si (Cz), implanted with H ions at RT to a dose of 3.5×10^{10} cm^{-2} and annealed at 150°C for 30 min. As-implanted spectra are also included for comparison (redrawn from Ref. 154, with permission).

This section concludes with an overview of low-energy hydrogen ion implantation of Si. Bruni *et al.*[171] have used transient capacitance, capacitance-voltage, and spreading resistance profiling to investigate the electrical properties of *p*-type Cz Si bombarded with 31 keV H_2^+ (equivalent to an energy of 15.5 keV) to a dose of 1.6×10^{16} H/cm^2. Isochronal annealing experiments were performed on implanted samples in vacuum in the temperature range 100–800°C. In particular, they investigated the interaction of hydrogen with implantation-induced defects, and the neutralization of shallow acceptor dopants (*i.e.*, B_s). Typical DLTS spectra obtained for these samples consisted of a single broad peak, whose amplitude decreased exponentially with the rate window. The Arrhenius plot of this peak deviated from linearity, and they assumed it was a superposition of two discrete defects. One of the defect peaks could be resolved using a filling pulse width of 0.01 ms, so that its activation energy was known. A fitting procedure was then employed to extract the energy of the second defect. This procedure revealed three hole traps H(0.23), H(0.33), and H(0.67) in the 15.5 keV H-implanted and annealed *p*-type Si. The values in brackets relate to the activation energies of defects relative to the valence band edge. Based on the assumptions that: (a) when the number *n* of H atoms belonging to the same vacancy increases, the electronic level associated with the complex V-H_n moves toward the valence band, (b) the completely decorated vacancy is not electrically active, and (c) the concentration of undecorated vacancies in their samples was negligible (peak hydrogen concentration was about six orders of magnitude greater than the bulk boron concentration), Bruni *et al.* speculated that H(0.67) and H(0.33) were due to the V-H_2 and V-H_3 complex, respectively.

Furthermore, Bruni *et al.*[171] used the amplitudes of the defect peaks as a rough estimate of the total concentration of hole traps in their samples. The relative DLTS signal amplitude is shown in Figure 34 as a function of annealing temperature. They concluded that for thermal annealing up to 300°C, hydrogen decorated vacancies, forming complexes with increasing thermal stability. That gave rise to H(0.33) and H(0.67), whose concentrations increased up to 250°C. The vacancies were completely decorated with hydrogen at 300°C (*i.e.*, formation of VH_4), and became electrically inactive. When $T \geq 400$°C, the vacancy-hydrogen are broken, inducing a partial vacancy depletion that restored the V-H_n electronic levels. Capacitance-voltage and spreading resistance measurements supported their model of defect evolution in their samples. There is at the present time too few studies on the electrical properties of low-energy

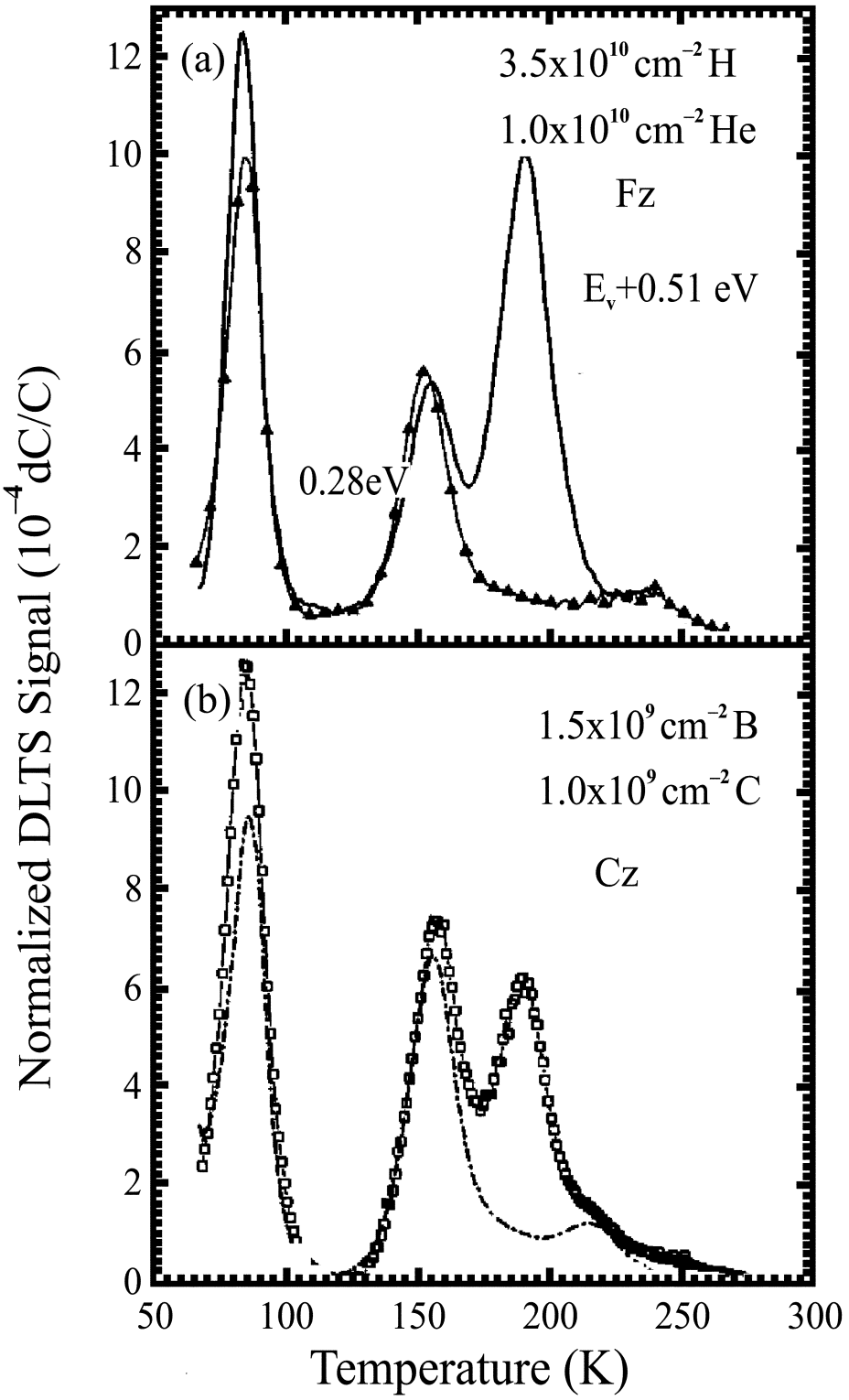

FIG. 33. (a) DLTS spectra of *p*-type Si (Fz), implanted with 0.3 MeV H and 5.35 MeV He ions at RT to a dose of 3.5×10^{10} and 1×10^{10} cm^{-2}, respectively. (b) DLTS spectra of *p*-type Si, Cz, implanted with 2.8 MeV C and 2 MeV B ions at RT to a dose of 1.5×10^{9} and 1×10^{9} cm^{-2}, respectively (redrawn from Ref. 154, with permission).

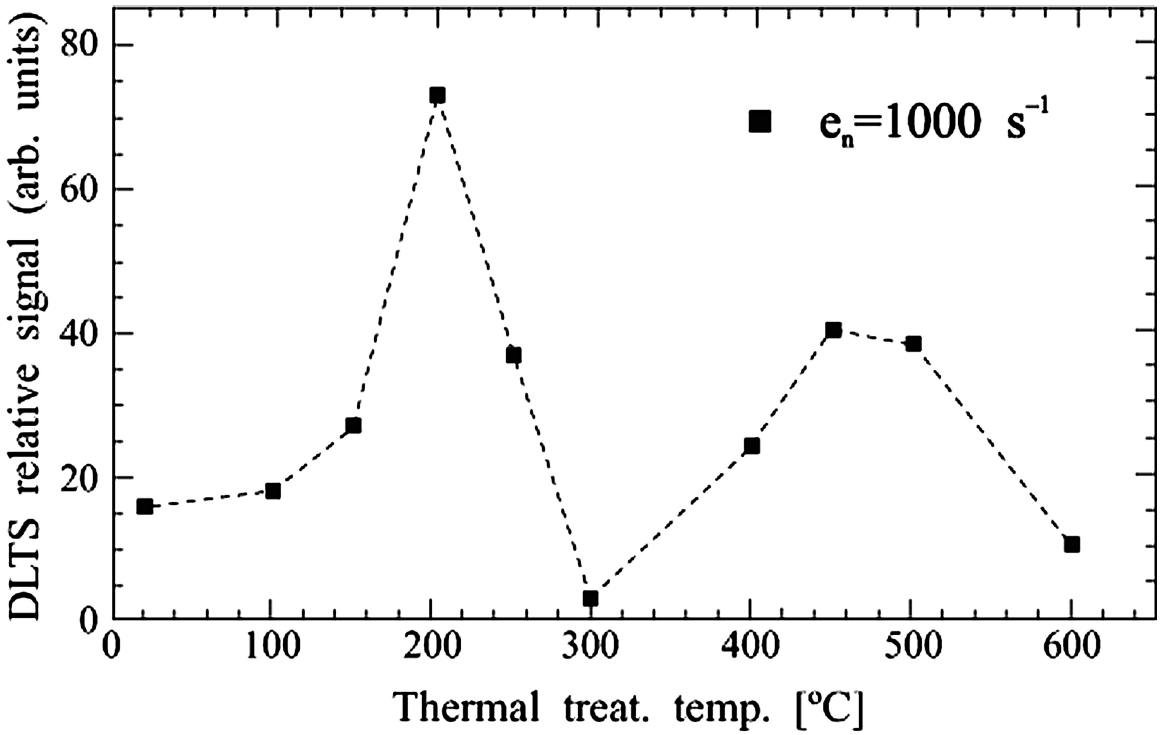

FIG. 34. Relative DLTS signal amplitude vs. sample annealing temperature (rate window: 1000 s^{-1}).[171]

hydrogen implanted *p*-type Si, especially in the high dose regime, for comparison with the results presented thus far. Moreover, theoretical calculations of the energy levels of the single vacancy decorated with hydrogen have yielded values, which are not only different, but also model dependent for deep level identification.[172,173]

More recently, Deenapanray[174] has studied the trap-limited migration of vacancy-type defects in 7.5 keV H-implanted *n*-type Cz Si (0.7–1.1 Ωcm). Samples were implanted to fluences in the range 1×10^{11} H cm^{-2} to 1×10^{15} H cm^{-2} at room temperature using a constant dose rate $\sim 10^{11}$ H cm^{-2} s^{-1}. The binary collision code MARLOWE[22–24] showed that the range of ions implanted 7° off the ⟨100⟩ direction was well within the zero-bias depletion region (∼0.3 μm) of SBDs used for electrical characterization of samples. A combination of DLTS and capacitance-voltage measurements showed that defects created in the top ∼0.25 μm were responsible for free carrier compensation to depths exceeding ∼1 μm. Figure 35a shows the DLTS spectra taken from samples implanted with 10^{11} H cm^{-2} [curve(a)], 10^{13} H cm^{-2} [curve(b)], and 10^{15} H cm^{-2} [curve(c)]. The main electron traps E3 ($\sim E_C - 0.28$ eV) and E4 ($\sim E_C - 0.43$ eV) were identified as the V-O-H complex and V-P-pair. Annealing at the modest temperature of 150°C for 20 min [spectrum (d)] removed ∼85% of E4, which followed the typical annealing property of the V-P-pair. The contribution of $V_2^{-/0}$ to E4 was also excluded based on the non-detection of the doubly negative charge state of the divacancy, and given that the V-P-pair is expected to be predominant in Cz samples with resistivity <1 Ω cm. The spectra in Figure 35a were recorded by probing sample depths between the edge of the zero bias depletion region and ∼1.2 μm. Consequently, the defect peak amplitude was taken as an estimate of the total defect concentration in an implanted sample.

The fluence dependence of the peak intensities of E3 and E4 are illustrated in Figure 35b. The peak intensity of E4 increased linearly with hydrogen fluence, whereas that of E3 showed a maximum at 1×10^{14} H cm^{-2}. This fluence dependence was in semiquantitative agreement with two distinct regimes for free carrier compensation in implanted samples. For fluences $\leq 10^{13}$ H cm^{-2}, the efficient trapping of O_i by single vacancies forms the V-O center, which then interacts with H to form the V-O-H complex. At the higher fluences, the formation of V-O-H became limited by both the consumption of the fixed concentration of O_i and the formation of electrically neutral V-O_2 and V-O-H_2 complexes. This is the cause of the cross-over in Figure 35b at a fluence of 10^{14} H cm^{-2} when the V-P pair became the dominant electron trap. Deenapanray[174] also correlated the introduction of the V-O-H complex and V-P pair with the free carrier concentration in implanted samples. A single electron trap with a characteristic diffusion length ∼0.29–0.31 μm was sufficient to account for the free carrier compensation for fluences $\leq 10^{13}$ H cm^{-2}, whereas an additional defect with characteristic diffusion length ∼0.070–0.075 μm was required to explain the compensation above 10^{14} H cm^{-2}.

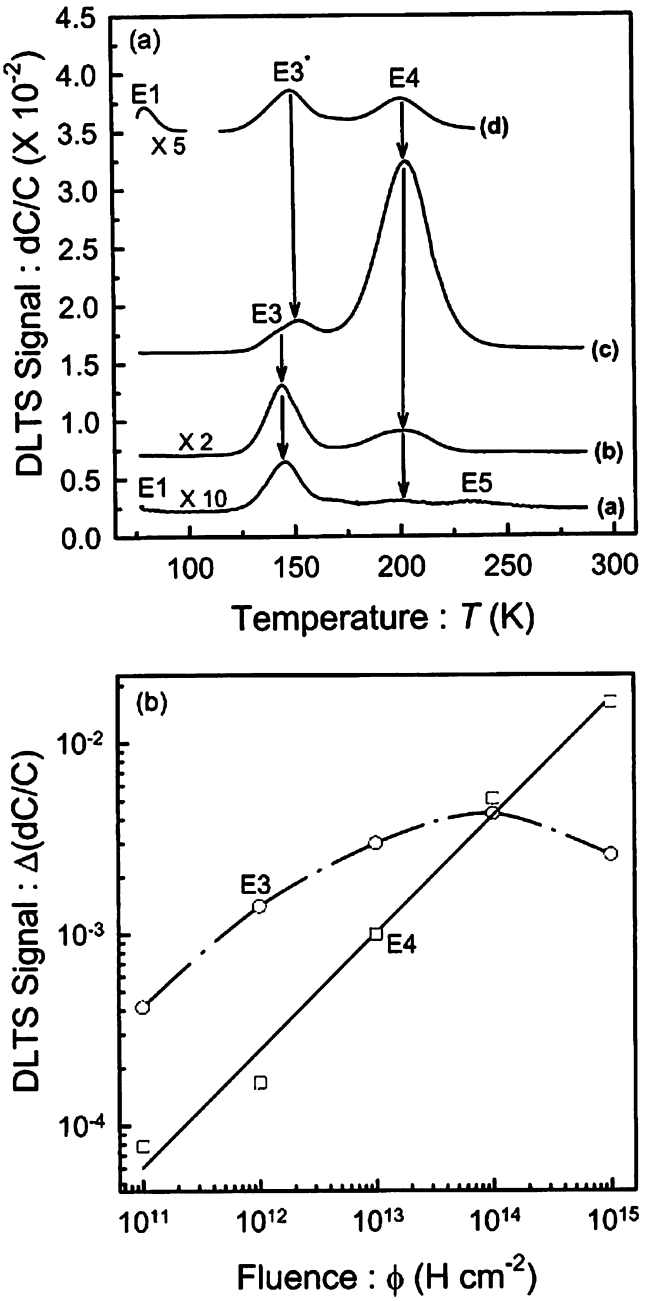

FIG. 35. (a) DLTS spectra from samples implanted with 10^{11}, 10^{13}, and 10^{15} H cm^{-2} (curves (a), (b), and (c), respectively). Spectrum (d) was measured from a sample implanted with 10^{15} H cm^{-2} and subsequently annealed under zero bias at 155°C from 20 min; (b) fluence dependence of the variation of the peak intensities of E3 and E4.[174]

5. CONCLUDING REMARKS

The electronic properties of primary defects created in both *n*- and *p*-type Si by electron-, proton- and alpha-particle irradiation have been reviewed. Although the focus has been on results obtained by deep level transient spectroscopy (DLTS), the authors have placed these results in a broader perspective by comparing them, to the best of their ability, with those obtained from other techniques that provide structural information about defects. In particular, the discussion has focused predominantly on the activation energy, electrical capture cross section, introduction rate, annealing kinetics, and physical structure of point defects in Si. The authors have also endeavored to encompass recent results obtained by high-resolution (or Laplace-) DLTS, which has significantly increased the spectroscopic ability of conventional DLTS. The behavior of hydrogen and its related defects has also been thoroughly discussed. The authors trust that this review will be of interest to both the scientific and technology communities. Furthermore, they sincerely hope that this work will stimulate the further review of defects generated by ion implantation, in particular by low energy ions, wherein interesting effects are observed due to the non-uniform creation of defects.

ACKNOWLEDGMENTS

The authors are grateful for the financial support of the National Research Foundation, South Africa. PNKD also acknowledges the financial support of the Australian Research Council. The authors owe gratitude to Walter E. Meyer and Simone Weidmann for compiling the figures used in this article. The authors are also indebted to Prof. Tony Peaker for his much appreciated comments on the manuscript.

REFERENCES

1. R. D. Rung, C. J. Dell'occa, and L. G. Walker, A Retrograde P-Well for Higher Density CMOS, *IEEE Trans. Electron. Devices* **28**, 1115 (1991).
2. J. L. Benton, J. Michel, L. C. Kimerling, D. C. Jacobson, Y.-H. Xie, D. J. Eaglesham, E. A. Fitzgerald, and J. M. Poate, The Electrical and Defect Properties of Erbium-Implanted Silicon, *J. Appl. Phys.* **70**, 2667 (1991).
3. E. A. White, K. T. Short, R. L. Dynes, J. P. Garno, and J. M. Gibson, Mesotaxy: Single-Crystal Growth of Buried $CoSi_2$ Layers, *Appl. Phys. Lett.* **50**, 95 (1987).
4. P. N. K. Deenapanray, Dynamics of the Ion Beam Induced Nitridation of Silicon, *J. Vac. Sci. Technol.* **A20**, 1261 (2002).
5. A. Mogro-Campero, R. P. Love, M. F. Chang, and R. F. Dyer, Localized Lifetime Control in Insulated Gate Transistors by Proton Implantation, *IEEE Trans. Electron Devices* **33**, 1667 (1986).
6. D. C. Sawko and J. Bartko, Production of Fast Switching Power Thyristors by Proton Irradation, *IEEE Nucl. Sci.* **30**, 1756 (1983).
7. C. Jagadish, B. G. Svensson, and N. Hauser, Point-Defects in n-Type Silicon Implanted with Low Doses of MeV Boron and Silicon Ions, *Semicond. Sci. Technol.* **8**, 481 (1993), and references therein.
8. J. W. Corbett, J. P. Karins, and T. Y. Tan, Ion-Induced Defects in Semiconductors, *Nucl. Instrum. Methods* **182–183**, 457 (1981).
9. D. V. Lang, Fast Capacitance Transient Apparatus: Application to ZnO and O Centers in GaP *p-n* Junctions, *J. Appl. Phys.* **45**, 3014 (1974).

10. D. V. Lang, Deep-Level Transient Spectroscopy: A New Method to Characterize Traps in Semiconductors, *J. Appl. Phys.* **45**, 3023 (1974).
11. L. C. Kimerling, Defects Characterization by Junction Spectroscopy, *Materials Research Society Proceedings, Vol 2: Defects in Semiconductors* (J. Narajan and T. Y. Tan, eds., North Holland, New York), p. 85, (1981).
12. L. Dobaczewski, P. Kaczor, I. D. Hawkins, and A. R. Peaker, Laplace Transform Deep-Level Transient Spectroscopic Studies of Defects in Semiconductors, *J. Appl. Phys.* **76**, 194 (1994).
13. J. H. Evans-Freeman, A. R. Peaker, I. D. Hawkins, P. Y. Y. Kan, J. Terry, L. Rubaldo, M. Ahmed, S. Watts, and L. Dobaczewski, High-Resolution DLTS Studies of Vacancy-Related Defects in Irradiated and in Ion-Implanted n-Type Silicon, *Mat. Sci. Semicon. Proc.* **3**, 237 (2000).
14. J. Lindhard, V. Nielsen, M. Scharff, and P. V. Thompsen, *Kgl. Dan. Vid. Selsk. Mat. fys. Medd.* **33**, 10 (1963).
15. O. B. Firsov, *Zh. Eksp. Teor. Fiz.* **34**, 447 (1958).
16. J. P. Biersack and L. G. Haggmark, A Monte Carlo Computer Program for the Transport of Energetic Ions in Amorphous Materials, *Nucl. Instrum. Methods* **174**, 257 (1980).
17. J. Lindhard and M. Scharff, Energy Dissipation by Ions in the keV Region, *Phys. Rev.* **124**, 128 (1961).
18. H. Z. Bethe, *Phys.* **76**, 293 (1932).
19. J. Lindhard, *Kgl. Dan. Vid. Selsk. Mat. fys. Medd.* **34**, 14 (1965).
20. J. Lindhard, M. Scharff, and H. Schiott, Range Concepts and Heavy Ion Ranges, *Kgl. Dan. Vid. Selsk. Mat. fys. Medd.* **33**, 14 (1963).
21. W. Eckstein, *Computer Simulation of Ion-Solid Interactions, Springer Ser. Mat. Sci., Vol. 10* (Springer, Berlin, Heidelberg) (1991).
22. M. T. Robinson, Computer Simulation Studies of High-Energy Collision Cascades, *Nucl. Instrum. Methods in Phys. Res.* **B67**, 396 (1992).
23. M. T. Robinson, The Temporal Development of Collision Cascades in the Binary-Collision Approximation, *Nucl. Instrum. Methods in Phys. Res.* **B48**, 408 (1990).
24. M. T. Robinson, Slowing-Down Time of Energetic Atoms in Solids, *Phys. Rev.* **B40**, 10717 (1989).
25. A. Hallén and M. Bakowski, Combined Proton and Electron Irradiation for Improved GTO Thyristors, *Solid-State Electron.* **32**, 1033 (1989).
26. G. L. Miller, D. V. Lang, and L. C. Kimerling, Capacitance Transient Spectroscopy. *Ann. Rev. Mater. Sci.* **7**, 377 (1977).
27. D. V. Lang and C. H. Henry, Nonradiative Recombination at Deep Levels in GaAs and GaP by Lattice-Relaxation Multiphonon Emission, *Phys. Rev. Lett.* **35**, 1525 (1975).
28. C. H. Henry and D. V. Lang, Nonradiative Capture and Recombination by Multiphonon Emission in GaAs and GaP, *Phys. Rev.* **B15**, 989 (1977).
29. J. A. Van Vechten and C. D. Thurmond, Entropy of Ionization and Temperature Variation of Ionization Levels of Defects in Semiconductors, *Phys. Rev.* **B14**, 3539 (1976).
30. C. O. Almbladh and G. J. Rees, Statistical Mechanics of Band States and Impurity States in Semiconductors, *J. Phys. C: Solid State Phys.* **14**, 4575 (1981).
31. D. V. Lang, Space-Charge Spectroscopy in Semiconductors, in *Thermally Stimulated Relaxation of Solids* (P. Braunlich, ed., Springer-Verlag, Berlin), pp. 93–133 (1979).
32. L. C. Kimerling, Influence of Deep Traps on the Measurement of Free-Carrier Distributions in Semiconductors by Junction Capacitance Techniques, *J. Appl. Phys.* **45**, 1839 (1974).
33. J. J. Shiau, A. L. Fahrenbruch, and R. H. Bube, Interpretation of Capacitance Versus Voltage Measurements in the Presence of a High Density of Deep Levels, *J. Appl. Phys.* **59**, 2879 (1986).
34. F. D. Auret, Considerations for Capacitance DLTS Measurements Using a Lock-In Amplifier, *Rev. Sci. Instrum.* **57**, 1597 (1986).
35. F. D. Auret and M. Nel, Single Scan Defect Identification by Deep Level Transient Spectroscopy Using a Two-Phase Lock-In Amplifier (*IQ*-DLTS), *J. Appl. Phys.* **63**, 973 (1988).
36. P. D. Kirchner, W. J. Schaff, G. N. Maracas, L. F. Eastman, T. I. Chappell, and C. M. Ransom, The Analysis of Exponential and Non-Exponential Transients in Deep-Level Transient Spectroscopy, *J. Appl. Phys.* **52**, 6462 (1981).
37. A. Cola, M. G. Lupo, and L. Vasanelli, Determination of Deep-Level Parameters by a New Analysis Method of Isothermal Capacitance Transients, *J. Appl. Phys.* **69**, 3072 (1991).
38. K. Ikossi-Anastasiou and K. P. Roenker, Refinements in the Method of Moments for Analysis of Multi-Exponential Capacitance Transients in Deep-Level Transient Spectroscopy, *J Appl. Phys.* **61**, 182 (1987).
39. D. D. Nolte and E. E. Haller, Optimization of the Energy Resolution of Deep Level Transient Spectroscopy, *J. Appl. Phys.* **62**, 900 (1987).
40. C. Eiche, D. Maier, M. Schneider, D. Sinerius, J. Weese, K. W. Benz, and J. Honerkamp, Analysis of Photoinduced Current Transient Spectroscopy (PICTS) Data by a Regularization Method, *J. Phys. Condens. Matter* **4**, 6131 (1992).
41. I. Thurzo, D. Pogany, and K. Gmucova, A Novel Algorithm for Higher Order Filtering in DLTS, *Solid-State Electron.* **35**, 1737 (1992).
42. G. A. Korn and T. M. Korn, in *Mathematical Handbook*, (McGraw-Hill, New York) (1968).
43. P. Deixler, J. Terry, I. D. Hawkins, J. H. Evans-Freeman, A. R. Peaker, L. Rubaldo, D. K. Maude, J.-C. Portal, L. Dobaczewski, K. Bonde Nielsen, A. Nylandsted Larsen, and A. Mesli, Laplace-Transform Deep-Level Transient Spectroscopy Studies of the *G*4 Gold–Hydrogen Complex in Silicon, *Appl. Phys. Lett.* **73**, 3126 (1998).
44. Y. Zohta and M. O. Watanabe, On the Determination of the Spatial Distribution of Deep Centres in Semiconducting Thin Films from Capacitance Transient Spectroscopy, *Jpn. J. Appl. Phys.* **53**, 1890 (1982).
45. J. Frenkel, On Pre-Breakdown Phenomena in Insulators and Electronic Semiconductors, *Phys. Rev.* **54**, 647 (1938).
46. D. Pons and S. Makram-Ebeid, Phonon Assisted Tunnel Emission from Deep Levels in GaAs, *J. de Physique* **40**, 1161 (1979).
47. S. Makram-Ebeid and M. Lannoo, Quantum Model for Phonon-Assisted Tunnel Ionization of Deep Levels in a Semiconductor, *Phys. Rev.* **B25**, 6406 (1982).
48. H. Lefevre and M. Schultz, Double Correlation Technique (DDLTS) for the Analysis of Deep Level Profiles in Semiconductors, *Appl. Phys.* **12**, 45 (1977).
49. T. Markvart, D. P. Parton, J. W. Peters, and A. F. W. Willoughby, DLTS of Recombination Centres in Semiconductors, *Materials Science Forum* **143–147**, 1381 (1994).

50. S. M. Sze, *Physics of Semiconductor Devices*, 2nd Ed., (John Wiley & Sons, Wiley Eastern Ltd., New Delhi), p. 37 (1981).
51. W. Schockley and W. T. Read, Statistics of the Recombination of Holes and Electrons, *Phys. Rev.* **87**, 835 (1952).
52. C. Jagadish and P. N. K. Deenapanray, in *Business Briefing Global Semiconductor Manufacturing Technology* (World Markets Research Centre, UK, January 2001), p. 76.
53. L. C. Kimerling and J. M. Poate, in *Lattice Defects in Semiconductors* (Inst. Phys. Conf. Ser. **23**), p. 126 (Proceedings 1974).
54. L. C. Kimerling, H. M. De Angelis, and J. W. Diebold, On the Role of Defect Charge State in the Stability of Point Defetcs in Silicon, *Solid State Commun.* **16**, 171 (1975).
55. L. C. Kimerling, New Developments in Defect Studies in Semiconductors, *IEEE Trans. Nucl. Sci.* **NS-23**, 6 (1976).
56. L. C. Kimerling, in *Radiation Effects in Semiconductors 1976*, IOP Conf. Proc. Ser. No. **31** (N. B. Urli and J. W. Corbett, eds., IOP, London), p. 221 (1977).
57. L. C. Kimerling, P. Blood, and W. M. Gibson, Defect States in Proton-Bombarded Silicon at T <300 K, in Defects and Radiation Effects in Semiconductors, 1978, (J. H. Albany, ed., IOP Conf. Ser. No. **46** IOP, London), p. 273 (1979).
58. H. M. De Angelis, J. W. Diebold, and L. C. Kimerling, Radiation Damage in III-V Compounds, in *Radiation Damage and Defects in Semiconductors* (London: IOP, 1973), p. 295.
59. G. D. Watkins, The Lattice Vacancy in Silicon, in *Deep Centers in Semiconductors* (S. Pantelides ed., Gordon and Breach, New York), pp. 147–183 (1986).
60. E. D. Wickner and D. P. Snowden, *Bull. Am. Phys. Soc.* **9**, 706 (1964).
61. L. J. Cheng and J. C. Corelli, Recovery of Electrical Properties in 45-MeV-Electron-Irradiated *n*-Type Si from 80 to 350°K, *Phys. Rev.* **140**, A2130 (1965).
62. G. D. Watkins and K. L. Brower, EPR Observation of the Isolated Interstitial Carbon Atom in Silicon, *Phys. Rev. Lett.* **36**, 1329 (1976).
63. G. D. Watkins, Intrinsic Point Defects in Semiconductors, in *Materials Science and Technology, Vol. 4, Electronic Structure and Properties of Semiconductors*, (W. Schroter, ed., VCH, Weinheim, 1991), Chapter 3.
64. G. D. Watkins, Vacancies and Interstitials and Their Interactions with Other Defects in Silicon, in *Proceedings of the Third International Symposium on Defects in Silicon (Electrochemical Society Proceedings Vol. 99-1)*, (T. Abe, W. M. Bullis, S. Kobayashi, W. Lin, and P. Wagner, eds., Pennington, New Jersey), pp. 38–52, (1999).
65. G. D. Watkins and J. R. Troxell, Negative U Properties of Point Defects in Silicon, *Phys. Rev. Lett.* **44**, 593 (1980).
66. G. D. Watkins, J. R. Troxell, and A. P. Chatterjee, Vacancies and Interstitials in Silicon, in *Defects and Radiation Effects in Semiconductors 1978* (Inst. of Phys. Conf. Ser. **46**, London, 1979), p. 16.
67. J. C. Brabant, M. Pugnet, J. Barbolla, and M. Brousseau, Studies of Defects Introduced by Electron Irradation at 4.2°K in P-Silicon by Thermally Stimulated Capacitance Technique, *J. Appl. Phys.* **47**, 4809 (1976).
68. J. C. Brabant, M. Pugnet, J. Barbolla, and M. Brousseau, Studies of Defects Introduced by Electron Irradiation at 4.2° k in Silicon by Thermally Stimulated Capacitance, in *Radiation Effects Semiconductors 1976*, (Inst. Phys. Conf. Ser. **31**, London, 1977) p. 200.
69. G. A. Baraff, E. O. Kane, and M. Schlüter, Theory of the Silicon Vacancy: An Anderson Negative-U System, *Phys. Rev.* **B21**, 5662 (1980).
70. G. D. Watkins, A. P. Chattergee, and R. D. Harris, Negative-U for Point Defects in Silicon, in *Defects and Radiation Effects in Semiconductors 1980*, (Inst. Conf. Ser. **59**, London, 1981) p. 199.
71. G. D. Watkins,Negative-U Properties for Point Defects in Silicon, in *Defects in Semiconductors*, (J. Narayan and T. Y. Tan, eds., North Holland, New York, 1981), p. 21.
72. G. D. Watkins, Defects in Irradiated Silicon: EPR of the Tin Vacancy Pair, *Phys. Rev.*, **B12**, 4383 (1975).
73. J. R. Troxell and G. D. Watkins, *Bull. Am. Phys. Soc.* **24**, 18 (1979).
74. J. W. Corbett, G. D. Watkins, R. M. Chrenko, and R. S. McDonald, Defects in Irradiated Silicon. II. Infrared Absorption of the Si-*A* Center, *Phys. Rev.* **121**, 1015 (1961).
75. J. W. Corbett and G. D. Watkins, Production of Divacancies and Vacancies by Electron Irradiation of Silicon, *Phys. Rev.* **138**, A555 (1965).
76. G. D. Watkins, in *Lattice Defects in Semiconductors* (Inst. Phys. Conf. Ser. **23**, London, 1975), p. 1.
77. C. A. J. Ammerlaan and G. D. Watkins, Electron Paramagnetic Resonance Detection of Optically Induced Divacancy Aligment in Silicon, *Phys. Rev.* **B5**, 3988 (1972).
78. A. H. Kalma and J. C. Corelli, Photoconductive Studies of Defects in Silicon: Divacancies Associated Energy Levels, *Phys. Rev.* **173**, 734 (1968).
79. G. D. Watkins and J. W. Corbett, Defects in Irradated Silicon: Electron Paramagnetic Resonance of the Divacancy, *Phys. Rev.* **138**, A543 (1965).
80. A. O. Evwaraye and E. Sun, Electron-Irradation-Induced Divacancies in Lighly Doped Silicon, *J. Appl. Phys.* **47**, 3776 (1976).
81. F. P. Wang, H. H. Sun, and F. Lu, Novel Electrical and Annealing Properties of Defects in Electron Irradated Silicon p^+-n Junctions, *J. Appl. Phys.* **68**, 1535 (1990).
82. E. V. Monakhov, B. S. Avset, A. Hallén, B. G. Svensson, Formation of a Double Acceptor Center During Divacancy Annealing in Low-Doped High-Purity Oxygenated Si, *Phys. Rev.* **B65**, 233207 (2002).
83. E. V. Monakhov, J. Wong-Leung, A. Y. Kuznetsov, C. Jagadish, and B. G. Svensson, Formation of a Double Acceptor Center During Divacancy Annealing in Low-Doped High-Purity Oxygenated Si, *Phys. Rev*. **B65** (24), 245201 (2002).
84. L. Dobaczewski, K. Gośoiński, Z. R. Zytkiewicz, K. Bonde Nielsen, L. Rubaldo, O. Andersen, and A. R. Peaker, Piezoscopic Deep Level Transient Spectroscopy Studies of the Silicon Divacancy, *Phys. Rev.* **B65**, 113203 (2002).
85. G. D. Watkins and J. W. Corbett, Defects in Irradiated Silicon. I. Electron Spin Resonance of the Si-*A* Center, *Phys. Rev.* **121**, 1001 (1961).
86. L. Dobaczewski, O. Andersen, L. Rubaldo, K. Gośoiński, V. P. Markevich, A. R. Peaker, and K. Bonde Nielsen, Saddle Point for Oxygen Reorientation in the Vicinity of a Silicon Vacancy, *Phys. Rev.* **B67**, 195204 (2003).
87. E. L. Elkin and G. D. Watkins, Defects Irradiated Silicon: Electron Paramagnetic Resonance and Electron–Nuclear Double

Resonance of the Arsenic– and Anitomy–Vacancy Pairs, *Phys. Rev.* **174**, 881 (1968).
88. A. O. Evwaraye, Annealing of Irradiation-Induced Defects in Arsenic-Doped Silicon, *J. Appl. Phys.* **48**, 1840 (1977).
89. V. P. Markevich, O. Andersen, I. F. Medvedeva, J. H. Evans-Freeman, I. D. Hawkins, L. I. Murin, L. Dobaczewski, and A. R. Evans Peaker, Defect Reactions Associated with the Dissociation of the Phosphorus–Vacancy Pair in Silicon, *Physica* **B308–310**, 513 (2001).
90. R. C. Newman and J. B. Willis, *J. Phys. Chem. Solids* **26**, 373 (1965).
91. A. R. Bean and R. C. Newman, Low Temperature Electron Irradiation of Silicon Containing Carbon, *Solid State Commun.* **8**, 175 (1970).
92. R. Woolley, E. C. Lightowlers, A. K. Tipping, M. Claybourn, and R. C. Newman, Electronic and Vibrational Absorption of Intersitial Carbon in Silicon, *Mat. Sci. Forum* **10–12**, 929 (1986).
93. K. Thonke, A. Teschner, and R. Sauer, New Photoluminescence Defect Spectra in Silicon Irradiated at 100 K: Observation of Interstitial Carbon, *Solid State Commun.* **61**, 24 (1987).
94. P. M. Mooney, L. J. Cheng, M. Suli, J. D. Gerson, and J. W. Corbett, Defect Energy Levels in Boron-Doped Silicon Irradiated with 1-MeV Electrons, *Phys. Rev.* **B15**, 3836 (1977).
95. R. D. Harris and G. D. Watkins, Interstitial Related Defects in n Type Silicon, in *The 13th International Conference on Defects in Semiconductors* (L. C. Kimerling and J. M. Parsey, Jr., eds., AIME, New York), p. 799 (1985).
96. L. W. Song and G. D. Watkins, EPR Identification of the Single-Acceptor State of Interstitial Carbon in Silicon, *Phys. Rev.* **B42**, 5759 (1990).
97. L. W. Song, X. D. Zhan, B. W. Benson, and G. D. Watkins, Bistable Interstitial-Carbon–Substitutional-Carbon Pair in Silicon, *Phys. Rev.* **B42**, 5765 (1990).
98. K. L. Brower, EPR of a Jahn-Teller Distorted (111) Carbon Interstitialcy in Irradiated Silicon, *Phys. Rev.* **B9**, 2607 (1974).
99. Y. H. Lee, L. J. Cheng, J. D. Gerson, P. M. Mooney, and G. W. Watkins, Carbon Interstitial in Electron-Irradiated Silicon, *Solid State Commun.* **21**, 109 (1997).
100. G. E. Jellison, Jr., Transient Capacitance Studies of an Electron Trap at E_c–E_T = 0.105 eV in Phosphorus-Doped Silicon, *J. Appl. Phys.* **53**, 5715 (1982).
101. A. Chantre and D. Bois, Metastable Defect Behavior in Silicon: Charge-State-Controlled Reorientation of Iron-Aluminum Pairs, *Phys. Rev.* **B31**, 7979 (1985).
102. J. L. Benton and M. Levinson, Metastable Defect Configurations in Semiconductors, in *Defects in Semiconductors II*, (S. Mahajan and J. W. Corbett, eds., North Holland, New York), p. 95, (1983).
103. L. W. Song, B. W. Benson, and G. D. Watkins, Identification of a Bistable Defect in Silicon: The Carbon Interstitial-Carbon Substitutional Pair, *Appl. Phys. Lett.* **51**, 1155 (1987).
104. J. W. Corbett, G. D. Watkins, and R. S. McDonald, New Oxygen Infrared Bands in Annealed Irradiated Silicon, *Phys. Rev.* **135**, A1381 (1964).
105. P. Pellegrino, P. Lévéque, J. Wong-Leung, C. Jagadish, and B. G. Svensson, Separation of Vacancy and Interstitial Depth Profiles in Ion-Implanted Silicon: Experimental Observation, *Appl. Phys. Lett.* **78**, 3442 (2001).
106. G. Davies, A. Oates, R. C. Newman, R. Woolley, E. C. Lightowlers, M. Binns, and J. Wilkes, Carbon Related Radiation Damage Centres in Czochralski Silicon, *J. Phys. C.* **19**, 841 (1986).
107. A. V. Yukhnevich and V. D. Tkachev, *Fiz. Tverd.* (Leningrad) **8**, 1264 (1966) [*Sov. Phys.—Solid State* **8**, 1004 (1966)].
108. J. M. Trombetta and G. D. Watkins, Identification of an Interstitial Carbon-Interstitial Oxygen Complex in Silicon, *Appl. Phys. Lett.* **51**, 1103 (1987).
109. E. Gürer, B. W. Benson, and G. D. Watkins, Configurational Metastability of Carbon Phosphorus Pair Defects in Silicon, *Mater. Sci. Forum* **83–87**, 339 (1992).
110. A. Chantre and L. C. Kimerling, Configurationally Multistable Defect in Silicon, *Appl. Phys. Lett.* **48**, 1000 (1986).
111. B. W. Benson, E. Gürer, and G. D. Watkins, Multi-Configurational Carbon-Antimony Pair in Silicon, *Mat. Sci. Forum* **38–41**, 391 (1989).
112. G. D. Watkins, Modification of Defect Structures in Semiconductors by Electronic Excitiation, *Reviews of Solid State Science* **4**, 279 (1990).
113. A. K. Tipping and R. C. Newman, The Diffusion Coefficient of Interstitial Carbon in Silicon, *Semicon. Sci. and Technol.* **2**, 315 (1987).
114. L. C. Kimerling, M. T. Asom, J. L. Benton, P. J. Drevonsky, and C. E. Caefer, Intersitial Defect Reactions in Silicon, *Mater. Sci. Forum* **38–41**, 141 (1989).
115. X. D. Zhan and G. D. Watkins, *Bull. Am. Phys. Soc.* **35**, 279 (1990).
116. P. J. Drevinsky, C. E. Caefer, S. P. Tobin, J. C. Mikkelsen, Jr., and L. C. Kimerling, Influence of Oxygen and Boron on Defects Production in Irradiated Silicon, in *Defects in Electronic Materials* (M. Stavola, S. J. Pearton, and G. Davies, eds., *Mat. Res. Soc. Proc.* **104**, Pittsburg, 1988), p. 167.
117. R. N. Hall, Kinetics of Hydrogen Defect Complex Formation in Ge and Si, in *The 13th International Conference on Defects in Semiconductors* (L. C. Kimerling and J. M. Parsey, Jr., eds., AIME, New York, 1985), p. 759.
118. T. S. Shi, S. N. Sahu, J. W. Corbett, and L. C. Snyder, *Scientia Sinica* **27**, 98 (1984).
119. S. J. Pearton, The Properties of Hydrogen in Crystalline Si, *J. Electron. Mater.* **14a**, 737 (1985).
120. J. L. Benton, C. J. Doherty, S. D. Ferris, D. L. Flamm, L. C. Kimerling, and H. J. Leamy, Hydrogen Passivation of Point Defects in Silicon, *Appl. Phys. Lett.* **36**, 670 (1980).
121. J. I. Pankove, D. E. Carlson, J. E. Berkeyheiser, and R. O. Wance, Neutralization of Shallow Acceptor Levels in Silicon by Atomic Hydrogen, *Phys. Rev. Lett.* **51**, 2224 (1983).
122. J. I. Pankove, P. J. Zanzucchi, C. W. Magee, and G. Lucovsky, Hydrogen Localization Near Boron in Silicon, *Appl. Phys. Lett.* **46**, 421 (1985).
123. N. M. Johnson, Mechanism for Hydrogen Compensation of Shallow-Acceptor Impurities in Single-Crystal Silicon, *Phys. Rev.* **B31**, 5525 (1985).
124. G. G. DeLeo and W. B. Fowler, Hydrogen-Acceptor Pairs in Silicon: Pairing Effect on the Hydrogen Vibrational Frequency, *Phys. Rev.* **B31**, 6861 (1985).
125. G. G. DeLeo and W. B. Fowler, Hydrogen-Acceptor Pairs in Silicon, *Phys. Rev. Lett.* **56**, 402 (1986).
126. M. Stavola, S. J. Pearton, J. Lopata, and W. C. Dautremont-Smith, Vibrational Characteristics of Acceptor-Hydrogen Complexes in Silicon, *Appl. Phys. Lett.* **50**, 1086 (1987).

127. B. B. Nielsen, J. U. Andersen, and S. J. Pearton, Lattice Location of Deuterium Interacting with the Boron Acceptor in Silicon, *Phys. Rev. Lett.* **60**, 321 (1988).
128. A. D. Marwick, G. S. Oehrlein, and N. M. Johnson, Structure of the Boron-Hydrogen Complex in Crystalline Silicon, *Phys. Rev.* **B36**, 4539 (1987).
129. S. J. Pearton, J. W. Corbett, and T. S. Shi, Hydrogen in Crysalline Semiconductors, *Appl. Phys.* **A43**, 153 (1987).
130. E. E. Haller, Hydrogen in Crystalline Semiconductors, *Semicond. Sci. Technol.* **6**, 73 (1991).
131. K. Irmscher, H. Klose, and K. Maass, Hydrogen Related Deep Levels in Proton-Bombarded Silicon, *J. Phys. C: Solid State Phys.* **17**, 6317 (1984).
132. B. Holm, K. Bonde Nielsen, and B. Bech Nielsen, Deep State of Hydrogen in Crystalline Silicon: Evidence for Metastability, *Phys. Rev. Lett.* **66**, 2360 (1991).
133. C. G. Van de Walle, Y. Bar-Yam, and S. T. Pantelides, Theory of Hydrogen Diffusion and Reactions in Crystalline Silicon, *Phys. Rev. Lett.* **60**, 2761 (1988).
134. C. G. Van de Walle, P. J. H. Denteneer, Y. Bar-Yam, and S. T. Pantelides, Theory of Hydrogen Diffusion and Reactions in Crystalline Silicon, *Phys. Rev.* **B39**, 10791 (1989).
135. Y. V. Gorelkinskii and N. N. Nevinnyi, *Sov. Tech. Phys. Lett.* **13**, 45 (1987).
136. A. L. Endröss, Charge-State-Dependent Hydrogen-Carbon-Related Deep Donor in Crystalline Silicon, *Phys. Rev. Lett.* **63**, 70 (1989).
137. A. L. Endröss, W. Krühler, and F. Koch, Electronic Properties of the Hydrogen-Carbon Complex in Crystalline Silicon, *J. Appl. Phys.* **72**, 2264 (1992).
138. P. J. H. Denteneer, C. G. Van de Walle, and S. T. Pantelides, Structure and Properties of Hydrogen-Impurity Pairs in Elemental Semiconductors, *Phys. Rev. Lett.* **62**, 1884 (1989).
139. W. Csaszar and A. L. Endröss, Anomalous Electronic Properties of a Hydrogen-Related Deep Donor in *c*-Si, *Phys. Rev. Lett.* **73**, 312 (1994).
140. Y. Kamiura, N. Ishiga, and Y. Yamashita, Structure and Stress Inducted Alignment of a Hydrogen Carbon Complex in Silicon, *Jpn. J. Appl. Phys.* **36**, L1419 (1997).
141. K. Fukuda, Y. Kamiura, and Y. Yamashita, Effects of Charge State on Stress-Induced Alignment and Relaxation of a Hydrogen Carbon Complex in Silicon, *Physica* **B273–274**, 184 (1999).
142. Y. Kamiura, M. Hayashi, Y. Nishiyama, S. Ohyama, and Y. Yamashita, Electronically Induced Instability of a Hydrogen-Carbon Complex in Silicon and its Dissociation Mechanism, *Jpn. J. Appl. Phys. Part 1* **36**, 6579 (1997).
143. M. Yoneta, Y. Kamiura, and F. Hashimoto, Chemical Etching-Induced Defects in Phosphorus-Doped Silicon, *J. Appl. Phys.* **70**, 1295 (1991).
144. G. Lucovsky, On the Photo-Ionization of Deep Impurity Centres in Semiconductors, *Solid State Commun.* **3**, 299 (1965).
145. D. M. Maric, P. F. Meier, and S. K. Estreicher, {H,B}, {H,C}, and {H,Si} Pairs in Silicon and Germanium, *Phys. Rev.* **B47**, 3620 (1993).
146. C. Kaneta and H. Kataama-Yoshida, Structural and Electronic Properties of Carbon-Hydrogen Complex in Silicon, *Mater. Sci. Forum.* **196–201**, 897 (1995).
147. A. Van Wieringen and N. Warmoltz, *Physica* **22**, 849 (1956).
148. O. Andersen, A. R. Peaker, L. Dobaczewski, K. Bonde Nielsen, B. Hourahine, R. Jones, P. R. Briddon, and S. Öberg, Electrical Activity of Carbon—Hydrogen Centers in Si, Continuous-Wave and Pulsed EPR Study of the Negatively Charged Silicon Vacancy with $S =$ and C_{3v} Symmetry in *n*-type 4*H*-SiC, *Phys. Rev.* **B66**, 235202 (2002).
149. M. W. Hüppi, Proton Irradiation of Silicon: Complete Electrical Characterization of the Induced Recombination Centers, *J. Appl. Phys.* **68**, 2702 (1990).
150. B. G. Svensson, A. Hállen, and B. U. R. Sundqvist, Hydrogen-Related Electron Traps in Proton-Bombarded Float Zone Silicon, *Mater. Sci. Eng.* **B4**, 285 (1989).
151. L. Palmetshofer and J. Reisinger, Defect Levels in H^+-, D^+-, and He^+-Bombarded Silicon, *J. Appl. Phys.* **72**, 2167 (1992).
152. K. Bonde Nielsen, L. Dobaczewski, K. Goscinski, R. Bendesen, O. Andersen, and B. Bech Nielsen, Deep Levels of Vacancy-Hydrogen Centers in Silicon Studied by Laplace DLTS, *Physica* **B273–274**, 167 (1999).
153. Y. Tokuda, H. Shimada, and A. Ito, Light-Illumination-Induced Transformation of Electron Traps in Hydrogen-Implanted *n*-Type Silicon, *J. Appl. Phys.* **86**, 5630 (1999).
154. S. Fatima, C. Jagadish, J. Lalita, B. G. Svensson, and A. Hállen, Hydrogen Interaction with Implantation Induced Point Defects in *p*-Type Silicon, *J. Appl. Phys.* **85**, 2562 (1999).
155. P. Lévêque, P. Pellegrino, A. Hallén, B. G. Svensson, and V. Privitera, Hydrogen-Related Defect Centers in Float-Zone and Epitaxial n-Type Proton Implanted Silicon, *Nucl. Instrum. Methods* **B174**, 297 (2001).
156. O. Feklisova and N. Yarykin, Transformation of Deep-Level Spectrum of Irradiated Silicon due to Hydrogenation Under Wet Chemical Etching, *Semicond. Sci. Technol.* **12**, 742 (1997).
157. O. Feklisova, N. Yarykin, Eu. Yakimov, and J. Weber, Hydrogen Interaction with Defects in Electron-Irradiated Silicon, *Physica* **B273–274**, 235 (1999).
158. A. R. Peaker, J. H. Evans-Freeman, P. Y. Y. Kan, L. Rubaldo, I. D. Hawkins, K. D. Vernon-Parry, and L. Dobaczewski, Hydrogen Reactions with Electron Irradiation Damage in Silicon, *Physica* **B273–274**, 243 (1999).
159. Y. Tokuda and T. Seki, Interaction of Hydrogen with the Vacancy-Oxygen Pair Produced in n-Type Silicon by Electron Irradiation, *Semicond. Sci. Technol.* **15**, 126 (2000).
160. Y. Ohmura, K. Takahashi, H. Saitoh, T. Kon, and A. Enosawa, Hydrogenation and Passivation of Electron-Beam-Induced Defects in n-Type Si, *Physica* **B273–274**, 228 (1999).
161. S. J. Pearton, Hydrogen Passivation of Gamma-Ray Induced Point Defects in Si, *Phys. Stat. Sol.* **A72**, K73 (1982).
162. J. L. Hastings, M. Gharaibeh, S. K. Estreicher, and P. A. Fedders, Hydrogen Interactions with Intrinsic Defects in Silicon, *Physica* **B273–274**, 216 (1999).
163. J. W. Corbett, J. C. Corelli, U. Desnica, and L. C. Snyder, *Microscopic Identification of Electronic Defects in Semiconductors*, (N. M. Johnson, S. G. Bishop, and D. Watkins, eds.), *Mater. Res. Soc. Symp. Proc.* **46**, 243 (1987).
164. K. Irmscher, Ph.D. Thesis, Humboldt Universität, Berlin, Germany, 1985.

165. J. Lalita, B. G. Svensson, C. Jagadish, and A. Hallén, Annealing Studies of Point Defects in Low Dose Mev Ion Implanted Silicon, *Nucl. Instrum. Methods* **B127–128**, 69 (1997).
166. P. Johannesen, B. Bech Nielsen, and J. R. Byberg, Identification of the Oxygen-Vacancy Defect Containing a Single Hydrogen Atom in Crystalline Silicon, *Phys. Rev.* **B61**, 4659 (2000).
167. G. L. Gutsev, G. S. Myakenkaya, V. V. Frolov, and V. B. Glazman, Nature of Hydrogen-Bonding in Si-A-Center, *Phys. Stat. Sol.* **153**, 659 (1989).
168. A. R. Peaker, Private Communication.
169. B. Bech Nielsen, P. Johannesen, P. Stallinga, K. Bonde Nielsen, and J. R. Byberg, Identification of the Silicon Vacancy Containing a Single Hydrogen Atom by EPR, *Phys. Rev. Lett.* **79**, 1507 (1997).
170. S. Fatima, Ph.D. Thesis, *Electrically Active Defects in Ion Implanted Si*, Australian National University, Canberra, Australia, 2000.
171. M. Bruni, D. Bisero, R. Tonini, G. Ottaviani, G. Queirolo, and R. Bottini, Electrical Studies on H-implanted Silicon, *Phys. Rev.* **B49**, 5291 (1994).
172. J. Bernholc, N. O. Lipari, S. T. Pantelides, and M. Scheffler, Electronic Structure of Deep *sp*-Bonded Substitutional Impurities in Silicon, *Phys. Rev.* **B26**, 5706 (1982).
173. G. L. Gutsev and G. S. Myakenkaya, The Acceptor States of Hydrogen in Silicon, *Phys. Stat. Sol.* **156**, 319 (1989).
174. P. N. K. Deenapanray, Trap-Limited Migration of Vacancy-Type Defects in 7.5 keV H^--Implanted Si, *Appl. Phys. Lett.* **80**, 1577 (2002).